UNIVERSITY OF SALERNO

DEPARTMENT OF CHEMISTRY AND BIOLOGY "A. Zambelli"

Ph. D. Course in Chemistry - XXXIII Cycle

Ph. D. Thesis in Chemistry

BIOINSPIRED SUPRAMOLECULAR CATALYSIS IN NANOCONFINED SPACE

Tutor:
Prof. Margherita De Rosa

Co-tutor:
Prof. Carmine Gaeta

Ph. D. Coordinator:
Prof. Claudio Pellecchia

Ph. D. Student:
Stefania Gambaro
8800100032

2020-2021

Who cares if one more light goes out?

Abstract

The nanoconfinement in Nature is the key for the selectivity of enzymatic reactions: when the substrates are confined in the enzyme pocket, overconcentration and proximity effects promote the reaction in very efficient and selective ways. For this reason, several artificial enzymes have been designed in order to mimic the modus operandi of natural enzymes. Among them, the self-assembled resorcin[4]arene capsule is one of the most investigated systems: its inner cavity looks like the enzyme active site, and like in an enzyme pocket, it can host the reagents in a selective way, can stabilize the intermediates and transition states of reactions by secondary interactions, and then, overconcentration and proximity effect leads to a reaction rate increasing. The most interesting aspect in conducting a reaction inside a cavity is that the reactivity of a substrate can be different from the classical one observed in bulk medium. In this regard, the main topic of the present PhD thesis is to extend the catalytic application of the hexameric resorcin[4]arene capsule.

Firstly, the use of the capsule was implemented in a Michael type Friedel-Crafts reaction between heteroarenes and nitroalkenes and in the synthesis of bis(heteroaryl)methanes, interesting building blocks for the synthesis of natural and unnatural porphyrin derivatives. The results indicated that the capsule promotes the reactions in efficient and selective fashion thanks to its H-bonding ability and its intrinsic Brønsted acidity.

In the second part of the thesis, the study was focused on the ability of the capsule to exert a supramolecular control over the composition of dynamic covalent libraries. The results clearly indicated that in the presence of the

capsule a kinetic and thermodynamic modulation of an imine-based dynamic covalent library was detected. This behavior was induced by a *predatory* effect of the capsule on specific constituent of the library.

Next, it was explored a Diels-Alder reaction promoted by carbocation catalysis in the nanoconfined space. The results demonstrated that the capsule promotes in situ generation of tritylium cation and prevents its quenching by encapsulation in the electron rich cavity.

Moreover, during my stay at the Institut Català d'Investigació Química, under the supervision of Prof. Pablo Ballester a new strapped calix[4]pyrrole was synthesized.

Table of Contents

Abstract **6**

Table of Contents **8**

List of Abbreviations **10**

Chapter 1. Introduction **12**

1.1 Supramolecular catalysis 12

1.2 Self-assembled capsules as supramolecular catalyst 16

1.3 Self-assembled capsules based on metal-ligand interactions 18

1.4 Self-assembled Capsules based on hydrogen bonds 21

1.4.1 Hexameric resorcinarene capsule as supramolecular nanoreactor 28

1.4.2 Hexameric resorcinarene capsule as catalyst 33

Chapter 2. Aim and Outlines of the thesis **43**

Chapter 3. Hexameric resorcinarene capsule as H-bonding catalyst in the construction of heterocyclic derivatives **45**

3.1 Introduction 45

3.2 Results and Discussion 53

3.2.1 Michael type Friedel Craft reaction promoted by CR_6 53

3.2.2 Synthesis of bis(heteroaryl)methanes promoted by CR_6 63

3.3 Conclusions 74

Chapter 4. Modulation of Dynamic Covalent Imine Libraries by the hexameric resorcinarene capsule **76**

4.1 Introduction 76

4.2 Results and discussion 79

4.2.1 Modulation of 2 x 1 DCLs in presence of CR_6 79

4.2.2 Modulation of 2 x 2 DCLs in presence of CR_6 96

4.3 Conclusions 99

Chapter 5. Hexameric resorcinarene capsule in the promotion of Lewis-Acid catalysis by the in-situ generation of a carbocation 100

5.1 Introduction 100

5.2 Results and discussion 103

5.3 Conclusions 110

Chapter 6. Summary 112

6.1 Final conclusions 112

Chapter 7. Experimental Section 113

7.1 General Remarks 113

7.2 General Procedures for the Alkylation of Heteroarenes by nitrostyrene and carbonyl compounds inside CR_6 114

7.3 General procedures for the modulation of imine-based DCLs..... 132

7.4 General Procedures for the Diels-Alder reaction 181

***List of publications* 187**

Appendix: Template Synthesis of a bis-calix[4]pyrrole macrocycle 189

A1. Introduction: Calix[4]pyrroles as receptors 189

A2. Results and discussion 194

A3. Conclusions 202

A4. Experimental Section 203

List of Abbreviations

AcOH	Acetic acid
br	broad
BHM	bis-(heteroaryl)methane
$BrCH_2COOH$	bromoacetic acid
DCM	dichloromethane
DC	dipolar cycloaddition
DCC	dynamic covalent chemistry
DCL	dynamic covalent library
DS	Diels-Alder
d	doublet
dba	dibenzylideneacetone
dd	double doublet
DMSO	dimethylsulfoxide
ee	enantiomeric excess
equiv.	equivalent(s)
ESI	Electrospray Ionization
FC	Friedel-Craft
h	hour(s)
H_2O	water
HOMO	Higher Occupied Molecular Orbital
HRMS	High Resolution Mass Spectrometry
i-Pr	isopropyl
LUMO	Lower Unoccupied Molecular Orbital
m	meta

MTFC	Michael-type Friedel-Craft
NMR	Nuclear Magnetic Resonance
o	ortho
rt	room temperature
s	singlet
t	triplet
t-Bu	*t*-butyl
TFA	trifluoroacetic acid

Chapter 1. Introduction

1.1 Supramolecular catalysis

Chemical transformations require making and breaking of chemical bonds and for most of them the presence of a catalyst is necessary in order to be synthetically effective. Thus, the study of catalysis is one of the fundamental topics in chemistry since it provides the tools necessary to increase reaction rate and selectivity, which is a crucial point for converting basic chemicals into useful products.

Historically, catalysis can be divided into heterogeneous and homogeneous catalysis, which includes transitions metal catalysis and organocatalysis; but in the last decade a new field, the so-called *supramolecular catalysis,* has attracted very much attention, considering the extensive number of articles present in literature[1].

Supramolecular catalysis can be considered a crossroad between catalysis and supramolecular chemistry[2] and from this point of view, the catalysis itself can be described as a supramolecular phenomenon when the catalyst recognizes the substrate and arranges the transition states for building the final products.

As nature is the first source of inspiration for supramolecular chemists, in the same way the natural enzymes represent a model for the design of

---

[1] a) P. Ballestrer, A. Vidal-Ferran, P. W. N. M. Van Leeuwen, *Adv. Catal.,* **2011**, *54*, 63; b) J. Liu, L. Chen, H. Cui, J. Zhang, L. Zhang, C.-Y. Su, *Chem. Soc. Rev.,* **2014**, *43*, 6011; c) J. J. Roach, R. A. Shenvi, *Nat. Chem.,* **2015**, *7*, 187; d) C. J. Brown, F. D. Toste, R. G. Bergman, K. N. Raymond, *Chem. Rev.,* **2015**, *115*, 3012.

[2] a) J. M. Lehn, *Science*, **1985**, *227*, 849, b) J. M. Lehn, *Supramolecular Chemistry: Concepts and Perspectives*, WILEY-VCH, **1995**.

supramolecular catalysts[3]. In fact, nature operates biochemical transformations that make life possible thanks to the presence of these astonishing catalytic agents. The natural enzymes are sophisticated polypeptidic molecules that present a hydrophobic pocket created by their defined three-dimensional structure, in which is located the active site. In this nanoconfined space the reactions take place with high chemo-, regio- and stereoselectivity[4]: firstly, specific substrates are bounded by multiple supramolecular interactions (hydrophobic interactions[5], hydrogen bonds[6], van der Walls interaction[7], etc) and reversible covalent interactions, then they are forced to react.

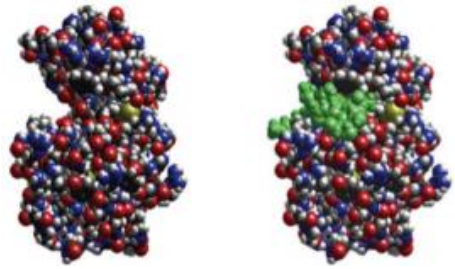

Figure 1. Example of substrate recognition (in green) by carboxypeptidase A.

The basic principles behind the enzymatic catalysis were proposed by Pauling over 50 years ago: molecular recognition (lock/key[8] and induced

---

[3] a) P. W. N. M. van Leeuwen, *Supramolecular Catalysis*, Wiley-VCH, Weinheim, **2008**; b) M. Raynal, P. Ballestrer, A. Vidal-Ferran, P. W. N. M. van Leeuwen, *Chem. Soc. Rev.* **2014**, *43*, 1660. c) J. Meeuwissen, J. N. H. Reek, *Nat. Chem.,* **2010**, *2*, 615

[4] a) C-H Wong, G. M. Whitesides*, Enzyme in synthetic organic chemistry*, Pergamon Press; **1994**; b) R. Breslow, *Acc. Chem. Res*., **1980**, *13*, 170; c) M. Raynal, P. Ballester, A. Vidal-Ferran, P. W. N. M. van Leeuwen, *Chem. Soc. Rev*., **2014**, *43*, 1734; d) J. Meeuwissen, J. N. H. Reek, *Nat. Chem*., **2010**, *2*, 61

[5] S. J.Teague, A. M. Davis, *Angew. Chem. Int. Ed. Engl*., **1999**, *38*, 736

[6] A. R. Fersht, J. P. Shi, J. Knill-Jones, D. A. Lowe, A. J. Wilkinson, D. M. Blow, P. Brick, P. Carter, M. M. Y. Waye, G. Winter, *Nature,* **1985**, *314*, 235.

[7] J. C.; Ma, D. A. Dougherty, *Chem. Rev*, **1997**, *97*, 1303

[8] E. Fischer, *Ber. Dtsch. Chem. Ges*., **1894**, *27*, 3189.

fit[9]) and stabilisation of the transition states of the reaction[10]; however the complete comprehension of enzyme catalysis is still matter of debate. Additionally, the natural enzymes present some practical disadvantages[11] such as a low operational stability, sensitivity of catalytic activity to environmental conditions, substrate specificity and high costs in preparation and purification. Hence the interest in developing new bioinspired systems, called artificial enzymes,[12] which can provide new tools to better understand the principle mechanisms of enzyme catalysis and then mimic the *modus operandi* of natural enzymes, in terms of efficiency and selectivity, without the drawbacks above mentioned[13].

There are two approaches in the design of artificial enzymes: the conventional route, consisting in replicating the enzyme active site, is proved not being successful because it is impossible to achieve nature's complexity on a synthetic level. The second route is “imitating” or mimicking the characteristic properties of enzymes, such as substrate recognition, stabilization of the transition state and absence of product inhibition, into a new system without replicating the structure of the enzyme’s active site itself.

It is accepted that a suitable microenvironment plays a crucial role when an enzymatic reaction is carried out: the substrates, hosted in the enzyme’s pocket, not only are forced to be close to each other and isolated from the surroundings (i.e solvent molecules), thus leading to an increase of the reactivity, but the inclusion into a restricted space can also lead the reagent

---

[9] D. E. Koshland Jr., *Proc. Natl. Acad. Sci. U. S. A*., **1958**, *44*, 98.
[10] a) L. Pauling, *Chem. And Eng. News*, **1946**, *10*, 1375; b) L. Pauling, *Nature*, **1948**, *161*, 707.
[11] Y. Yin, Z. Dong, Q. Luo, J. Liu, *Prog. Polym. Sci*., **2012**, *37*, 1476.
[12] a) J. A. Kirby, *Angew. Chem. Int. Ed*., **1996**, *35*, 707; b) E. Kuah, S. Toh, J. Yee, Q. Ma, Z. Gao, *Chem. Eur. J.*, **2016**, *22*, 8404.
[13] J. A. Kirby, F. Hollfelder, *From Enzyme Models to Model Enzymes*, RSC Publishing, **2009**.

molecules to react each other with specific geometric constraints, leading to reaction products with a certain regio- and stereoselectivity[14]. So, a fundamental step in order to create an efficient artificial enzyme is the design of a supramolecular systems (host) able to confine the substrates. Today, supramolecular chemistry offers many synthetic cavity-containing macrocycles which have found applications as supramolecular catalysts, including cyclodextrins[15], cucurbiturilis[16], cavitands[17] and calix[4]arenes[18]. Thanks to the presence of a cavity, they are capable to isolate the chemical reactants from the surrounding medium and thanks to the local higher concentration and orientation effect, they can promote a reaction with a specific path. However, due to the small dimension of the cavity and the difficulty in obtaining larger receptors, in the nineties, several research groups have started to study the catalytic application of new supramolecular hosts with bigger inner cavity as the nanocapsules[19], which from now on will be the main topic of the introduction.

---

[14] S. Tehila, J. W. Koblenz, J. N. H. Reek, *Chem. Soc. Rev.,* **2008**, *37*, 62.

[15] a) E. Iglesias, *J. Am. Chem. Soc.* **1998**, *120*, 13057; b) J. Báscuas, L. García-Río, J. R. Leis, *Org. Biomol. Chem*., **2004**, *2*, 1186; c) N. Basilio, L. García-Río, J. A. Moreira, M. Pessego, *J. Org. Chem.,* **2010**, *75*, 848; d) R. Breslow; D. S. Dong, *Chem. Rev*., **1998**, *98*, 1997.

[16] a) J. Lagona, P. Mukhopadhyay, S. Chakrabarti, L. Isaacs, *Angew. Chem., Int. Ed.* **2005**, *44*, 4844; b) W. M. Nau, M. Florea, K. I. Assaf, *Isr. J. Chem.,* **2011**, *51*, 559; c) B. C. Pemberton, R. Raghunathan, S. Volla, J. Sivaguru, *Chem. Eur. J*., **2012**, *18*, 12178.

[17] a) A. Gissot J. Rebek Jr., *J. Am. Chem. Soc*. **2004**, *126*, 7424; b) R. J. Hooley, J. Rebek Jr., *J. Am. Chem. Soc*., **2005**, *127*, 11904; c) R. J. Hooley, J. Rebek Jr., *Org. Biomol. Chem*. **2007**, *5*, 3631; d) K. E. Djernes, O. Moshe, M. Mettry, D. D. Richards, R. J. Hooley, *Org. Lett*., **2012**, *14*, 788.

[18] a) A. Casnati, M. Fabbi, N. Pelizzi, A. Pochini, F. Sansone, R. Ungaro, E. Di Modugno, G. Tarzia, *Bioorg. Med. Chem. Lett*., **1996**, *6*, 2699; b) P. Molenveld, J. F. J. Engbersen, D. N. Reinhoudt, *Chem. Soc. Rev.,* **2000**, *29*, 75; c) Y. Molard, C. Bureau, H. P. Lopez, R. Lamartine, J. B. R. de Vains, *Tetrahedron Lett*., **1999**, *40*, 6383.

[19] L. Catti, Q. Zhang, K. Tiefenbacher, *Chem. Eur. J.,* **2016**, 22, 9060.

1.2 Self-assembled capsules as supramolecular catalyst

Molecular capsules are a special class of host molecules with a complex three-dimensional structure which delimitates an internal space, *i.e.* the microenvironment to accommodate guests. They are divided into two classes: capsules based on covalent interactions[20] and those based on non-covalent interactions, called also self-assembled or supramolecular capsules[21]. The latter present several advantages over their covalent counterparts: in the self-assembled capsule the guest exchange in-and-out is often easier compared to their covalent counterparts[22] since this can occur via partial dissociation of the capsule. Additionally, the construction of noncovalent capsule does not require the tedious multistep synthesis, which is mandatory for the formation of covalent ones.

The self-assembled capsules are composed of two or more building blocks able to self-assemble in solution sealed together by multiple secondary interactions such as hydrogen bonds or metal-ligand interactions. However, the driving force for the self-assembly of stable capsule is the complementarity in terms of size, shape and binding site of the building blocks. In fact, poor complementarity will destabilize the forming complex, while high complementary leads to a stable capsule. Additionally, the reversible and directional nature of these interactions makes possible the self-control and self-correction, leading to the formation of a thermodynamically stable capsule, fig. 2.

---

[20] a) J. Canceill, M. Cesario, A. Collet, C. Pascard, J. *Chem. Soc. Chem. Comm*., **1985**, *6*, 361; b) D. J. Cram, S. Karbach, Y.H. Kim, L. Baczynskyj, G.W. Kalleymeyn, *J. Am. Chem. Soc*., **1985**, *107*, 2575; c) A. Asadi, D. Ajami, J. Rebek Jr., *Chem. Sci.*, **2013**, *4*, 12125.

[21] T.S. Koblenz, J. Wassenaar, J.N.H. Reek, *Chem. Soc. Rev*., **2008**, *37*, 247.

[22] a) M.E. Tanner, C. B. Knobler, D. J. Cram, *J. Am. Chem. Soc.,* **1990**, *112*, 1659; b) J. C. Sherman, *Tetrahedron*, **1995**, *51*, 3395.

Even if both interactions enjoy facile reversibility and reliable directionality, hydrogen bonds offer greater plasticity and faster equilibration[23], while metal-ligand bonds typically offer greater strength and more rigidity.

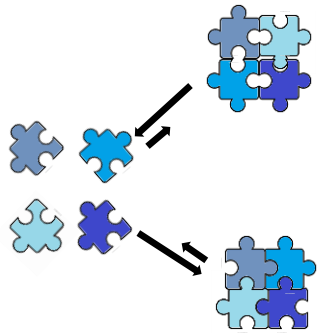

Figure 2. Self-correction in the self-assembly of a stable supramolecular capsule.

The key features of the self-assembled capsules such as the selective guest recognition and their reversible encapsulation, which depend on size, shape and complementarity between the guest and the cavity of the capsule, make them useful tools for catalysis. For these reasons, the self-assembled capsules have been widely applied as nanoreactors[24] for several reactions. Additionally, the use of self-assembled capsules in catalysis gives the opportunity to get more insight into reactivity of the molecules in a well-defined nanospace.

[23] P. M. Pihko, *Hydrogen Bonding in Organic Synthesis*, Wiley-VCH, Weinheim, **2009.**
[24] M. Yoshizawa, J. K. Klosterman, M. Fujita, *Angew. Chem. Int. Ed.*, **2009**, *48*, 3418.

1.3 Self-assembled capsules based on metal-ligand interactions

The self-assembly of synthetic building blocks through metal-ligand interactions can result in a well-defined cage-like structure[25]. Unlike H-bonded capsule, the guest exchange occurs by expansion of the apertures of the capsule[26]. Raymond and co-workers have developed a chiral tetrahedral $[Ga_4L_6]^{12-}$ complex, **CA**, with an octahedral coordination geometry, where the ligand is a 1,5-bis(2,3dihydroxybenzamido)naphthalene unit[27], fig. 3.

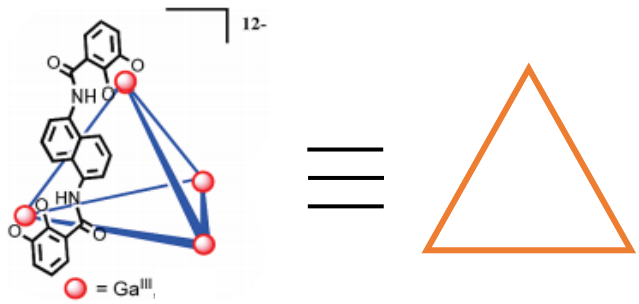

Figure 3. Tetrahedral M_4L_6 coordination cage **CA.**

The metal ions are located at the corners of a tetrahedron and the ligand spans the edge of the tetrahedron. Since each metal ion is coordinated by three bidentate moieties that belong to three different ligands, they are chiral (Δ or Λ).

The negative charge of the cage **CA** makes it soluble in polar solvent and consequently, in combination with the presence of a hydrophobic cavity of

[25] M. J. Wiester, P. A. Ulmann, C.A. Mirkin, *Angew. Chem. Int. Ed.,* **2011**, *50*, 114.
[26] M. D. Pluth, K. N. Raymond, *Chem. Soc. Rev.*, **2007**, *36*, 161.
[27] D. Fiedler, D. H. Leung, R. G. Bergman, K. N. Raymond, *Acc. Chem. Res.*, **2005**, *38*, 351.

300-500 Å^3, **CA** proved to be a good host for several species in water, such as tropylium cation[28], phosphonium species[29] and metal complexes[30]. Additionally, the cage **CA** shows interesting catalytic ability: it promotes Aza-Cope rearrangements[31], allylic alcohols isomerization[32] and Nazarov cyclization[33]. In the latter case, the self-assembled host **CA** promotes the cyclization of pentadienol **1** selectively into cyclopentadiene **2**. However, the reaction is affected by product inhibition: **CA** binds more strongly **2** than the reagent **1**, hampering the repeating of the catalytic cycle. The strategy used to overcome this problem is converting the product in a poor guest by the addition of maleimide **3** into the reaction mixture, which readily reacts with **2**, giving the Diels-Alder adduct **4**, for which **CA** does not show any significant affinity, fig. 4.

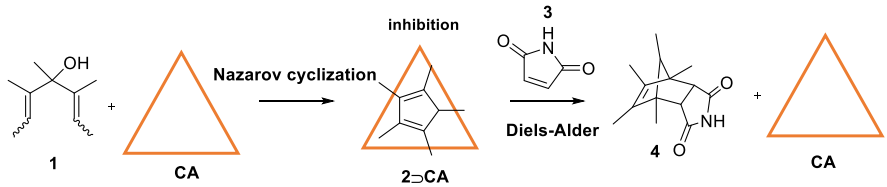

Figure 4. Schematic rapresentation of a Nazarov cyclization promoted by **A.**

Remarkably, the reaction in presence of **CA** shows a rate acceleration on the order of 10^6 and thus, its catalytic activity is comparable to those found in enzymatic systems: probably the local higher concentration and the

[28] J. L. Brumaghim, M. Michels, D. Pagliero, K. N. Raymond, *Eur. J. Org. Chem.*, **2004**, *24*, 5115.
[29] M. Ziegler, J. L. Brumaghim, K. N. Raymond, *Angew. Chem. Int. Ed.*, **2000**, *39*, 4119.
[30] D.Fiedler, R. G. Bergman, K. N. Raymond, *Angew. Chem. Int. Ed.*, **2006**, *45*, 745.
[31] C. J.Brown, G. R. Bergman, K. N. Raymond, *J. Am. Chem. Soc.*, **2009**, *131*, 17530.
[32] Leung, D. H.; G. R. Bergman, K. N., Raymond, *J. Am. Chem. Soc.*, **2007**, *129*, 2746.
[33] C. J Hastings, G. R. Bergman, K. N. Raymond, *J. Am. Chem. Soc.*, **2010**, *132*, 6938.

enhanced reactivity of the alcohol upon the encapsulation play a key role in a such reactivity activity.

Another interesting capsule based on metal-ligand coordination was reported by Fujita's group[34], the self-assembled octahedral $[M_6L_4]^{12+}$ cage **CB** composed of six *cis*-protected square planar Pd^{2+} complexes, e.g. $[Pd(en)]^{2+}$, and four 2,4,6-tris(4-pyridyl)-1,3,5-triazine as ligands, fig. 5. The metal complexes are situated at the corners of the octahedron and the ligands occupy the eight faces of the octahedron.

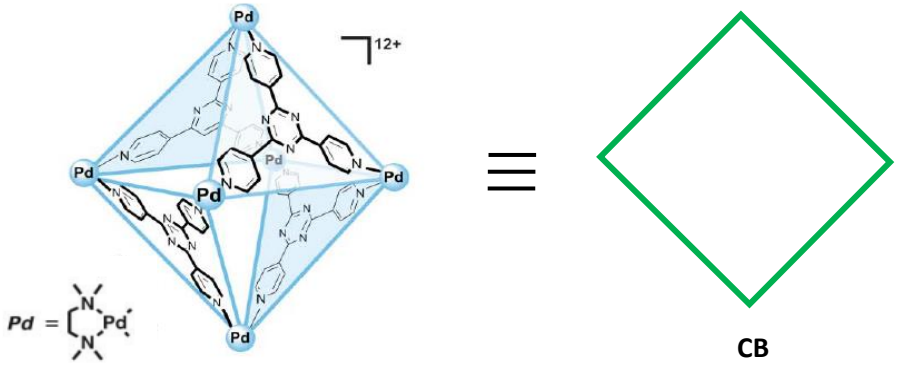

Figure 5. Tetrahedral M_6L_4 coordination cage **CB.**

The positive charge of the cage makes it soluble in water and thus, **CB** can strongly bind a variety of anionic and neutral guests such as adamantine and ferrocene in water[35]. In addition to the host/guest properties, this cage found wide applications as a nanoreactor for several reactions. Its performance in the Diels-alder reaction in water[36] between 9-

[34]M. Fujita, M. Tominaga, A. Hori, B. Therrien, *Acc. Chem. Res.*, **2005**, *38*, 371.
[35] A) M. Yoshizawa, J. K. Klosterman, M. Fujita, *Angew. Chem., Int. Ed.*, **2009**, *48*, 3418; b) M. Yoshizawa, M. Fujita, *Bull. Chem. Soc. Jpn.*, **2010**, *83*, 609.
[36] M. Yoshizawa, M. Tamura, M. Fujita, *Science*, **2006**, *312*, 251.

(hydroxymethyl)-anthracene **5** and *N*-cyclohexylmaleimide **6** is interesting, fig. 6. In presence of **CB** an unusual regioselectivity was observed: the *syn*-1,4-Diels-Alder adduct **7** was detected, while the reaction normally leads to the 9,10-Diels-Alder adduct **8**. The reaction selectivity can be explained by the forced relative orientation of the reagents **5** and **6** by the cavity of the nanocage **CB** upon encapsulation in the cavity of the nanocage **CB**.

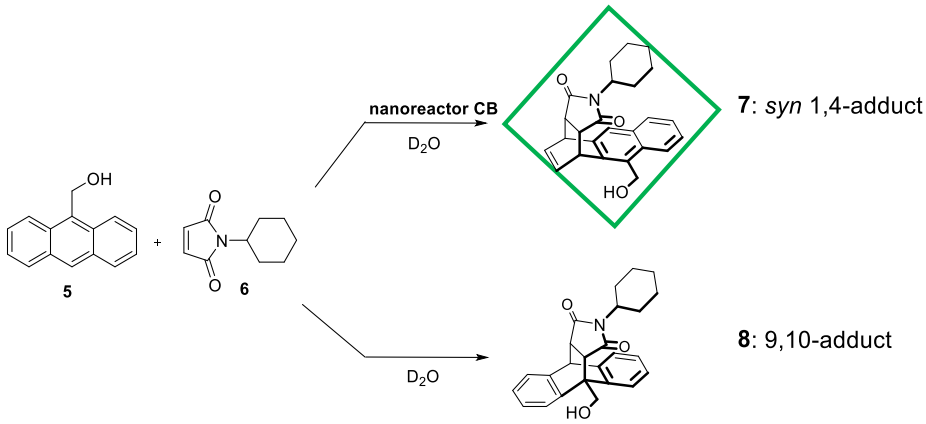

Figure 6. Schematic representation of Diels-Alder reaction with and without **CB.**

1.4 Self-assembled Capsules based on hydrogen bonds

Among several examples reported in the literature, the hydrogen-bonded self-assembled capsules have played a crucial role in biomimetic catalysis[37]. They started to become famous when in 1995 Rebek reported a self-assembled hydrogen-bonded system[38], the so-called "softball", in which two glycoluril units are sealed by 16 hydrogen bonds with an internal volume of 400 Å^3, fig. 7.

---

[37] a) F. Hof, S. L. Craig, C. Nuckolls, J. Rebek, Jr., *Angew. Chem. Int. Ed.,* **2002**, *41*, 1488; b) J. Rebek, Jr., *Hydrogen-Bonded Capsules: Molecular Behavior in Small Spaces*, World Scientific, Singapore, **2015**.
[38] a) C. Valdés, U. P. Spitz, S. W. Kubik, J. Rebek, Jr., *Angew. Chem. Int. Ed. Engl.*, **1995**, *34*, 1885; b) J. Kang, J. Santamaria, G. Hilmersson, J. Rebek, Jr. *J. Am. Chem. Soc.*, **1998**, *120*, 7389.

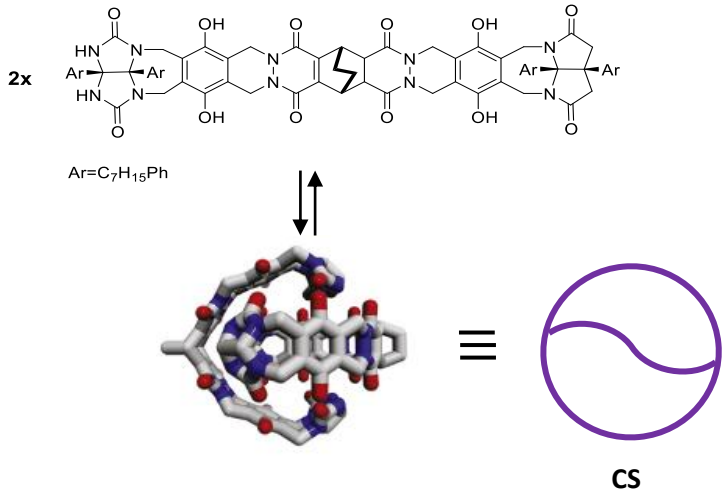

Figure 7. Rebek's softball **CS.**

In 1997, it was demonstrated that the softball **CS** promotes the Diels–Alder[39] reaction between *p*-benzoquinone **9** and cyclohexadiene **10**, fig. 8. Unfortunately, the reaction suffers from product inhibition, which can be overcome optimizing the size and shape of the reagent with the aim of forming a product with a low affinity for the capsule. Interestingly, when the cyclohexadiene **10** was replaced by 2,5-dimethylthiophene dioxide, the reaction rate was enhanced by the "softball" with a 75% yield after 4 days at 40°C, while only 17% yield was achieved in the absence of the nanoreactor **CS**.

[39] J. Kang, J. Rebek, *Nature*, **1997**, *385*, 50.

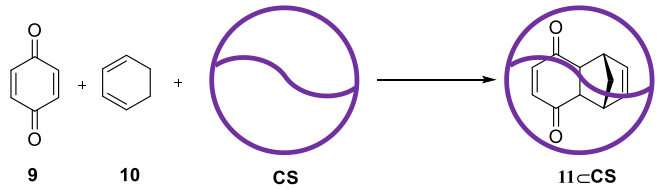

Figure 8. Schematic representation of a Diels-alder reaction promoted by the softball **CS.**

Successively, the same group has reported the cylindrical capsule **CD**[40] formed by the self-assembly of two resorcin[4]arene cavitands, sealed by 16 hydrogen bonds, with an internal volume of 425 Å^3.

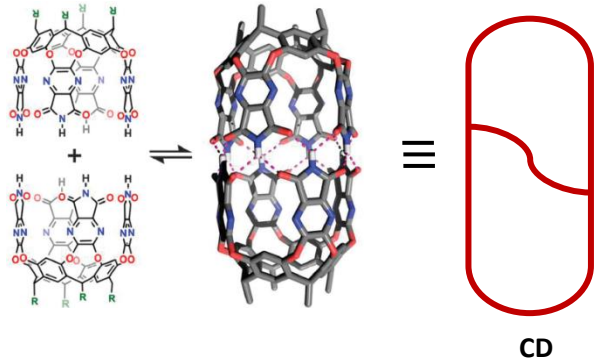

Figure 9. Rebek's cylindrical capsule **CD.**

This cylindrical capsule has been applied as a nanoreactor for the 1,3-dipolar cycloaddition between phenyl azide **12** and phenyl acetylene **13**. The two substrates can be simultaneously encapsulated in the cavity of the capsule and the cavity size forces the guest orientation edge-to-edge, giving

[40] J. Chen, J. Rebek, Jr., *Org. Lett.* **2002**, *4*, 327.

exclusively in 1,4 triazole **14,** in contrast to the free reactions that produces a 1:1 mixture of 1,4 -and 1,5 triazoles in low yield, fig. 10.

Additionally, the capsule **CD** is also substrate size selective: replacing the phenyl azide with larger azides as 1-naphtyl azide or 4-biphencyl azide no rate acceleration was observed.

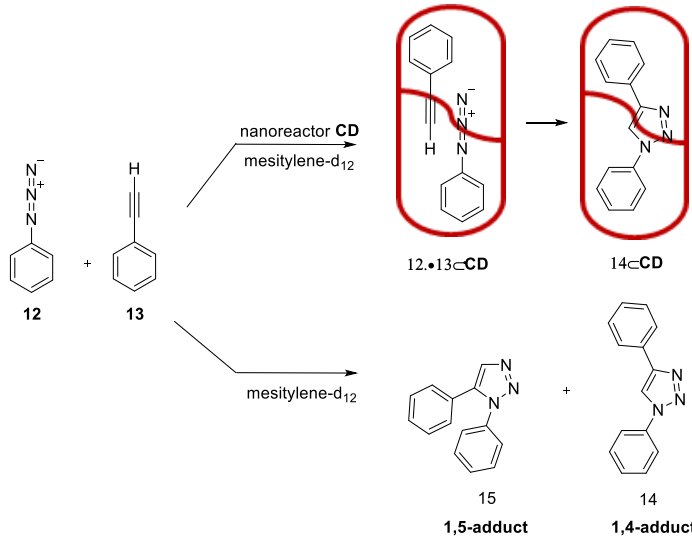

Figure 10. Schematic representation of 1,3-dipolar cycloaddition in presence and in absence of **CD.**

Recently, the attention has been focused on the employment of one of the largest known self-assembling capsules in organic solvents: the hexameric resorcin[4]arene capsule **CR_6**, reported for the first time by Atwood and MacGillivray[41].

[41] L. R. MacGillivray, J. L. Atwood, *Nature*, **1997**, *389*, 469.

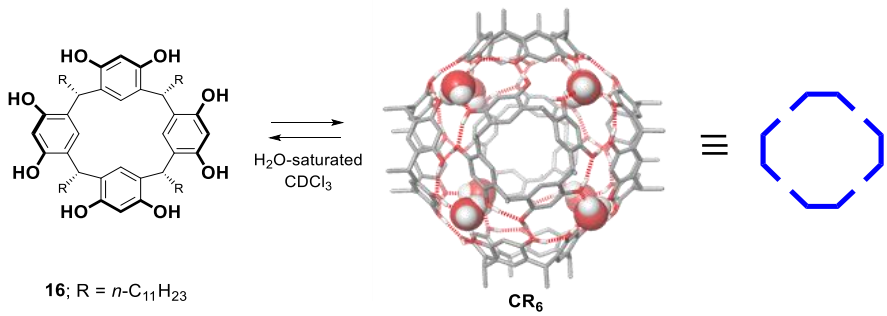

Figure 11. Self-assembly of six resorcin[4]arenes in the hexameric capsule **CR$_6$**.

Resorcin[4]arenes are synthetic organic macrocycles able to form a hemispherical structure. These macrocycles are synthesized easily in gram scale by condensation in acidic environment of resorcinol with an aldehyde[42]. Using long aldehydes, the solubility of the resorcin[4]arene in organic solvents is highly increased.

In 1997 MacGilliwray and Atwood demonstrated that in solid state the resorcin[4]arene forms a racemic mixture of pseudospherical hexamers sealed by 60 hydrogen bond. The X-ray structure of **CR$_6$** resembles a cube: at the corners are located eight water molecules, which develop three hydrogen bonds with the OH group of the three neighbouring resorcin[4]arene units, located on the side of the cube. Additionally, four of these bridging water molecules donate two hydrogen bonds (Fig. 12, H_2O drawn in blue), completing their hydrogen-bond-donating valence. The other four bridging water molecules, donating a single hydrogen bond (Fig. 12, green), present one hydrogen-bond-donating free valence. This pseudospherical aggregate has a cavity of 1375 Å^3.

[42] a) A. G. S. Hoegberg, *J. Am. Chem. Soc.*, **1980**, *102*, 6046; b) A. G. S. Hoegborg, *J. Org. Chem.*, **1980**, *45*, 4498.

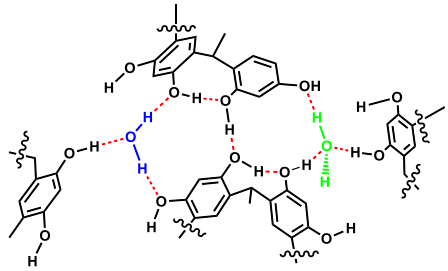

Figure 12. Chemical structure of the model representing a bridging water molecule fully H-bonded (in blue) and one with hydrogen-bond-donating free valence (in green).

Later, Cohen[43] and co-workers, thanks to NMR diffusion experiments, demonstrated that the C-undecyl-resorcin[4]arene self-assembles in wet apolar solvent, such as chloroform or benzene, in the same hexameric structure observed in the crystal state, with six to eight solvent molecules filling the cavity[44].

In the same years, Rebek's group demonstrated by NMR spectroscopy the encapsulation of quaternary ammonium salts thanks to the cation-π interactions with the internal electron rich surface of the capsule[45].

Furthermore, Tiefenbacher and co-workers reported the encapsulation of neutral guest as tertiary amines[46]. Briefly, the authors have carried out several encapsulation experiments of amines with different pK_a demonstrating that the driving force for their encapsulation is the protonation mediated by the hexamer, which acts as a Brønsted acid, with a pK_a value 5.5-6.0. The acidity of the capsule can be attributed to the anion

---

[43] L. Avram, Y. Cohen, *J. Am. Chem. Soc.*, **2002**, *124*, 15148.
[44] A. Shivanyuk, J. Rebek Jr., *J. Am. Chem. Soc.*, **2003**, *125*, 3432.
[45] a) A. Shivanyuk, J. Rebek Jr., *Proc. Natl. Acad. Sci. USA*, **2001**, *98*, 7662; b) E. S. Barrett, T. J. Dale, J. Rebek Jr., *J. Am. Chem. Soc.,* **2008**, *130,* 2344.
[46] Q. Zhang, K. Tiefenbacher, *J. Am. Chem. Soc.*, **2013**, *135*, 16213, b) J. M. Köster, K. Tiefenbacher, *Chem. Cat. Chem.*, **2018**, *10*, 2941.

stabilization thanks to the delocalization of the negative charge along the structure of the self-assembled capsule. Additionally, quantum mechanical (QM) calculations reported by Neri[47] and co-workers have estimated a pK_a of the four bridged water molecules with hydrogen-bond-donating free valence (green in Fig. 12) of about 2.5, whereas the mean pK_a value of all OH groups of **CR_6** is 6.1; which is in agreement with the experimental value. The hexamer can encapsulate also neutral species through H-bonding such as carboxylic acid[48], aminoacids[49] and alcohols[50]. In the latter case, surprisingly, in presence of 2-ethylhexanol, it was observed that six of eight water molecules at the corners of the cube are replaced by alcohol molecules leading to a hexameric structure sealed by 50 hydrogen bonding interactions[51].

In the last decade, the hexameric resorcin[4]arene capsule was widely used as an artificial enzyme; its use in supramolecular catalysis is encouraged by the simple synthesis of the monomer combined with the host-guest properties of the hexamer. In fact, several examples have been reported in which **CR_6** works as nanoreactor: the large cavity allows the co-encapsulation of both catalyst and substrates. In these cases, the nanoreactor CR_6 is able to promote the reaction thanks to the synergic interplay of both confinement and local overconcentration effect of the catalyst and substrates[52].

---

[47] P. La Manna, C. Talotta, G. Floresta, M. De Rosa, A. Soriente, A. Rescifina, C. Gaeta, P. Neri, *Angew. Chem. Int. Ed.*, **2018**, *57*, 5423

[48] T. E. Salem, I. Baruch, L.; Avram, Y.; Cohen, L. C. Palmer, J. Rebek, Jr., *Proc. Natl. Acad. Sci. USA*, **2006**, *103*, 12296.

[49] a) Y. Aoyama, Y. Tanaka, Y. H. Toi, H. Ogoshi, *J. Am. Chem. Soc.*, **1988**, *110*, 634; b) Y. Aoyama, Y. Nonaka, Y. Tanaka, Y. H. Toi, H. Ogoshi, *J. Chem. Soc., Perkin. Trans.*, **1989**, *2*, *1025.*

[50] S. Slovak, Y.Cohen, *Chem. Eur. J.*, **2012**, *18*, 8515.

[51] O. Ugono, K. T. Holman, *Chem. Commun.*, **2006**, 2144.

[52] G. Borsato, A. Scarso, *Organic Nanoreactors: From Molecular to Supramolecular Organic Compound*, Academic Press, London, **2016**.

Interestingly, the hexamer can act as catalyst itself by the stabilization of intermediates and transition states. In many examples, an unusual reaction outcome can be observed because of the nanoconfinement.

1.4.1 Hexameric resorcinarene capsule as supramolecular nanoreactor

Several reports have been presented in the literature in which the hexameric capsule acts as a container for substrates and catalyst[53].

A remarkable example, reported by Tiefenbacher and co-workers, in which **CR_6** works as a nanoreactor is the iminium reduction of unsaturated aldehydes[54]. The authors showed that, if L-proline, α,β-unsaturated aldehyde **17** and Hantzsch ester **18**, as reductive agent, were mixed in water-saturated $CDCl_3$ at 30°C in the presence of **CR_6**, the product **19** was obtained in 93% yield with a good enantioselectivity in favour of the (*S*) enantiomer (74% ee). Carrying out the reaction with L-proline in absence of **CR_6** capsule, **19** was obtained in low yield and only 9% ee (*S*) fig. 13. In order to justify the enantioselective modulation, the authors proposed a model in which, upon encapsulation of the substrates and iminium formation, this was bound to the inner wall of the capsule cavity by cation-π interactions with the less hindered face. Consequently, the attack of the nucleophile occurred from the *syn*-face with respect to the bulky Y group. Naturally, if the reaction was performed in bulk solution the attack from the *syn*-face was not favored. The example reported by Tiefenbacher shows the

---

[53]a) G. La Sorella, L. Sperni, P. Ballester, G. Strukul, A. Scarso, *Catal. Sci. Technol.*, **2016**, *6*, 6031; b) G. La Sorella, L. Sperni, P. Ballester, G. Strukul, A. Scarso, *Adv. Synth. Catal.*, **2016**, *358*, 3443.

[54] a) T. M. Bräuer, Q. Zhang, K. Tiefenbacher, *Angew. Chem. Int. Ed.*, ***2016***, *55*, 7698; b) T. M. Bräuer, Q. Zhang, K. Tiefenbacher, *J. Am. Chem. Soc.*, **2017**, *139*, 17500

ability of **CR$_6$** to exert a control not only on the reaction efficiency, but also on the enantioselectivity.

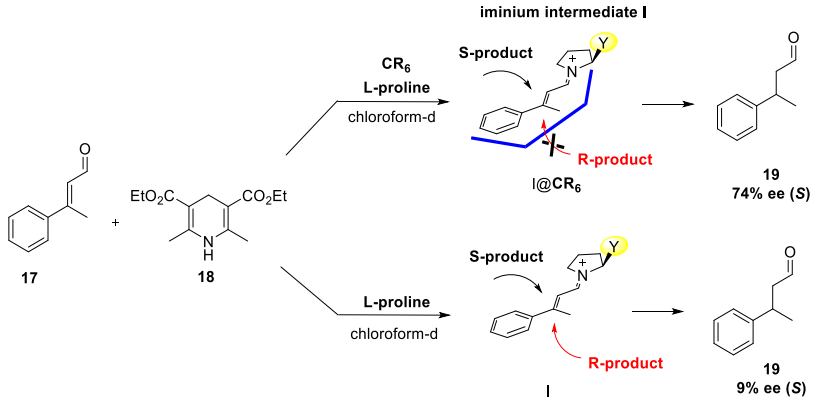

Figure 13. Schematic representation of 1,3-dipolar cycloaddition in presence and in absence of **CR$_6$**.

Another interesting application of the hexamer as nanoreactor is provided by Neri and co-workers[55]. They have studied the feasibility of a 1,3-dipolar cycloaddition between nitrones and α,β-unsaturated aldehydes inside the nanoreactor **CR$_6$**.

The cycloaddition between nitrone **20** and (E)- crotonaldehyde **21** can in principle lead to 4- and 5-formyl regioisomers, **22** and **23**, as two *endo*- and *exo*-diastereomers, in two possible enantiomeric forms, fig. 14.

[55] P. La Manna, M. De Rosa, C. Talotta, C. Gaeta, A. Soriente, G. Floresta, A. Rescifina, P. Neri, *Org. Chem. Front.*, **2018**, *5*, 827.

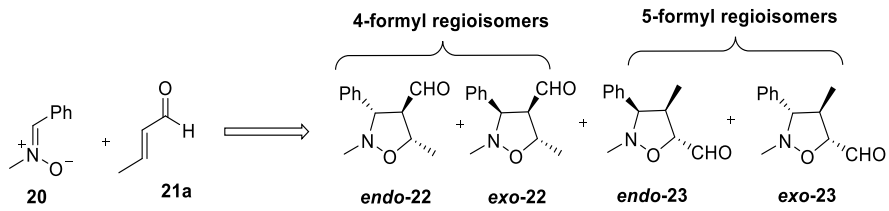

Figure 14 Possible regio- and stereoisomers of the 1,3-dipolar cycloaddition of nitrone **20** with (E)-crotonaldehyde **21a**.

When the reaction was carried out in presence of **CR_6** the 4-formyl regioisomer **22** was preferentially formed in 90% yield in a high regioisomeric ratio of 98/2 with respect to isomer **23**. Additionally, a high *endo*-**22**/*exo*-**23** diasteroisomeric ratio of 84/14 was observed and an ee value of 95% was measured in favour of the 4*R* enantiomer of *endo*-**22**. Interestingly, the use of L-proline without the nanoreactor was ineffective: no product was detected. According to the QM calculation, fig. 15, the key step in this reaction is the iminium intermediate formation inside the cavity of the capsule, catalyzed by the intrinsic acidity of **CR_6**. Therefore, QM calculations also indicated that the iminium was bounded to the internal cavity of CR_6 by H-bond interaction between the carboxylic moiety of the L-proline and a bridging water molecule, thus explaining the selectivity.

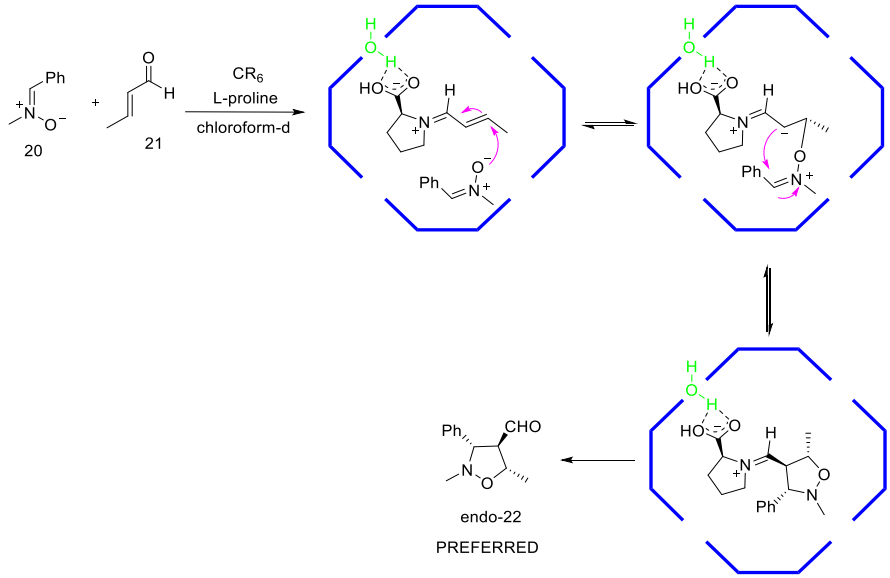

Figure 15. Proposed mechanism of 1,3-DC between nitrone **20** and (E)-crotonaldehyde **21** in presence of **CR6**.

So, the conclusion was that the hexamer behaved like an artificial enzymatic system able to control simultaneously the regiochemistry and the stereochemistry (both, diastereo- and enantioselectivity) of the 1,3-dipolar cycloaddition.

One the most fascinating aspect of natural enzymes is their ability to select a substrate from a complex mixture of potential candidates[56]. An example of this substrate selectivity was reported by Scarso and co-workers in the synthesis of amides, starting from a mixture of linear carboxylic acids and primary amines, using EDC•HCl **27** as condensing agent[57], fig. 16. Interestingly, when the reaction was carried out in presence of **CR6**, only shorter amides were formed, while in the absence of the capsule, a mixture

[56] A. C. H. Jans, A. Gomez-Suarez, S. P. Nolan, J. N. H. Reek, *Chem. Eur. J.*, **2016**, *22*, 14836.
[57] S. Giust, G. La Sorella, L. Sperni, G. Strukul, A. Scarso, *Chem. Commun.*, **2015**, *51*, 1658.

of comparable amounts of all the possible amides is detected, fig. 16. These results suggested that, **CR$_6$** can modulate the reaction outcome by substrate selectivity, which in this case is tuned by steric effects.

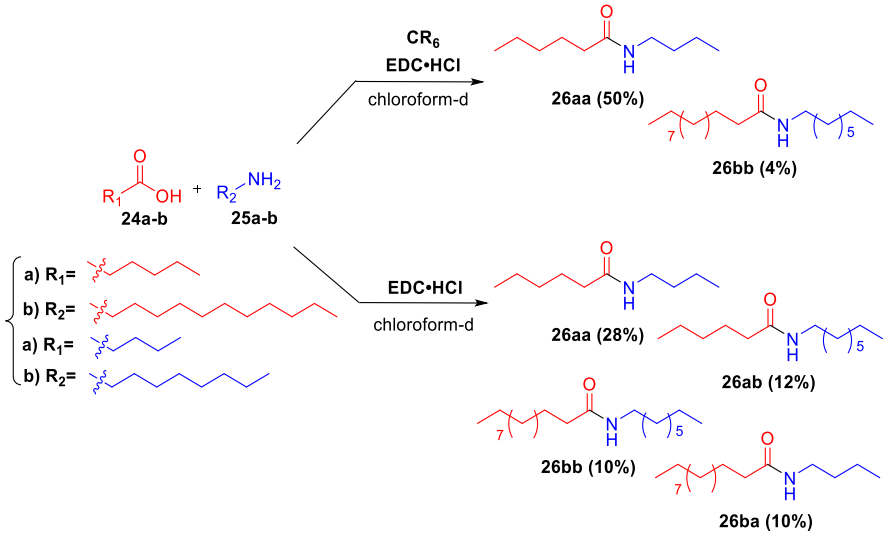

Figure 16. Schematic representation of competition experiment between carboxylic acids **24a-b** and amines **25a-b** in presence and in absence of **CR$_6$**.

Another notable examples, reported by the same group, in which **CR$_6$** exploited its function as nanoreactor concern the sulfoxidation of thioethers[58] and the hydration of aromatic alkyne[59]. In the latter case, the combination of catalytic amount of **CR$_6$** and HBF_4 catalyzed the hydration of aromatic alkynes **28a-c** to their corresponding methyl ketones **29a-c**, fig. 17 Additionally, it was demonstrated the sensitivity of the reaction to the size of the substrates: **29a**, which derives from the smaller alkyne **28a**, was obtained with a 98% yield, whereas **28b** and **28c**, because of the sterically demanding size of the starting alkyne, were obtained in lower yields.

---

[58] G. La Sorella, L. Sperni, P. Ballester, G. Strukul, A. Scarso, *Adv. Synth. Catal.*, **2016**, *358*, 3443.
[59] G. La Sorella, L. Sperni, P. Ballester, G. Strukul, A. Scarso, *Catal. Sci. Technol.*, **2016**, *6*, 6031.

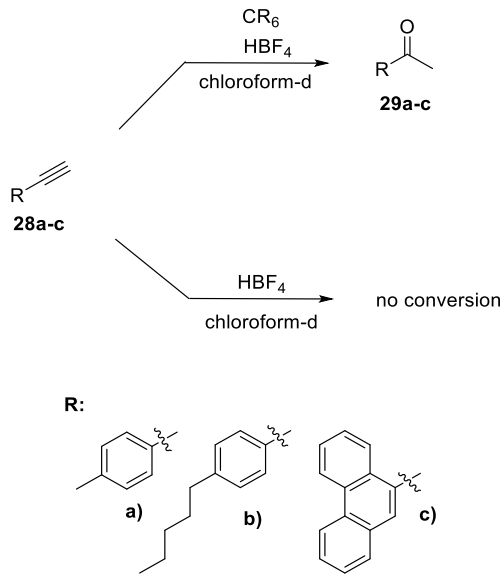

Figure 17. Schematic representation of hydration of aromatic alkynes in presence and in absence of **CR6**.

1.4.2 Hexameric resorcinarene capsule as catalyst

In literature, examples of application of the resorcin[4]arene capsule as a real organocatalyst are the majority[60]. This is a consequence of the several properties of the hexamer:

- Ability to stabilize cationic intermediates through cation-π interactions;
- Mild Brønsted acidity: the hexamer has a pK_a= 5.5-6.0.
- Ability to act as hydrogen-bonding catalyst thanks to the bridging water molecules with a donating free valence.

[60] a) G. La Sorella, L. Sperni, G. Strukul, A. Scarso, *Chem. Cat. Chem.*, **2015**, *7*, 291; b) L. Catti, K. Tiefenbacher, *Chem. Commun.*, **2015**, *51*, 892.

The first interesting example is reported by Tiefenbacher[61] and co-workers in which the combination of the weak acidity of the capsule and its ability to stabilize cationic intermediates and related transition states plays a crucial role in the tail-to-head cyclization (THT)[62] of linear terpene derivatives. They found that substrates like geraniol **40** and geranyl acetate **41** are activated inside the cavity of the capsule because of the presence of allylic moieties with leaving groups sensitive to acidic conditions, such as hydroxyl or acetate groups. These substrates according to the proposed biosynthesis of cyclic terpenes, fig. 18, can be converted into the intermediate allylic cation **31,** which, by intramolecular cyclization reaction, isomerization and reactions with nucleophiles, can be further converted into a wide variety of cyclic terpenes.

In nature there are specific enzymes, named terpene cyclases[63], able to promote this kind of reaction in a very selective way, starting from linear precursors bearing phosphate as leaving group. The key feature of the enzyme selection is based on the ability of the enzyme to isolate the substrate inside the pocket, stabilize the allylic carbocation and force the folding of the intermediate to get only certain compounds.

---

[61] Q. Zhang, K. Tiefenbacher, *Nat. Chem.*, **2015**, *7*, 197.
[62] S. V. Pronin, R. A. Shenvi, *Nature Chem.*, **2012**, *4*, 915.
[63] D. W. Christianson, *Chem. Rev.*, **2006**, *106*, 3412.

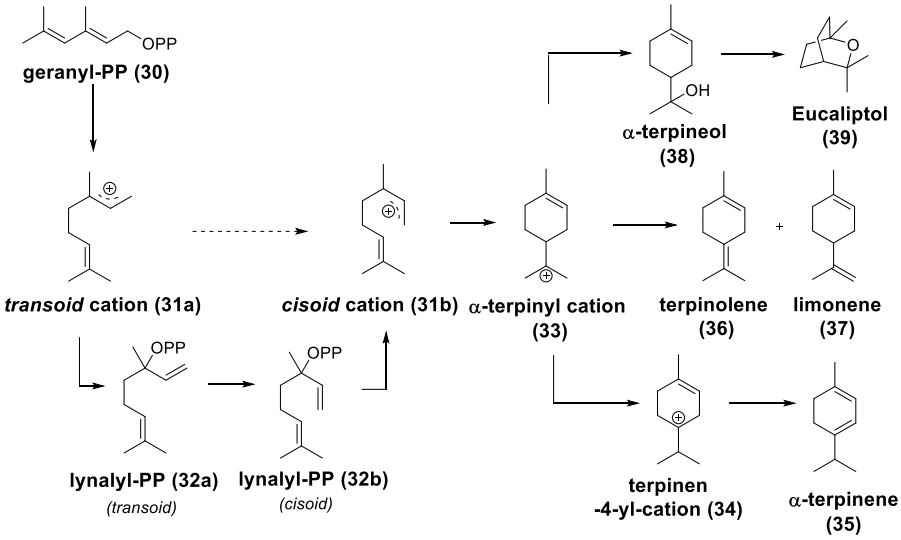

Figure 18. Proposed biosynthesis of cyclic terpene natural products.

The hexameric **CR$_6$** capsule was able to mimic the enzyme pocket of cyclase enzymes. In fact, when geraniol **40** was encapsulated inside **CR$_6$**, it was converted in 72 h into eucaliptol **39** and α-terpinene **35**. In detail, the composition of the mixture changed over the reaction time: after 10 h linalool **32** was the major product in the mixture, which is the result of the nucleophilic water attack to the allylic carbocation **31**, fig. 19. Later *α*-terpinene **35** and α-terpineol **38** started to form and at 30 h the mixture is composed by **32**, **35** and **38**. Finally linalool **32** and α-terpineol **38** were converted into eucaliptol **39** leading to final composition of the mixture. The formation of these cyclic terpenes from linear geraniol is an unprecedented result that underlines the product selectivity features possible using the resorcinarene capsule.

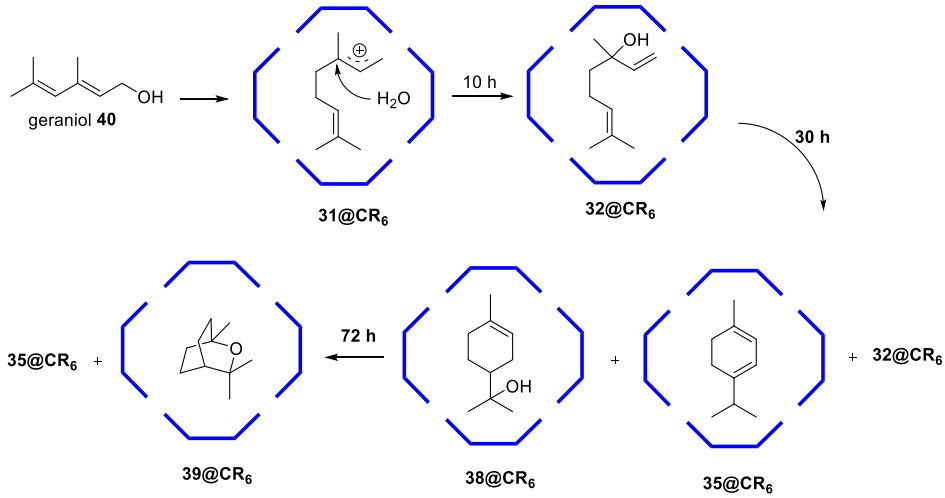

Figure 19. Schematic representation of THT reaction of geraniol **40** promoted by **CR6**.

Later[64], the same group reported that geranyl acetate **41** cyclized into α-terpinene **35** thanks to the combined action of capsule **CR6** and DCl (or HCl, in trace amounts). The authors suggested that the capsule can be described as an apoenzyme, while the corresponding holoenzyme, catalytically effective, was formed upon protonation by trace amounts of acid, fig. 20. Additionally, the use of geranyl acetate **41** limits the interceptions of cationic intermediates by the cleaved leaving group. In this case, it is possible to continue the propagation of cation charge leading selectively the α-terpinene **35**, which is an impressive result to obtain in solution: it is the first non-stop tail to head cyclization realized in solution using a supramolecular catalyst.

[64] Q. Zhang, L. Catti, J. Pleiss, K. Tiefenbacher, *J. Am. Chem. Soc.*, **2017**, *139*, 11482.

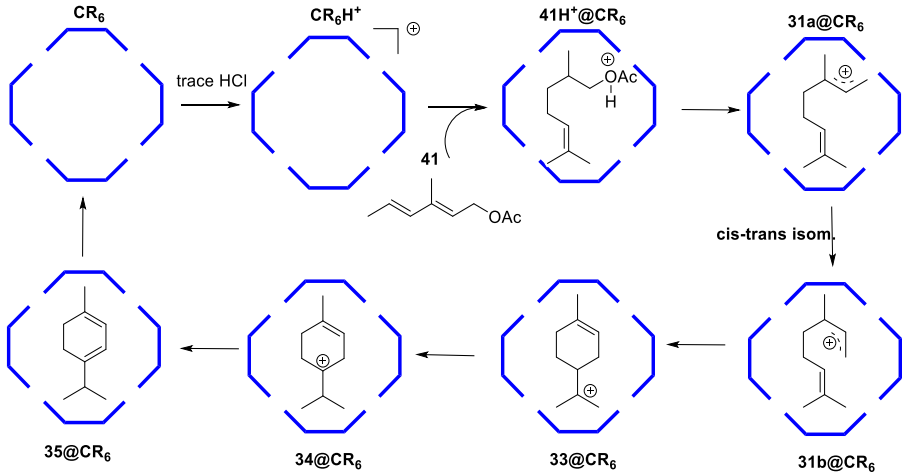

Figure 20. Proposed mechanism for the THT reaction of geranyl acetate **41** promoted by **CR$_6$**/HCl.

A deep investigation of the possible mechanism of action of the capsule led to the conclusion that a direct *transoid-cisoid* isomerization of the carbocation **31** should be possible and maybe is possible also in the natural cyclase enzymes, fig. 20.

The same group has demonstrated the ability of the capsule to promote the more changeling THT cyclization of sesquiterpenes[65]. In this case, the double bond's geometry of the linear precursors is the key in the product selectivity. In fact, when the linear sesquiterpene (2E,6Z)-farnesyl acetate **42** was cyclized in the presence of **CR$_6$**/HCl, the main product is the δ-selinene **44** (18%), while starting from (2Z,6E)-**42** or (2Z,6Z)-**42** only a trace amount of δ-selinene was detected, but mainly **46**, **47, 48** and **49**. These results suggested that the 1,10-cyclization, which is the key step for the synthesis of δ-selinene, occurs only for the E conformation of the double

[65] Q. Zhang, K. Tiefenbacher, *Angew. Chem. Int. Ed.*, **2019**, *58*, 12688.

bond between C_2 and C_3 of the precursor, while an alternative pathway, the 1,6-cyclization, prevails when the precursors present the Z conformation of the double bond between C_2 and C_3, fig. 21.

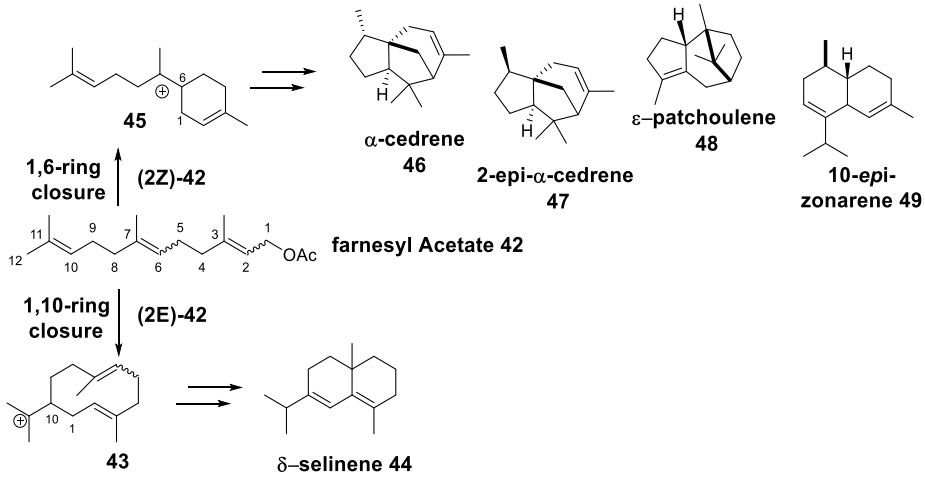

Figure 21. Proposed mechanism for the THT reaction of farnesyl acetate **42** promoted by **CR_6**/HCl.

Another interesting example of CR_6 as catalyst was reported by Strukul and co-workers for the hydration reaction of isonitriles into *N*-formylamides[66]: heating at 60°C the isonitrile **50** in the presence of the capsule **CR_6**, the complete conversion of the reagent into *N*-formylamide **51** was observed, meanwhile in the absence of the capsule no product was detected, fig. 22.

[66] G. Bianchini, G. L. Sorella, N. Canever, A. Scarso, G. Strukul, *Chem.Commun.*, **2013**, *49*, 5322.

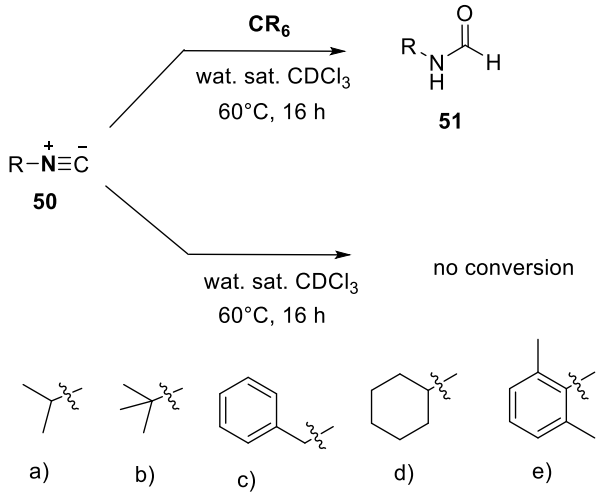

Figure 22. Schematic representation of the hydration of isonitrile with and without **CR6**.

The authors suggested that the catalytic activity of the capsule is based on its mild Brønsted acidity, which favours the protonation of the isonitrile unit. Additionally, the catalytic activity of the capsule was affected by the size and shape properties of the substrate: for **50a**, **50c**, **50d**, quantitative hydrolysis was observed within 18 h in the presence of **CR6**, whereas lower conversions were detected for substrates **51b** and **51e**.

Next, the same group has demonstrated the ability of **CR6** in the promotion of a metal-free isomerization of epoxide to the corresponding carbonyl compound[67].

[67] T. Caneva, L. Sperni, G. Strukul, A. Scarso, *RSC Adv.*, **2016**, *6*, 83505.

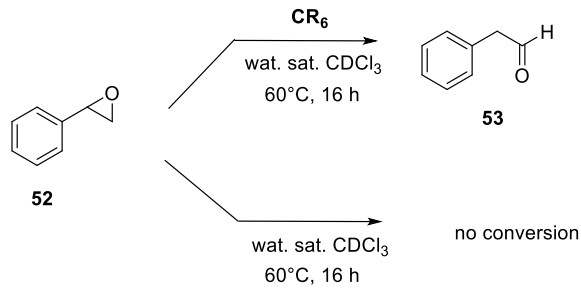

Figure 23. Schematic representation of epoxide isomerization with and without **CR6**.

The presence of the hexamer leads to the formation of the carbonyl compound with a quantitative yield after 18h at 60°C, while no hint of product was detected in absence of **CR6**, fig. 23. It is known that the isomerization of epoxides to carbonyl compounds is an acid-catalyzed reaction and for this reason, control experiments were carried out replacing the capsule with acetic acid as a catalyst and no formation of **53** was observed. This clearly indicates that both the Brønsted acidity and the cavity effect of **CR6** work in a synergistic fashion.

Recently, Neri and co-workers, have disclosed the ability of **CR6** in the promotion of a Friedel-Craft reaction of various arenes and heteroarenes with benzyl chloride by H-bond catalysis[47]. Interestingly, when the *N*-methylpyrrole **54a** was used as substrate, the reaction in presence of the capsule led the formation of the β–adduct in high yield (80%) and regioselectivity, while in absence of **CR6** no conversion was observed, fig. 24.

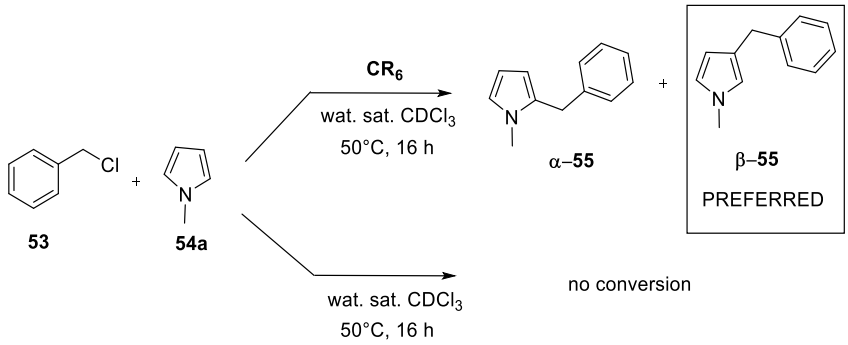

Figure 24. Schematic representation of Friedel-Craft reaction with and without **CR₆**

The ability of **CR₆** to promote the reaction was explained by QM calculations. They have indicated that benzyl chloride **53** is activated inside the cavity by an H-bond interaction with a bridged water molecule, making the C-Cl bond susceptible to the nucleophilic attack.

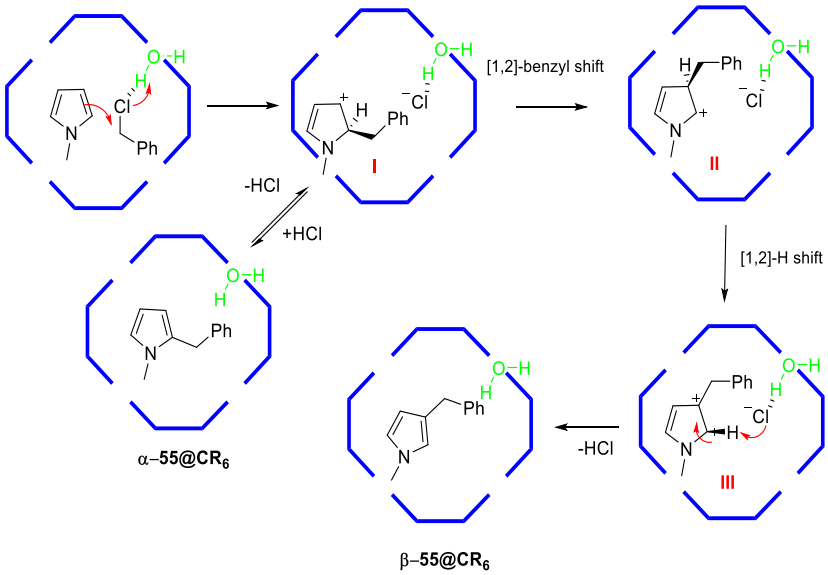

Figure 25. Proposed mechanism for the Friedel-Craft reaction promoted by **CR₆**.

Additionally, on the basis of QM calculations the authors rationalized the unusual regioselectivity output with the mechanism depicted in fig. 25. In detail, after the encapsulation of both reagents and the polarization of the C-Cl bond by H-bond interaction, the α-attack of *N*-methylpyrrole **54a** lead to the cationic intermediate I. At this point, this intermediate I can be directly converted into the α-regioisomer, or it can evolve into the intermediate II by [1,2]-benzyl shift, which by loss of the proton is further converted in the β-adduct. The driving force of the regioselectivity is related to the stability of the encapsulated products: β-**55**@CR_6 is thermodynamically more stable than α-**55**@**CR_6**. For this reason, over the time, the reaction affords the thermodynamic product.

Summarizing, the calculations confirm the catalytically relevant role of the capsule and particularly, the calculations highlight that the capsule not only affected the reaction efficiency, but also the reaction outcome favouring an uncommon regioselectivity.

Chapter 2. Aim and Outlines of the thesis

Considering the many efforts that have been done to developed artificial enzymes for organic reactions, the main goal of this research project is to further investigate the ability as biomimetic catalyst of the self-assembled resorcin[4]arene capsule **CR_6**. At this regard, the study described in Chapter 2 deals with the organocatalytic application of **CR_6** in the construction of relevant *N*-heterocycle containing building blocks in mild conditions.

Next, since the phenomena of adaptation represent the key reason of living systems' evolution, the study reported in the chapter 3 is focused on the ability of a dynamic covalent library to adapt to the presence of **CR_6**, considered as an external stimulus capable of driving the equilibrium in one or other direction.

Chapter 4 concerns the capability of **CR_6** to generate in situ a carbocation such as tritylium cation, a useful Lewis acid catalyst for different types of reactions. The capsule promotes the Diels-Alder reaction inside the nanoconfined cavity.

At the end of the thesis, an Appendix describes the research project carried out at the Institut Català d'Investigació Química (ICIQ), under the supervision of Prof. Pablo Ballester, which deals with the synthesis of a new *strapped* calix[4]pyrrole.

In Figure 26 the outlines of the next chapters are summarized.

Chapter 3

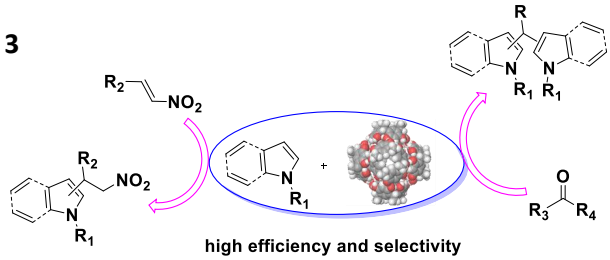

Chapter 4

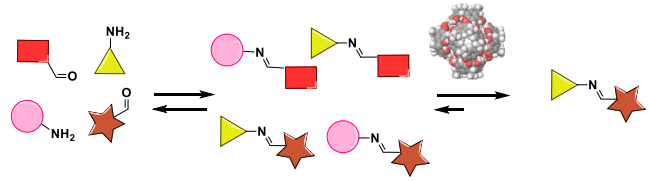

Chapter 5

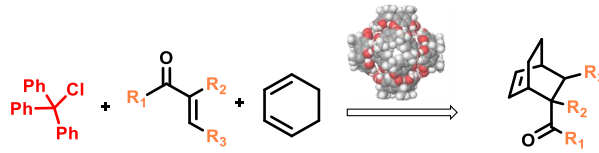

Appendix

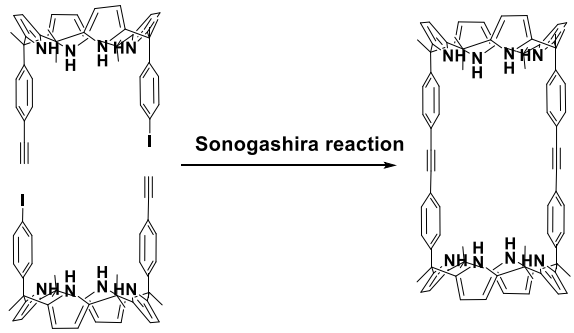

Figure 26. Outlines of the present research Ph. D project.

Chapter 3. Hexameric resorcinarene capsule as H-bonding catalyst in the construction of heterocyclic derivatives

3.1 Introduction

Aromatic *N*-heterocycles, and in particular pyrrole and indole containing ones, are ubiquitous important units in nature: they possess physiological and pharmacological properties and are constituents of many biologically important molecules[68].

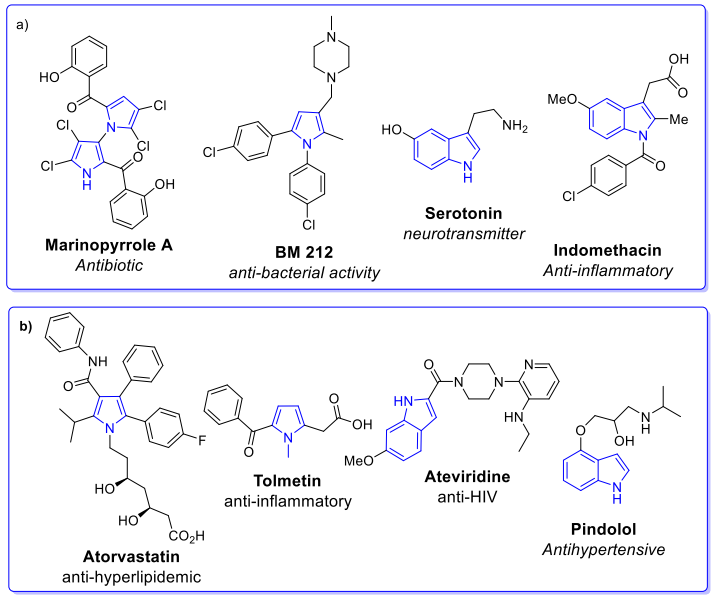

Figure 27. Examples of a) natural and b) pharmaceutical products containing pyrrole/indole ring.

---

[68]a) A. P. Kozikowski, Comprehensive Heterocyclic Chemistry; Katritzky, A. R., Rees, C. W., Eds.; Pergamon: New York, **1984**; b) H. Fan, J. Peng, M. T. Hamann, J.-F. Hu, *Chem. Rev.*, **2008**, *108*, 264; c) J. Kochanowska-Karamyan, M. T. Hamann, *Chem. Rev.*, **2010**, *110*, 4489; d) J. A. Joule, K. Mills, *Heterocyclic Chemistry* (5th ed.), Wiley, Chichester (U.K.), **2010**; e) A. Ramirez, S. Garcia-Rubio, *Curr. Med. Chem.*, **2003**, *10*, 1891.

Therefore, development of synthetic methods of indole and pyrrole derivatives have been widely studied. They are electron-rich heteroaromatic compounds and hence their predominant chemical reactivity is its attack by electrophiles and subsequent substitution reaction[69].

The electrophilic substitution of aromatic molecules proceeds via a two - step sequence: at first, the electrophile E^+ is added to the heterocycle providing a positively charged intermediate, the Wheland intermediate (usually the rate determining step), then the elimination of H^+ leads to the final product.

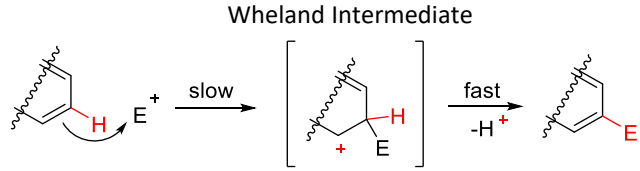

Figura 28. Electrophilic substitution of aromatic compounds.

Functionalization of heteroaromatic systems in a regioselective way has been always a changeling task: the insertion of a desired substituent at a specific position is in fact stymied by the intrinsic reactivity of the ring. In fact, the introduction and removal of functional groups (protection/activation) is usually required in order to achieve satisfactory levels of chemo- as well as regio-selectivity[70].

---

[69] a) V. Bhardwaj, D. Gumber, V. Abbot, S. Dhiman, P. Sharma, *RSC Adv.*, **2015**, *5*, 15233; b) G. W. Gribble, *Indole Ring Synthesis: From Natural Products to Drug Discovery* (1st ed.), Wiley, Chichester (U.K.), **2016**; c) M. Bandini, A. Melloni, S. Tommasi, A. Umani-Ronchi, Synlett **2005**, *8*, 1199.
[70] C. Schmuck, D. Rupprecht, *Synthesis* **2007**, *20*, 3095.

Furthermore, pyrrole and indole are susceptible to chemical degradation as they are rather easily oxidized; this further hampers their synthesis and especially their isolation and purification.

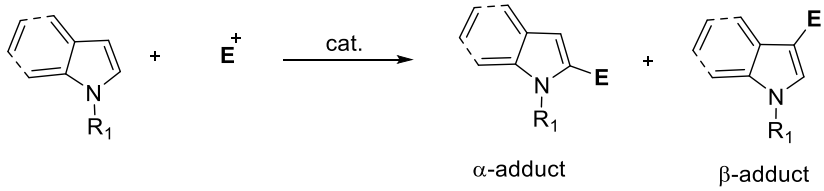

Figura 29. Regioselectivity of aromatic substitution on indole/pyrrole ring.

There are several ways to perform the alkylation of heteroarenes, with the main differences lying in the nature of the electrophile utilized[71]. Among them, the reaction between heteroarenes and electron-deficient C=C bond represents some of the most useful and reliable approaches. This type of addition has also been visualized as a Michael-type Friedel–Crafts reaction (MTFC), as this leads to direct alkylation of aromatic and heteroaromatic compounds.

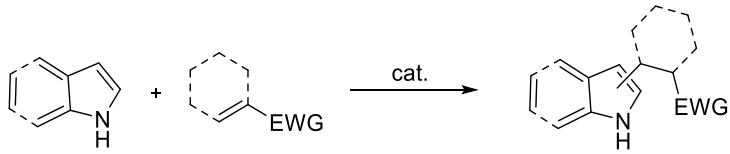

Figure 30. Catalytic Michael-type Friedel-Craft alkylation of indole/pyrrole (EWG: COX, NO_2).

The nucleophilic conjugate addition of pyrrole/indole to nitroolefins has been known for a long time[72] and offers an interesting synthetic versatility

[71] M. Bandini, A. Eichholzer, *Angew. Chem. Int. Ed.*, **2009**, *48*, 9608
[72] a) G. R. Humphrey, J. T. Kuethe, *Chem. Rev.*, **2006**, *106*, 2875; b) W. E. Noland, P. J. Hartman, *J. Am. Chem. Soc.*, **1954**, *76*, 3227; c) W. E. Noland, G. M. Christensen, G. L. Saur, G. G. S. Dutton, J. *Am. Chem. Soc.*, **1955**, *77*, 456; d) W. E. Noland, R. A. Hovden, *J. Org. Chem.*, **1959**, *24*, 894.

since the NO_2 group can be converted in different functionality[73]. For example, the β-indolylnitroalkanes **58** can be easily converted into "triptans", **58c**, melatonin derivatives **58a**, 1,2,3,4-tetrahydro-b-carbolines (THBCs, **58b**), fig. 31.

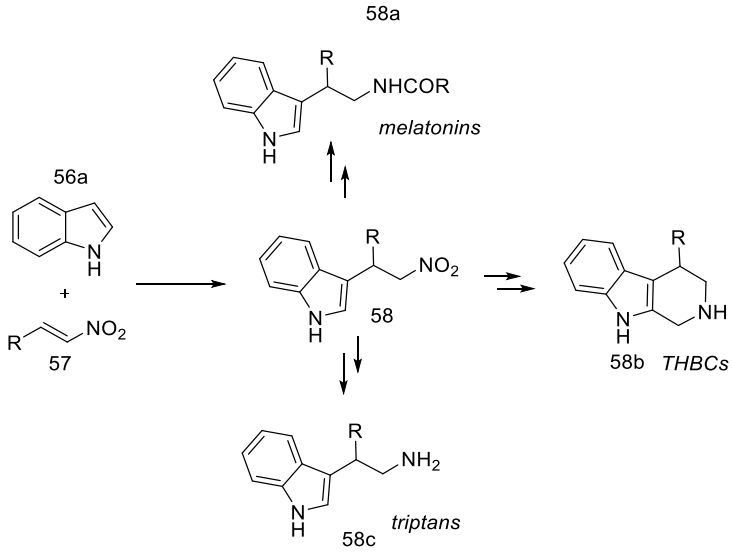

Figure 31. Indolylnitroalkanes: versatile intermediates in organic synthesis.

MTFC of indoles and pyrroles to nitroolefins has been well documented in the literature using Brønsted[74] or Lewis acids[75]. However, acid-catalyzed

[73]N. Ono, *The Nitro Group in Organic Synthesis*, Wiley-VCH, New York, **2001.**

[74] a) J. Szmuszkovicz, *J. Am. Chem. Soc.* **1975**, *79*, 2819; b) W. E Noland, G. M. Christensen, G. L. Sauer, G. G. S. Dutton, *J. Am. Chem. Soc.*, **1955**, 77, 456; c) Z. Iqbal, A. H. Jackson, K. R. N. Rao, *Tetrahedron Lett.*, **1988**, *29*, 2577. d) S.-L. You, Q. Cai, M. Zeng *Chem. Soc. Rev.*, **2009**, *38*, 2190; e) E. Marués-López, A. Alcaine, T. Tejero, R. P. Herrera, *Eur. J. Org. Chem.*, **2011**, 3700; f) R.-J. Tang, T. Milcent, B. Crousse *RSC Adv.*, **2018**, 8, 10314.

[75] a) M. M. Ala, R. Varala, S. V. Adapa, *Tetrahedron Lett.* **2003**, *44*, 5115; b) I. Komoto, S, Kobayashi, *Org. Lett.*, **2002, *7*,** 1115; c) P. E. Harrington, M. A. Kerr, *Synlett,* **1996**, *38*, 1047.

MTFC requires a careful control over the acidity to avoid the undesirable side reactions such as dimerization and polymerization[76].

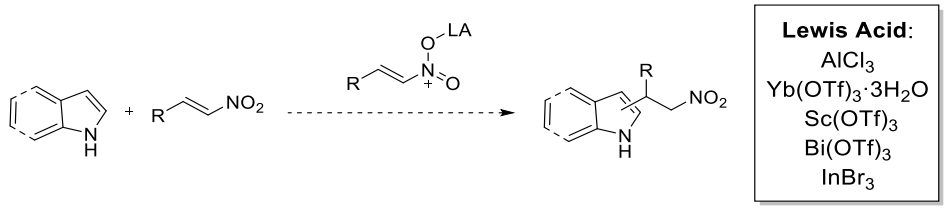

Figure 32. MTFC of indole/pyrrole promoted by Lewis Acid.

Then, other drawbacks are the use of expensive stoichiometric amounts of Lewis acidic catalysts and toxic heavy metals, long reaction times and air sensitive conditions.

Hence, searching for cheaper, simpler, and more efficient procedures, including metal free catalysts, is very attractive. In the last decade, several H-bond donor catalysts have been developed: 2-aminopyridium ions[77], boronate urea[78], fluorinated alcohols[79] and thio(urea) derivatives, which represent the preferred general catalytic system in the promotion of the MTFC[80], where the activation of the electrophile is mediated by a bidentate hydrogen bonding.

---

[76] a) C. Lin, J. Hsu, M. N. V- Sastry, H. Fang, *Tetrahedron*, 2005, **61**, 11751; b) N. Azizi, F. Arynasab, M. R. Saidi, *Org. Biomol. Chem.*, **2006**, *4*, 4275; C) L. T. An, J. P. Zou, L.L. Zhang, Y. Zhang, *Tetrahedron Lett.,* **2007**, *48*, 4297; d) G. Sri Hari, M. Nagaraju, M. Marthanda Murthy, *Synthetic Commun.,* **2008**, *38*, 100.
[77] N. Takenaka, R. S. Sarangthem, S. K. Seerla, *Org. Lett*., **2007**, *9*, 2819.
[78] J. Cai, P. Wu, Y. Wan, *Synlett*, **2008**, *8*, 1193.
[79] R. Tang, T. Milcent, B. Crousse, *RSC Adv.*, **2018**, *8*, 10314.
[80] G. Dessole, R. P. Herrera, A. Ricci, *SynLett*, **2004**, *13*, 2374.

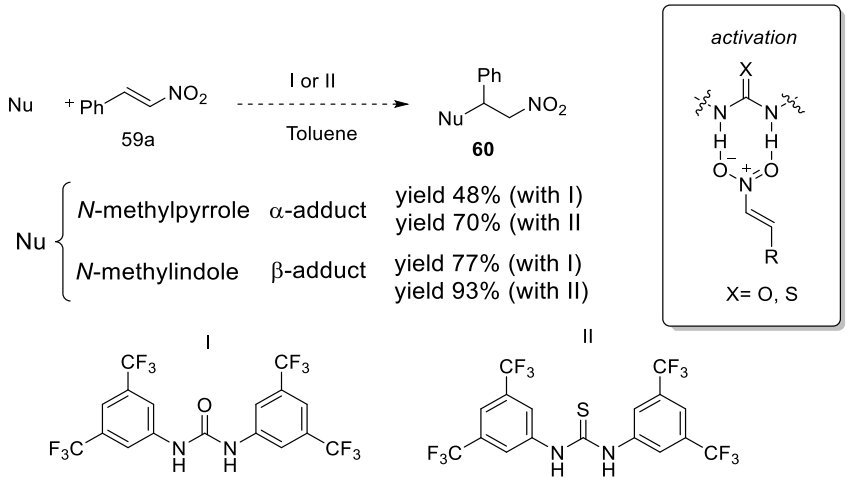

Figure 33. MTFC of indole/pyrrole promoted by (thio)urea based catalyst.

Another useful approach to functionalize the pyrrole/indole ring is the acid condensation with different carbonyl compounds, such as esters, aldehydes, ketones and amides. This procedure has been applied effectively in total synthesis of various families of natural products[81]. In particular, the condensation reaction of appropriate aldehydes or ketones with pyrrole **54b** ring affords dipyrromethanes[82], essential scaffolds for the synthesis of macrocycles, natural porphirines[83] and porphyrin analogues. Additionally, most of them found application as flavours and food additives[84].

---

[81] a) P. S. Baran, J. M. Richter, *J. Am. Chem. Soc.*, **2005**, 127, 15394; b) P. S. Baran, T. J. Maimone, J. M. Richter, *Nature*, ***2007***, *446*, 404; c) P. S., Baran, J. M. Richter, *J. Am. Chem. Soc.*, **2004**, *126*, 7450; d) P. S. Baran; J. M. Richter, J. M.; D. W. Lin, *Angew. Chem., Int. Ed.*, **2005**, *44*, 609.

[82] *B. F. O. Nascimento, S. M. M. Lopes, M. Pineiro, T. M. V. D Pinho E Melo, Molecules,* ***2019****, 24, 4348.*

[83] a) A. K., Burrell, D. L. Officer, P. G. Plieger, D. C. W. Reid, *Chem. Rev.*, **2001**, *101*, 2751; b) W. -S., Cho, and C.-H Lee, *Bull. Korean Chem. Soc.*, **1998**, *19*, 314 c) J. K. Laha, S. Dhanalekshmi, M. Taniguchi, A. Ambroise, J. S.Lindsey, *Org. Processes Rev. Dev.,* **2003**, *7*, 799.

[84] a) M. Stoll, M. Winter, F. Gautschi, I. Flamment, B. Willhalm, *Helv. Chim. Acta,* **1967**, *50*, 628; b) C. Frattini, C. Bicchi, C.; Barettini, G. M. Nano, *J. Agric. Food Chem*. **1977**, *25*, 1238 c) M. Shimoda, T. J. Shibamoto, *Agric. FoodChem*., **1990**, 38, 802.

In this reaction, the resulting pyrrolyl-carbinol **61** is usually not isolated, the acidic conditions catalyse the loss of water producing the 2-alkylidene-pyrrolium cation **62**, that is itself a reactive electrophile. At this point, the reaction proceeds through the attack of a second molecule of pyrrole to the cation, fig. 34, leading to the formation of α-dipyrromethane.

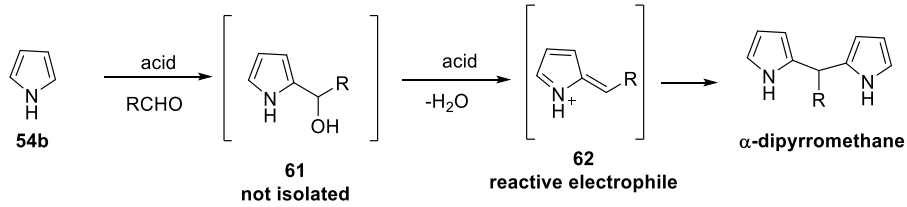

Figure 34. Synthesis of α-dipyrromethane.

In the same way, indole **56aa** can react with aldehydes and ketones under acid catalysis, leading to the bis(indolyl)methane, which constitutes a common class of structures isolated from natural sources and with a broad spectrum of biological activities[85], fig. 35.

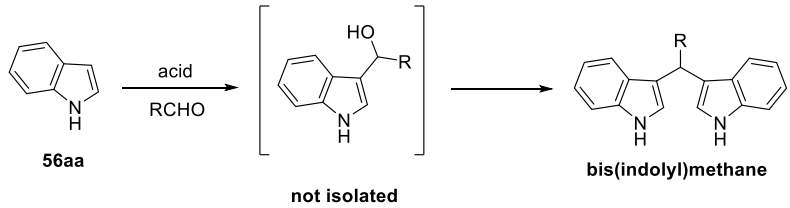

Figure 35. Synthesis of bis(indolyl)alkanes.

Various methods have been developed for the synthesis of bis(heteroaryl)methanes (BHM). Some of them involve the reaction with

[85] a) P. Galletti, A. Quintavalla, C. Ventrici, G. Giannini, W. Cabri, D. Giacomini, *New J. Chem.* **2010**, *34*, 2861; b) A. Srivastava, A. Agarwal, S. K. Gupta, N. Jain, *RSC Adv*. **2016**, *6*, 23008; c) V. Jamsheena, G. Shilpa, J. Saranya, N. A. Harry, R. S. Lankalapalli, S. Priya, *Chem. Biol. Interact.,* **2016**, *247*, 11; d) T. Das, S. Debnath, R. Maiti, D. K. Maiti, *J. Org. Chem.,* **2017**, *82*, 688; e) S. Sakemiand, H. H.Sun*, J. Org. Chem*., **1991**, *56*, 4304.

alcohols and acetals under oxidative conditions[86]. However, the protocol most used to get access of BHM involves the use of aldehydes activated by either Bronsted and Lewis acids[87], although some procedures still suffered from drawbacks such as harsh reaction conditions[88], use of big excess of heterocycle[89], difficulty in recovering the expensive catalysts[90] and most of all regioselectivity and polyalkylations troubles.

Hence, with the aim to develop new organocatalytic strategies and prompted by the recent results of my research group on the catalytic role of the bridging water molecules of the self-assembled resorcinarene capsule **CR_6** in the activation of substrates through H-bonding[55], we have envisioned that the capsule **CR_6** could promote the addition of electrophiles such as nitrostyrenes and carbonylic compounds on pyrrole/indole skeleton, fig. 36.

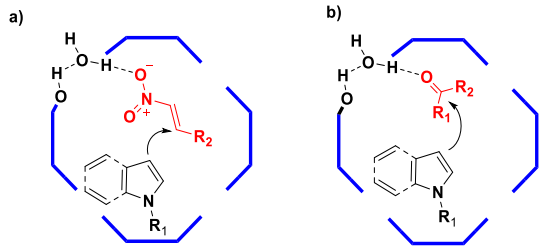

Figure 36. Proposed activation step of a) nitrostyrene and b) carbonyl substrates toward the addition of pyrrole/indole.

---

[86] a) Y.-Y. He, X.-X. Sun, G.-H. Li, G.-J. Mei, F. Shi, J. Org. Chem**., 2017**, *82*, 246, b) N.-X. Zhu, C.-W. Zhao, J.-C. Wang, Y.-A. Li, Y.-B. Dong, *Chem. Commun.,* **2016**, *52*, 12702.

[87] A. Palmieri, M. Petrini, R. R. Shaikh, *Org. Biomol. Chem.*,**2010**, 8, 1259, b) W. Qiang, X., Liu, T. –P. Loh. *ACS Sustain. Chem. Eng*., **2019**, *7*, 8429; c) J. S. Yadav, B. V. S. Reddy, S. Sunitha, *Adv. Synth. Catal*. **2003,** *345*, 349; d) C. Karami, H. Ahmadian, M. Nouri, F. Jamshidi, H. Mohammadi, K. Ghodrati, A. Farrokhi, Z. Hamidi, *Catal. Commun*., **2012**, *27*, 92.

[88] A. Wang, X. Liu, Z. Su, H. Jing, *Catal. Sci. Technol*., **2014**, *4*, 71.

[89] a) P. D. Rao, P. D. Dhanalekshmi, B. J. Littler, J. S. Lindsey*, J. Org. Chem*., **2000**, *65*, 7323; b) C. Biaggi, M. Benaglia, L. Raimondi, F. Cozzi, *Tetrahedron* **2006**, *62,* 123759.

[90] S. Khaksar, S. M. Ostad, *J. Fluorine Chem*., **2011**, *132*, 937.

3.2 Results and Discussion

3.2.1 Michael type Friedel Craft reaction promoted by CR_6

Firstly, we have evaluated the feasibility of a MTFC reaction between aromatic heterocycles and nitroalkenes.

The reaction of *N*-methylpyrrole **54a** with β-nitrostyrene **59a**, scheme 1, was chosen as reaction model. Initially, we tested the influence of the capsule on the reaction outcome. When the reaction was performed in the presence of 26 mol% of $\mathbf{CR_6}$ in water-saturated $CDCl_3$ at 30°C, we obtained the product **63aa** in 77% yield with a regioselectivity α/β of 86/14. Furthermore, no polyalkylated products were observed (entry 1, Table 1). On the contrary, performing the reaction in absence of the nanoreactor $\mathbf{CR_6}$ led to the total recovery of the starting materials, also extending the reaction times. This result represents a first evidence that $\mathbf{CR_6}$ plays a role in the activation of the MTFC reaction between **54a** and **59a**. Next, we performed a series of experiments under different reaction conditions in order to optimize the efficiency of the reaction.

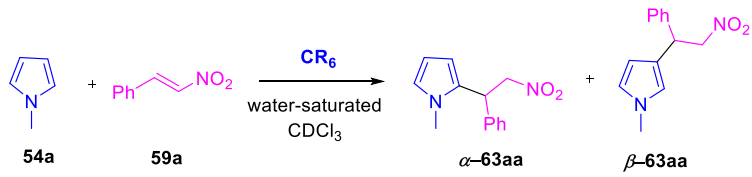

Scheme 1. MTFC reaction between *N*-methylpyrrole **54a** and β-nitrostyrene **59a.**

Table 1. Optimization of the reaction conditions for MTFC reaction between **54a** and **59a.**

Entry	solvent	54a:59a	CR_6	T (°C)	t (h)	Yield (%)[b]	α-63aa/β-63aa[c]
1	$CDCl_3$	4:1	yes	30	4	77	86/14
2[d]	$CDCl_3$	4:1	no	30	16	NR	-
3	$CDCl_3$	4:1	yes	50	2	94	80/20
4	$CDCl_3$	4:1	no	50	16	NR	-
5	$CHCl_3$	4:1	yes	50	2	99	83/17
6	$CHCl_3$	1:1	yes	50	2	81[e]	65/35
7	$CHCl_3$	1:4	yes	50	2	97[f]	-

[a] 0.16 mmol of **59a** and 26% mol **CR_6** in 1.1 mL of wat. Sat. solvent. [b] Yields of the isolated products by chromatography on column. [c] Determined by ^{1}H NMR analysis. [d] Only starting materials were recovered. [e] 9% of disubstituted product was obtained. [f] The reaction gave an inseparable mixture of dialkylated adducts.

Increasing the reaction temperature to 50 °C, the adducts α-**63aa** and β-**63aa** were obtained in 94% yield after 2h, while there was no substantial difference in the regioselectivity (entry 3, Table 1). On the contrary, performing the reaction in absence of **CR_6**, no products were detected (entry 4, Table 1,). Additionally, the use of non-deuterated chloroform as solvent (entry 5, Table 1) did not affect the reaction efficiency which remained unchanged with respect to the reaction in $CDCl_3$ (entry 3, Table 1). Interestingly, the variation in molar ratio **54a/59a** showed a remarkable effect on the reaction trend. When the reaction was carried out with **54a/59a** in 1:1 ratio, we observed a decrease in terms of efficiency and regioselectivity (α-**63aa/**β-**63aa** ratio 65/35), with the presence also of disubstituted products (entry 6, Table 1). Instead, using an excess of β-

nitrostyrene **59a**, we observed the exclusive formation of disubstituted products (entry 7, table 1,).

Further studies were focused on clarifying the role of **CR$_6$** in this reaction. According to a protocol previously reported[55,56], a series of control experiments were carried out. In detail, when the reaction was run in presence of the hexamethonium iodide (HMI), which is known to be a high affinity guest for **CR$_6$**, no product was observed. A plausible explanation for this result is that HMI occupies the cavity of the capsule and prevents the incoming of **54a** and **59a**, thus acting as an inhibitor, fig. 37. Therefore, the reaction occurs within capsule **CR$_6$**.

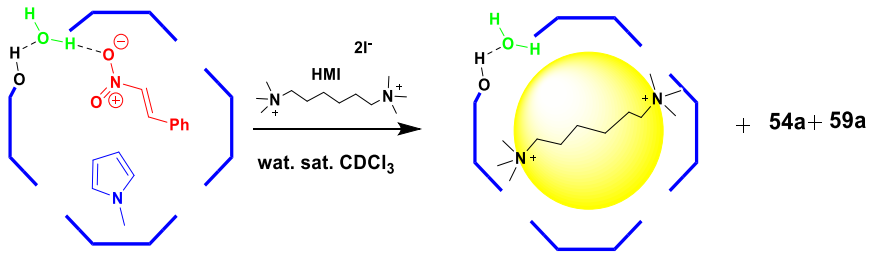

Figure 37. Mechanism of the inhibition of the capsule **CR$_6$** in the presence of hexamethonium guest.

Further evidence was provided when the reaction was carried out in presence of DMSO, a competitive H-bond solvent able to disaggregate the capsule, no conversion into **63aa** was detected, (entry 2, Table 2). Next, when the reaction was performed replacing **CR$_6$** with its monomeric unit, 4-dodecyl-resorcinol, only traces of **63aa** were observed, confirming the importance of the three-dimensional capsular structure, (entry 3, Table 2). Thus, these control experiments provided the first proof that the reaction took place inside the cavity of **CR$_6$.** Further evidence came from the

NMR study regarding the proofs of the encapsulation of the reagents **54a** and **59a** inside the nanoconfined space of **CR_6**. Recently, my research group have reported a detailed 2D NMR study which demonstrated the encapsulation of *N*-methylpyrrole **54a** inside **CR_6**[47,55]. The encapsulation of β-nitrostyrene **59a** inside **CR_6** was proved by a 2D-EXSY experiment of the mixture **59a/CR_6.** In fact, the presence of exchange cross-peaks between the vinyl protons of **59a**, respectively outside and inside the capsule, confirmed the incorporation of **59a** within **CR_6**, (fig. S1, in the experimental section).

Table 2. Control experiments of MTFC between **54a** and **59a**

Entry	Capsule (mol%)	Additive (equiv.)[b]	Yield (%)[c]	α-63aa/β-63aa[c]
1[e]	26	HMI (18)[f]	NR	—
2[d,e]	26	DMSO (10)[f]	NR	—
3	—	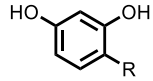 R= *n*-$C_{12}H_{25}$ (24)	trace	—
4	—	AcOH (1)	NR	—
5	—	$BrCH_2COOH$ (1)	17	59/41
6	—	TFA (1)	34	78/22

[a]Reaction conditions: **54a** (0.59 M), **59a** (0.15 M), **CR_6** (0.039 M) in 1.1 mL of water-saturated $CHCl_3$ at 50 °C for 2h. [b] Amount of additive respect to β-nitrostyrene **59a**. [c] Yields of the isolated products by chromatography on column. [d]Determined by ^1H NMR analysis. [e] Reaction time = 16 h. [f]

As stated before, Brønsted acid catalysts[74] generally promote this reaction through the activation of the nitroolefins towards the conjugate addition of the heterocyclic compounds. Tiefenbacher and Zhang have reported that the capsule itself can act as a mild Brønsted acid with a pk_a value of about 5.5-6.0[46] and, more recently, it is extimated a local pk_a value of ≈2.5 for the four bridged-water molecules with one H-bond donating free valence[55]. Hence, we sought to define if the catalytic activity of **CR_6** was due to its Brønsted acidity. We tested various common Brønsted acids with a pk_a value comparable to the capsule's ones such as AcOH (pk_a = 4.76) and $BrCH_2COOH$ (pk_a = 2.86). The reaction in the presence of AcOH led to no conversion into **63aa** (entry 2, Table 2), whereas the acidity of $BrCH_2COOH$ promotes the reactions with poor yield and in not selective way (entry 3, Table 2). Finally, we have also tested the stronger trifluoroacetic acid, TFA, (entry 5, Table 2) and, in this case, we got **63aa** in 34% yield with a complex mixture of byproducts. So, based on the collected data, we can conclude that the reaction takes place inside the cavity of the capsule and moreover, that the solely mild Brønsted acidity of **CR_6** is not enough to promote the MTFC reaction between **54a** and **59a**.

At this point, with the optimized reaction conditions illustrated in entry 5, Table 1, the substrate scope of the reaction was investigated. Firstly, we studied the influence of the nature of the Michael acceptor, table 2. The catalytic system proved to be compatible with all the β-nitrostyrene derivatives tested, affording the products in good or high yields. The α-regioisomer was the preferred one, regardless of the nature and the relative position on the aromatic ring of the substituents (Table 3).

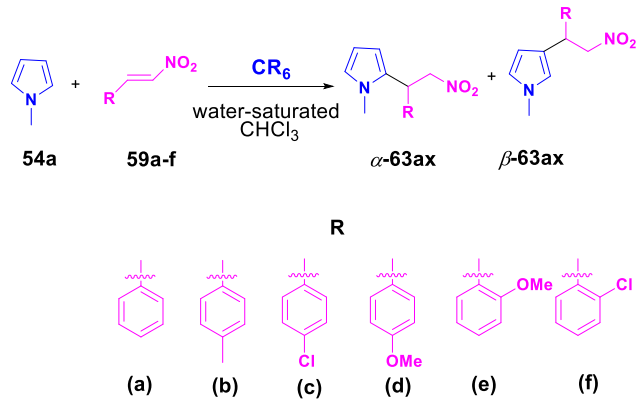

Scheme 2. MFTC between **54a** and **59a-f.**

Table 3. Scope study for the conjugate addition of *N*-methyl pyrrole **54a** to various nitroolefins **59a–f.**

Entry[a]	59	Yield (%)[b]	α-63ax/β-63ax[c]
1	**59a**	99	83/17
2	**59b**	99	80/20
3	**59c**	95	77/23
4	**59d**	92	85/15
5	**59e**[d]	70	60/40
6	**59f**[d]	80	60/40

[a] Reaction conditions: **54a** (0.59 M), **59a-f** (0.15 M), **CR_6** (0.039 M), wat. sat. $CHCl_3$ (1.1 mL), reaction time 2 h unless otherwise specified. [b]Yields of the isolated products by chromatography on column. [d]Determined by ^{1}H NMR analysis. [e]Reaction time = 16 h. [f]

However, with *ortho*-substituents on the β-nitrostyrene, the reaction required more time for the total conversion and a higher amount of the β-regioisomer was detected (entries 5-6, Table 3). This regioselectivity could

be explained in terms of steric hindrance: the substituent in the *ortho*-position of **59e** and **59f** could drive the attack on the β-position.

Next, the efficiency of the reaction with different heterocyclic rings was investigated, scheme 3.

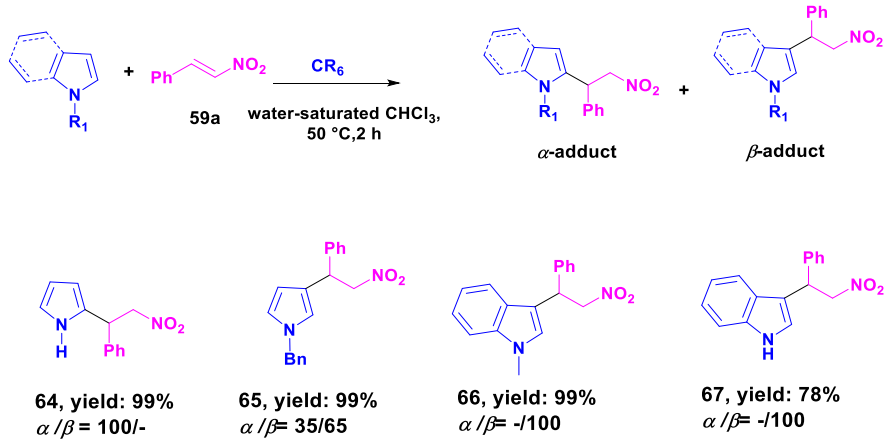

Scheme 3. Scope study for the conjugate addition of different heterocyclic rings to **59a**[91].

When the pyrrole was used in reaction with **59a**, a complete α-regioselectivity was observed. Interestingly, the β-isomer is the preferred product when the more sterically demanding *N*-benzyl pyrrole was used. These results suggested that the steric hindrance at the nitrogen atom of pyrrole drives the regioselectivity of the reaction. Using indole and *N*-methylindole, the reaction led to the β-adducts in 78% and 99% yield respectively. The best efficiency

[91] Reaction conditions: indoles or pyrroles (0.59 M), **59a** (0.15 M), **CR6** (0.039 M), wat. sat. $CHCl_3$ (1.1 mL), reaction time 2 h. Yields of the isolated products by chromatography on column. α/β determined by ^{1}H NMR analysis.

observed in the latter case is probably due to the substitution on nitrogen atom that probably prevents side reactions.

Summarizing, the experimental data showed that the capsule **CR_6** not only plays a role in the activation of the MTFC reaction, but also exerts a control over the regioselectivity outcome.

In order to explain the experimental data and to get more insight into the reaction mechanism, quantum mechanical studies were performed[92]. For this purpose, the reaction between **59a** and **54a** was chosen as a representative model. The calculation results indicated that the reaction proceeds as depicted in scheme 4 with the energy profile shown in the figure 38.

[92] Quantum mechanical studies were performed by Prof. A. Rescifina and co-workers, Università degli Studi di Catania.

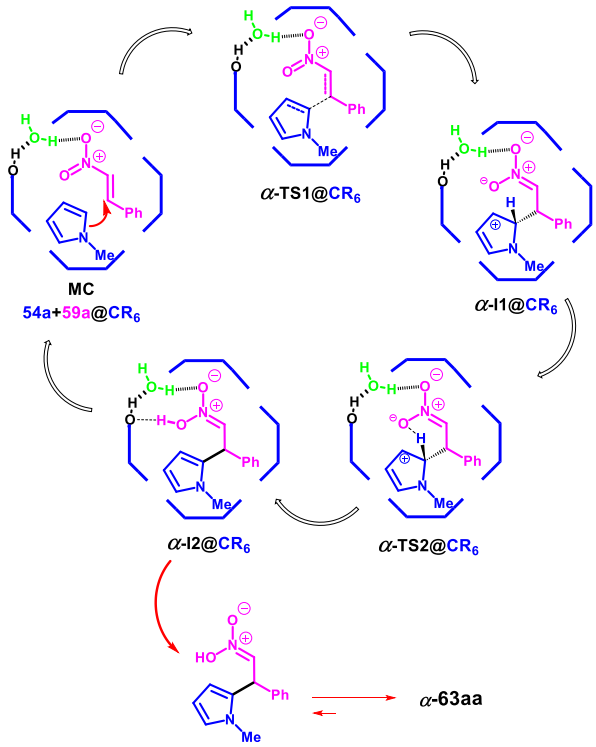

Scheme 4. *Alpha* channel for the *in silico* studies of the MTFC inside **CR$_6$**.

According to the proposed mechanism (Scheme 4), the first step is the encapsulation of both reagents (**54a** and **59a**) inside the capsule, forming the hetero binary complex (MC). Interestingly, the nitrostyrene **59a** is activated towards the nucleophilic attack by a H-bond interaction between one oxygen atom of the nitro group and a bridged water molecule presenting a H-bond free valence. Following the *α*-path, the attack of **54a** to the Michael acceptor led to the intermediate *α*-I1, which can re-aromatize, through the *α*-TS2, to the intermediate *α*-I2, in which the nitronic acid tautomer of the compound ***α*-63aa** is stabilized by two H-bonds. Next, the expulsion of the tautomer by encapsulation of the

reagents allows the repeating of the catalytic cycle. The expulsion of the nitro acid tautomer and its conversion into the most stable α-**63aa** outside the capsule **CR$_6$** is in total agreement with the absence of product inhibition. The route for the formation of the β-**63aa** adduct proceeds in a similar way to the previous one and regarding the regioselectivity aspect, the preferred formation of the α-regioisomer is due to the difference in the Gibbs free energy in the TS1: the β-attack led to a β-TS1 higher than the corresponding α-TS1 by 1.17 kcal/mol, fig. 38.

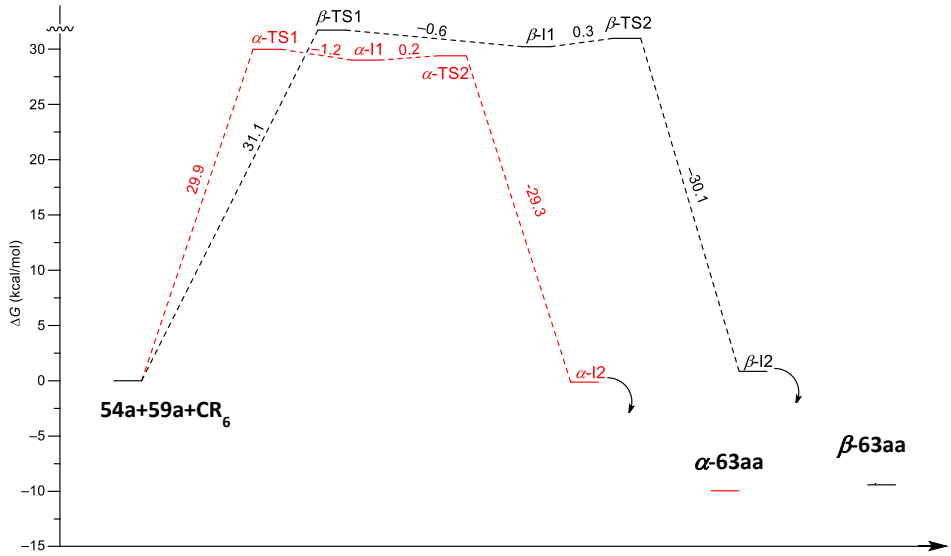

Figure 38. Gibbs free energy profiles for *alpha* (in red) and *beta* (in black) paths within **CR$_6$**.

Additionally, considering the very high value of the Gibbs free activation energy for the reaction without any catalyst (α-TS1, $\Delta G^{\ddagger}$ = 38.32 kcal/mol, Table S1, in the experimental section), the reaction

without **CR_6** does not take place (entry 4, Table 1). In the same way, the use of AcOH is not sufficient to overcome this barrier (entry 4, Table 2), whereas the process is activated by TFA but in a non-selective way because of the simultaneous activation of the nitro-aci tautomerism route[93] with the formation of nitronic acid derivatives that can be easily degraded into complex mixture, leading a low yield (entry 6, Table 2).

In conclusion, the experimental and computation data showed the ability of **CR_6** in the promotion of MTFC between heteroarenes and nitrostyrenes thanks the activation of the latter by H-bonding interaction and in the prevention of the products' degradation by encapsulation.

3.2.2 Synthesis of bis(heteroaryl)methanes promoted by CR_6

In order to further expand the catalytic application of capsule **CR_6,** we have tested its ability in promoting the synthesis of bis(heteroaryl)methanes by reaction between aldehydes and pyruvates with aromatic heterocycles. Our study started with a survey of reaction conditions, choosing the reaction between *N*-methylpyrrole **54a** and ethyl pyruvate **68a** as model reaction, scheme 5.

[93] a) V. G. Avakyan, O. V. Fateyev, *Russ. Chem. Bull.*, **1993**, *42*, 90; b) I. Erden, J. R. Keeffe, F. P. Xu, J. B. Zheng, *J. Am. Chem. Soc.*, **1993**, *115*, 9834.

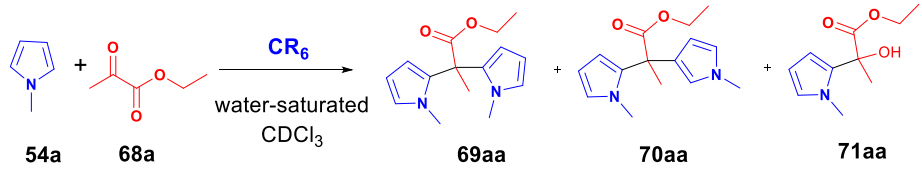

Scheme 5. Reaction between *N*-methylpyrrole **54a** and ethyl pyruvate **68a.**

Table 4. Optimization of the reaction condition for the synthesis of bis(heteroaryl)methanes between **54a** and **68a.**

Entry[a]	Capsule (26 mol%)	T (°C)	54a/68a	Yield (%)[b]	69aa (%)[c]	70aa (%)[c]	71aa (%)[c]
1	Yes	30	1/1	35	23	4	8
	No			---	---	---	---
2	Yes	50	1/1	43	23	4	9
	No			---	---	---	---
3	Yes	10	1/1	20	10	5	5
	No			---	---	---	---
4	Yes	30	2/1	60	40	5	15
	No			---	---	---	---
5	Yes	30	4/1	98	60	10	28
	No			---	---	---	---

[a]Reactions were performed on a 0.16 mmol scale of **68a, CR$_6$** (0.26 equiv.) in water saturated $CDCl_3$ (1.1 mL) under stirring for 16h at 30°C. [b]Isolated yield. [c] Determined by ^{1}H NMR spectroscopy.

When the reaction was carried out in the presence of 26% mol of **CR$_6$** in water-saturated $CDCl_3$ at 30°C and with a 1/1 ratio of **54a/68a**, the *meso*-α,α-substituted dipyrromethane **69aa** in 23% yield was obtained as major product, while a minimal amount of α,β–linked dipyrromethane **70aa** and monoalkylated adduct **71aa** were observed (entry 1, Table 4). Interestingly, running the reaction under the same reaction conditions but without **CR$_6$**,

no products were detected (entry 1, Table 4). This is the first evidence of the catalytic role of **CR_6** in this reaction and different reaction conditions were evaluated in order to improve the efficiency. For example, carrying out the reaction at 50°C has only a small effect on the yield (entry 2, Table 4), while changing the molar ratio of **54a/68a** has a significant effect on the reaction outcome (entry 4-5, Table 4). When an excess of **54a** was used, we observed an increase of the reaction efficiency in terms of yield, with no difference in the product selectivity. On the basis of these results, the capsule **CR_6** plays a role in this promotion and a series of control experiments, according to a protocol previously mentioned, confirmed that the reaction took place inside **CR_6**. In detail, the first experiment involves the use of a competitive cationic guest, such as tetrabutylammonium tetrafluoroborate: it occupies the cavity of capsule **CR_6** acting as an inhibitor and thus prevents the reactants from entering within the cavity[54]. The second one involves the use of DMSO, which, competing with the H-bonding network responsible of the self-assembly of the capsule, favours its disaggregation. In both experiments, no hint of products was detected, confirming that the reaction took place in the nanoconfined space of **CR_6**. Further proofs came from the NMR studies on the encapsulation of the reagents: in the DOSY experiment of the mixture **68a/CR_6** the diffusion coefficient of incapsulated **68a** was aligned with those of the capsule, thus probing its internalization in **CR_6,** (Fig. S3, in the experimental section). Furthermore, in the 2D-EXSY (Fig. S2, in the experimental section), exchange cross peaks between **68a** incapsulated and free were detected.

Encouraged by these conclusions and with the optimized reaction conditions in the hand, we studied the generality of reaction.

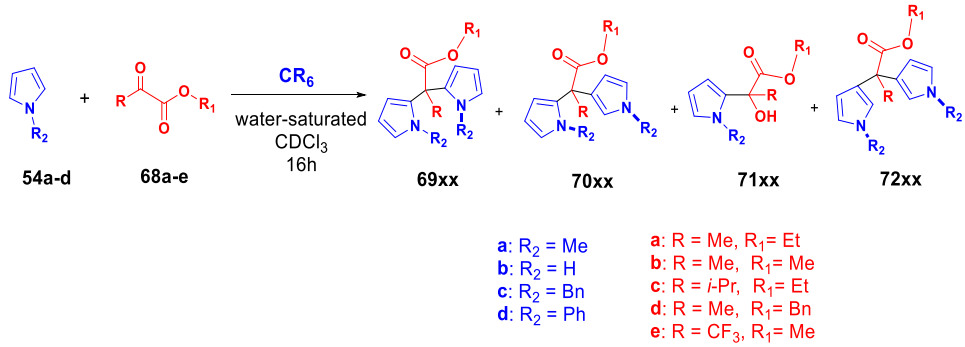

Scheme 6: Reaction between pyrroles **54a-d** and α-ketoesters **68a-e.**

Table 5. Scope of the reaction with pyrroles **54a-d** and α-ketoesters **68a-e.**

Entry [a]	CR_6	54	68	Yield (%)[b]	69xx (%)[c]	70xx (%)[c]	71xx (%)[c]	72xx (%)[c]
	Yes			98	60	10	28	---
1		**54a**	**68a**					
	No			---	---	---	---	---
	Yes			99	90	---	---	---
2[d]		**54a**	**68b**					
	No			---	---	---	---	---
	Yes			55	---	---	55	---
3		**54a**	**68c**					
	No			---	---	---	---	---
	Yes			76	38	38	---	---
4		**54a**	**68d**					
	No			---	---	---	---	---
	Yes			99	---	---	99	---
5		**54a**	**68e**					
	No			35	---	---	35	---
	Yes			99	99	----	---	---
6		**54b**	**68a**					
	No			---	---	----	---	---

	Yes			98	----	----	98	---
7		**54b**	**68e**					
	No			38	---	----	38	---
	Yes			50	----	----	----	50
8		**54d**	**68a**					
	No			---	----	----	----	---
	Yes			65	---	---	65	---
9		**54c**	**68a**					
	No			--	---	---	---	---

[a] Reactions were performed on a 0.16 mmol scale using **54a-d** (4 equiv.), **68a-e** (1 equiv.), and capsule **CR_6** (0.26 equiv.) in water saturated $CDCl_3$ (1.1 mL) under stirring for 16h at 30°C. [b] Isolated yield. [c] Determined by ^1H NMR spectroscopy. [d] 9% of adduct of pyrrole with two molecules of pyruvate is present.

Interestingly, it was found that the reaction outcome is influenced by the α-ketoester nature, Table 5. Using the α-ketoester with a methyl group **68b**, the reaction led to the formation of α,α–dipyrromethane **69ba** as only product in high yield (entry 2, Table 5), while in presence of α-ketoester **68c**, bearing the sterically demanding isopropyl group, no trace of dipyrromethane was detected: only mono adduct **71ac** was obtained in 50 % yield (entry 3, Table 5). In the same way, the α-ketoester **68e**, bearing a trifluoromethyl group, when reacted either with **54a** and **54b**, is totally converted into the mono-alkylated adducts **71af** and **71bf** (entries 5 and 7, Table 5).

Additionally, carrying out the reaction with the α-ketoester **68d** (R'=Bn) and **54a**, α,α- and α,β-dipyrromethanes, **69ad** and **70ad** in 1/1 ratio were observed with no trace of mono-adduct product (entry 4, Table 5).

Considering the nature of the nucleophile, the reaction between pyrrole **54a** and **68a** led to the total conversion in the α,α-dipyrromethane **69aa** (entry 6, Table 5), whereas the use of **54c**, pyrrole bearing the benzyl group, the mono-adduct **71ca** was obtained selectively and in good yield. (entry 9, Table 5). Interestingly, when *N*-phenyl pyrrole **54d** was used, the selective formation of a β,β-dipyrromethane **72da** was observed, (entry 9, Table 5). The selective formation of β,β–dialkylated products was also observed starting from indole derivatives: the reaction led to β,β-**73axx** bis(indolyl)methane in high yield independently by the nature of both reagents (Table 6).

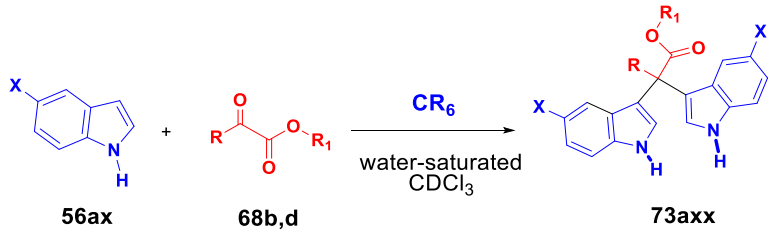

aa: X= H
ab: X= Me
ac: X= OMe
ad: R= Br

b: R= Me, R_1= Me
d: R= Me, R_1= Bn

Scheme 7. Reaction with indoles **56ax** and α-ketoesters **68b,d.**

Table 6. Scope of the reaction with indoles **56ax** and α-ketoesters **68b,d.**

Entry[a]	56ax	68	Yield 73axx (%)[b]
1	56aa	68b	86
2	56ab	68b	90
3	56ac	68b	88
4	56ad	68b	85

5	56aa	68d	80

[a]Reactions were performed on a 0.16 mmol scale using **56ax** (4 equiv.), **68b,d** (1 equiv.) and capsule **CR$_6$** (0.26 equiv.) in water saturated $CDCl_3$ (1.1 mL) under stirring for 16h at 30°C. [b]Isolated yield.

Considering these results, we proposed the stepwise mechanism depicted in fig. 39.

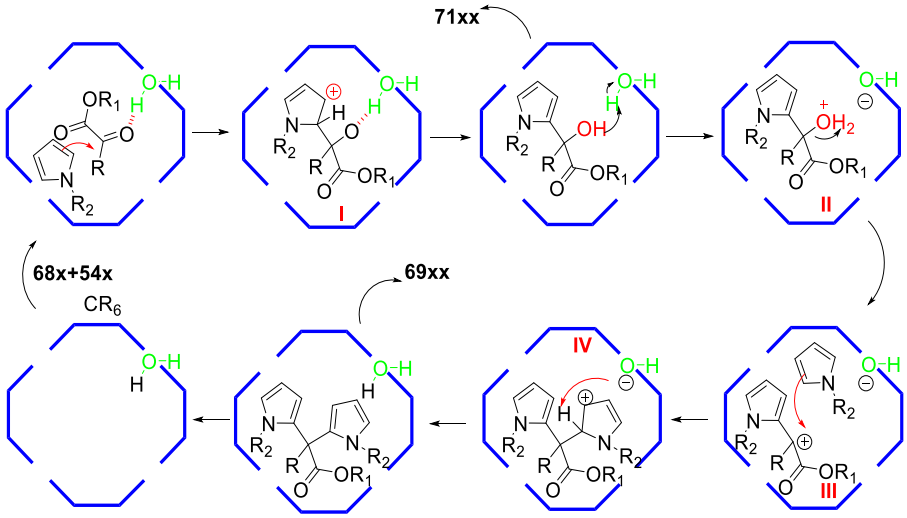

Figure 39. Proposed mechanism for the formation of the products **69xx** and **71xx** inside the nanocavity of **CR$_6$**.

According to the mechanism, the first step involves the encapsulation of both reagents inside **CR$_6$** and the α-ketoester is activated towards the nucleophilic of **54a** by H-bond interaction with a bridged water molecule. The nucleophilic attack leads to the cationic intermediate I, stabilized by H-bonding and cation⋯π interactions, which, after re-aromatization, is converted in the alcohol derivative **71aa**. At this point, based on the local acidity of the bridged water molecules with H-bond donating free valence

(pK_a ≈ 2.5), the intermediate **71aa** can be further derivatized: the protonation of the OH group and the loss of water, lead to the formation of the carbocation III, that can be attacked by a second molecule of **54a**, forming, after the re-aromatization, the bis-alkylated adduct **69aa**.

Summarizing, the formation of the carbocation III presents the key step for the synthesis of bis alkylated-adducts, and its formation is supported by the findings that when the reaction was carried out using **68e**, the α-ketoester bearing a trifluoromethyl moiety, only mono-alkylated product was isolated: the electron-withdrawing group disfavours the formation of carbocation **III.**

Then, with the aim to extend the scope of the reaction between **54a** and carbonyl compounds inside the nanocavity of the **CR_6**, we tested the procedure with aldehydes. The reaction between **54a** and benzaldehyde **74a** was chosen as reaction model, scheme 8.

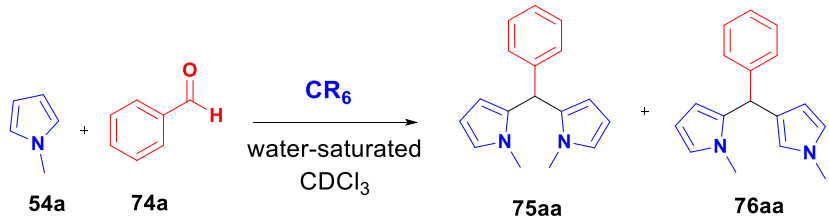

Scheme 8. Reaction between *N*-methylpyrrole **54a** and benzaldehyde **74a.**

Table 7 Optimization reaction conditions for the reaction between **54a** and benzaldehyde **74a.**

Entry[a]	Capsule	T (°C)	54a/74a	Yield (%)[b]	75aa (%)[c]	76aa (%)[c,d]
	Yes			38	34	4
1		50°C	1/1			
	No			---	---	---
	Yes			60	54	6
2		50°C	2/1			
	No			---	---	---
	Yes			97	87	10
3		50°C	4/1			
	No			---	---	---
	Yes			20	18	2
4		25°C	4/1			
	No			---	---	---

[a]Reactions were performed on a 0.16 mmol scale using **54a** (from 1 to 4 equiv.), **74a** (1 equiv.), and capsule **CR_6** (0.26 equiv.) in water saturated $CDCl_3$ (1.1 mL) under stirring for 16h. [b] Overall yield of Isolated products. [c]Determined by ^{1}H NMR spectroscopy. [d]The column gave an inseparable mixture with regioisomer and the yield was calculated by integration of the respective ^{1}H NMR signals of the regioisomers in the isolated fractions.

The reaction between **54a** and **74a** in equimolar ratio in presence of 26%mol of **CR_6** led to the formation of α,α-dipyrromethane **75aa** in 34% with a minimal amount of α,β-dialkylated adduct (entry 1, Table 7). Interestingly, no conversion was observed when the reaction was carried out in absence of **CR_6**. This is the evidence that **CR_6** promotes even this reaction and further experiments were conducted in order to improve the reaction efficiency. In detail, it was found that an excess of **54a** (entry 3, Table 7) had a positive effect on the reaction: α,α-dipyrromethane **75** was obtained with 87% yield as main product. With the optimized reaction

conditions, we have evaluated the substrate scope in order to determine the generality of the reaction, table 8.

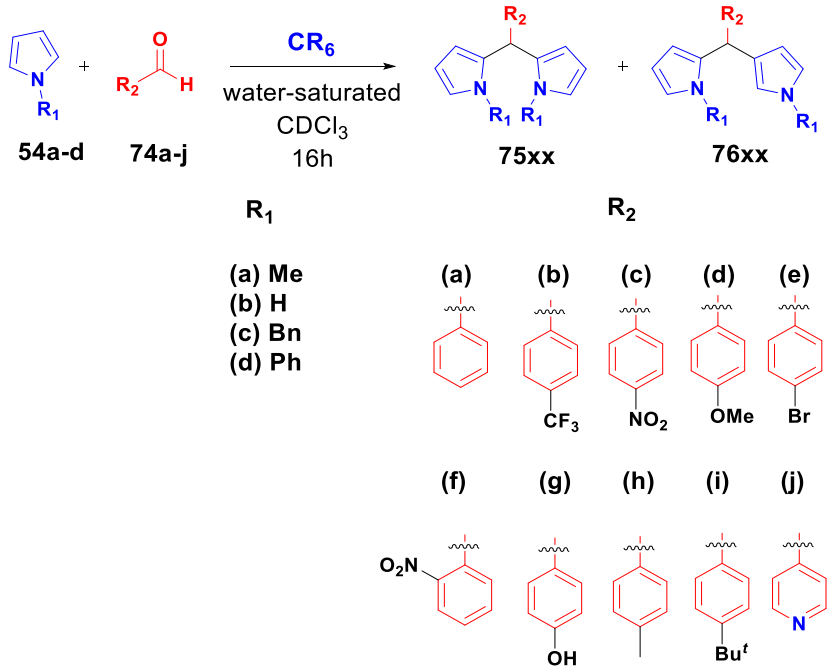

Scheme 9 Reaction with different pyrroles **54a-d** and aldehydes **74a-j**.

Table 8. Scope of the reaction with different pyrroles **54a-d** and aldehydes **74a-j**.

Entry[a]	54	74	Yield (%)[b]	75xx (%)[c]	76xx (%)[c,d]
1	54b	74a	70	70[e]	---
2	54c	74a	---	---	---
3	54d	74a	---	---	---
4	54a	74b	98	88	10
5	54a	74c	98	96	2

6[f]	54a	74d	98	96	2
7	54a	74e	95	93	2
8	54a	74f	99	90	9
9[f]	54a	74g	98	96	2
10	54a	74h	97	95	2
11	54a	74i	97	91	6
12	54a	74j	85	76	9

[a]Reactions were performed on a 0.16 mmol scale using **54a-d** (4 equiv.), **74a-j** (1 equiv.), and capsule **CR_6** (0.26 equiv.) in water saturated $CDCl_3$ (1.1 mL) under stirring for 16h at 50 °C. [b] Overall yield of Isolated products. [c]Determined by ^{1}H NMR spectroscopy. [d]The column gave an inseparable mixture with regioisomer and the yield was calculated by integration of the respective ^{1}H NMR signals of the regioisomers in the isolated fractions. [e] ^{1}H NMR spectrum of the crude reaction mixture showed presence of other species obtained after chromathography purification as a complex and inseparable fraction not characterized. [f]These reactions were performed under stirring for 48h at 50 °C.

It was found that the nature of the benzaldehyde **74a-j** has no effect on the regioselectivity: **CR_6** promotes the reaction in efficient way affording α,α-adducts as the major product (Table 8). Additionally, carrying out the reaction with pyrrole bearing sterically demanding groups, no conversion into products was observed (entries 2-3, Table 8), while using *N*-methylindole **56b** as nucleophile, the reaction proceeded in a very efficient and selective way: only β,β-adducts **77** were observed (Table 9).

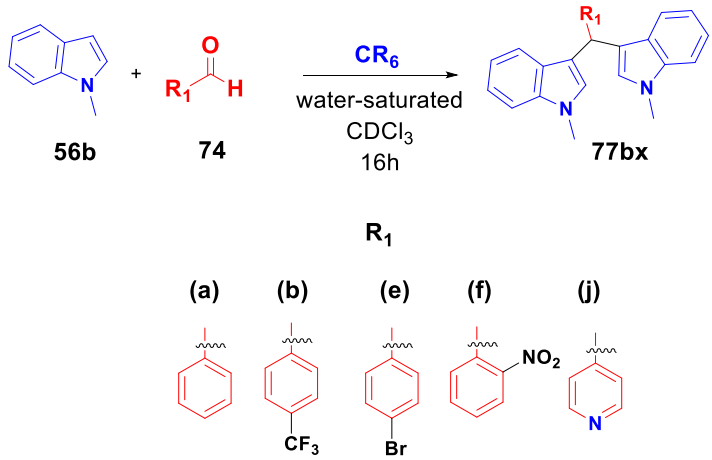

Scheme 10 Reaction with *N*-methylindole **56b** and benzaldehydes **74a, b, d, e, j**.

Table 9. Scope of the reaction between indole **56b** and benzaldehydes **74a, b, d, e, j**.

Entry[a]	74	Yield (%)[b]
1	74a	97
2	74b	98
3	74e	98
4	74f	97
5	74j	98

[a]Reactions were performed on a 0.16 mmol scale using **56b** (4 equiv.), **74** (1 equiv.), and capsule **CR$_6$** (0.26 equiv.) in water saturated $CDCl_3$ (1.1 mL) under stirring for 16h at 50 °C. [b]Isolated yield.

3.3 Conclusions

We have showed that the hexameric capsule **CR$_6$** is able to promote the reaction between nitrostyrene and carbonylic compounds (aldehydes and α-ketoesters) with pyrroles and indoles, affording relevant compounds,

such as bis(heteroaryl)methanes and nitroalkene derivatives, interesting building blocks for the construction of more complex structures. Interestingly, capsule **CR_6** shows a double function: 1) it can act as H-bond catalyst thanks to the H-bond donor capabilities of its bridging water molecules and thus, it can activate the substrates towards the nucleophilic addition of the heterocycles, and 2) it provides a nanoconfined environment able to confine the reactants, stabilize the reaction intermediates and also prevents product degradation. The synergistic interplay between these two features exerts a control on the reaction outcome both in term of efficiency and selectivity.

Chapter 4. Modulation of Dynamic Covalent Imine Libraries by the hexameric resorcinarene capsule

4.1 Introduction

In a single cell, several simultaneous reactions occur without interference, leading to products with very high level of chemo-, regio-, and stereoselectivity[4]. This perfect control is a consequence of a long process of evolution[94]: living organisms have to *adapt* to constantly changing environmental conditions to ensure the survival of the respective species. However, the adaptation is not a prerogative (or perquisite) to living organisms, in fact, simple chemical systems[95] present the same attitude: they can respond to the application of a *stimulus.* At a molecular level, such dynamic behaviour is achieved thanks to the presence of reversible covalent bond and it is matter of study of dynamic covalent chemistry (DCC).[96] In detail, DCC implements reversible chemical reactions to generate dynamic covalent libraries (DCLs) under thermodynamic control. In such a dynamic system, building blocks and products are continuously interconverting thus enabling in respond to a stimulus or external factor by

---

[94] C. Darwin in *On the Origin of Species by Means of Natural Selection, or the Preservation of Favoured Races in the Struggle for Life*, John Murray, London, **1859.**

[95] a) J.-M.Lehn, *Chem. Eur. J.* **1999**, *5*, 2455; b) J.-M Lehn, *Proc. Natl. Acad. Sci. U. S. A.*, **2002**, *99*, 4763; c) J.-M. Lehn, *Chem. Soc. Rev.* **2007**, *36*, 151; d) J.-M. Lehn, *Angew. Chem., Int. Ed.*, **2013**, *52*, 2836; e) J.-M. Lehn, *Angew. Chem. Int. Ed.*, **2015**, *54*, 3276.

[96] a) Y. Jin, C. Yu, R. J. Denman, W. Zhang, *Chem. Soc. Rev.,* **2013**, *42*, 6634; b) W. Zhang, Y. Jin, *Dynamic Covalent Chemistry: Principles, Reactions, and Applications,* First Edition, John Wiley & Sons Ltd., Chichester (UK), **2018**; c) P. Frei, R. Hevey, B. Ernst, *Chem. Eur. J.,* **2019**, *25*, 60; d) Q. Ji, R. C. Lirag, O. Š. Miljanić, *Chem. Soc. Rev.*, **2014**, *43*, 1873.

shifting its equilibrium composition according to Le Chatelier's principle.

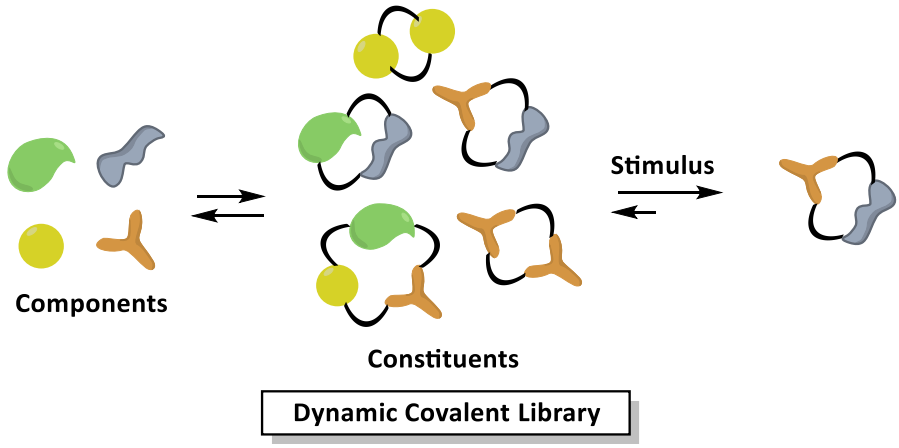

Figure 40. Adaptation of a dynamic covalent library to the application of stimulus.

DCLs can be influenced by either physical stimulus, such as temperature[97], crystallization[98] and distillation[99] or by chemical effectors, such as ligands or receptors. In this latter case, the modulation is driven by a complementarity (in term of shape and supramolecular interactions) between one constituent of the DCL and the effector[100]. For example, an interesting case of supramolecular modulation of a DCL was reported by Sanders[101] and co-workers in which a dynamic library modulates its products distribution after addition of a guest: the equilibrium of cyclic hydrazone-based pseudopeptides formed by 10 species, was shifted toward only the cyclic trimer able to selectively bind the lithium cation, fig. 41.

---

[97] P. N. W. Baxter, J.-M.; Lehn, K. Rissanen, *Chem. Commun.,* **1997**, 1323.
[98] C. Chow, S. Fujii, J.-M. Lehn, *Chem. Commun.*, **2007**, 43635.
[99] a) K. Osowska, O. Š. Miljanić, *Angew. Chem. Int. Ed.,* **2011**, *50*, 8345 (b) Q. Ji, O. Š. Miljanić, *J. Org. Chem.,* **2013**, *78*, 12710.
[100] G. R. L. Cousins, R. L. E. Furlan, Y.-F. Ng, J. E.; Redman, J. K. M. Sanders, *Angew. Chem. Int. Ed.,* **2001**, *40*, 423.
[101] R. L. E.Furlan, Y.-F.Ng, S.; Otto, J. K.M. Sanders, *J. Am. Chem. Soc.,* **2001**, *123*, 8876.

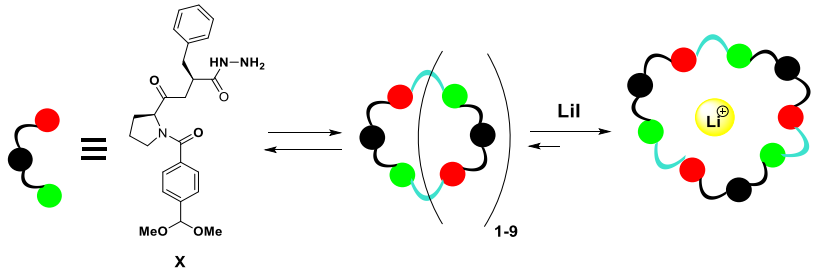

Figure 41. DCLs of cyclic pseudopeptides driven by template effect.

Among a series of possible reversible reactions[102], the formation of imines by the reaction of carbonyl compounds with an amine is one of the most widely employed to set up a DCLs[103]. This reaction is one of the oldest and most ubiquitous reactions in organic chemistry. There are many different factors which can influence the equilibrium: external ones, such as temperature, pH, solvent and concentrations or internal factors[104], such as steric and electronic features of the substrates, fig. 42. Additionally, the wide tolerance towards a broad variety of substituents allows the generation of DCLs with a broad structural diversity[105].

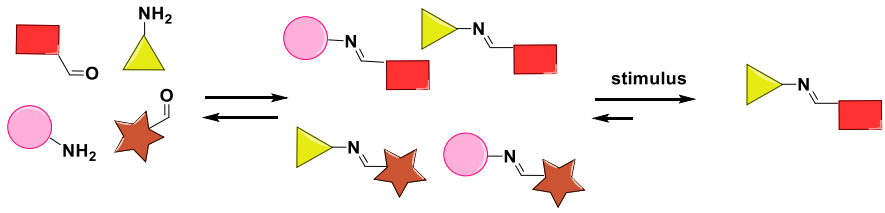

Figure 42. Adaptation of an imine based DCLs to a stimulus.

---

[102] a) P. T. Corbett, J. Leclaire, L. Vial, K. R. West, J.-L. Wietor, J. K. M. Sanders S. Otto, *Chem. Rev.*, **2006**, **106**, 3652; b) O. Ramstrom, J.-M. Lehn, *Nat. Rev. Drug Discovery*, **2002**, *1*, 26; c) S. J. Rowan, S. J. Cantrill, G. R. L. Cousins, J. K. M. Sanders, J. F. Stoddart, *Angew. Chem., Int. Ed.*, **2002**, *41*, 8982.
[103] C. Godoy-Alcantar, A. K. Yatsimirsky, J.-M. Lehn, *J. Phys. Org. Chem.*, ***2005***, *18*, 979
[104] M. He, J.-M. Lehn *J. Am. Chem. Soc.*, **2019**, *46*, 18560.
[105] A. Hermann, *Org. Biomol. Chem*., **2009**, *7*, 31954.

On the basis that the self-assembled resorcinarene capsule **CR_6** finds widely application as biomimetic catalyst because i) it presents a big electron-rich cavity to host neutral and cationic guests[46] ii) acts as H-bond catalyst and as mild Brønsted acid (pk_a 5.5-6.0)[47] and iii) shows interesting reagent and product selectivity, we wanted to investigate if **CR_6** is able to exert a supramolecular control over an imine based dynamic library.

4.2 Results and discussion

4.2.1 Modulation of 2 x 1 DCLs in presence of CR_6

Before starting the investigation on the DCLs, we needed to assess the bevahior of **CR_6** in the formation of imines in single experiment and for this initial study we focused our attention on the synthesis of imines **A74a** and **A74b**, starting from from *p*-chloroaniline **A,** benzaldehyde **74a** and *p*-trifluoromethylbenzaldehyde **74b**, respectively, scheme 11.

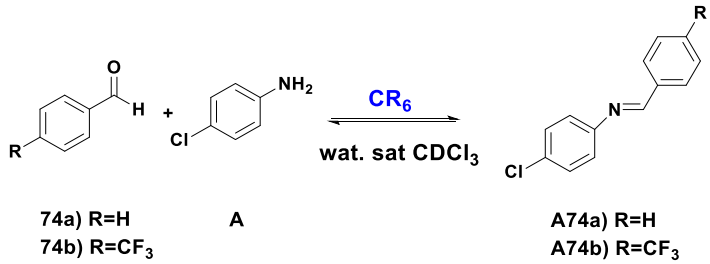

Scheme 11. Synthesis of imines **A74a** and **A74b** in presence of **CR_6**

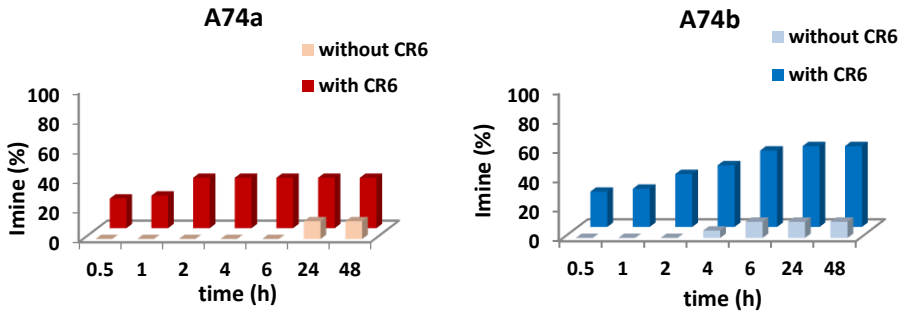

Figure 43. Formation of imines **A74a** (left) and **A74b** (right) during the single experiments in the presence or in the absence of the capsule **CR_6**.

In detail, the experiments were carried out in water saturated $CDCl_3$ at 30°C using aniline and aldehyde in equimolar ratio (42.3 mM) in the presence (42.3 Mm) or in absence of **CR_6**. The reactions were monitored as a function of time by quantitative ^{1}H NMR (qNMR) spectroscopy using 1,1,2,2-tetracloroethane (TCE) as internal standard. The imine-signals were integrated with respect to the signal of TCE, after addition of DMSO in order to disaggregate **CR_6.**

It was found that in both cases, **CR_6** sped up the formation of imines **74a** and **74b:** when we performed the reaction between **74a** and **A** in presence of **CR_6** the equilibrium was reached after 2h, leading to 34% of **A74a**, while without **CR_6** it was possible to detect the imine with 12% conversion only after 24h. When **74b** was mixed with **A** in presence of **CR_6**, the imine **A74b** reached an equilibrium value of 60% after 24h, while the reaction was slowed in absence of **CR_6**, fig. 43. These preliminary results indicated that **CR_6** promoted the formation of both imines and prompted us to investigate an imine based DCL with **A74a** and **A74b** as constituents and three

components, *p*-chloroaniline **A,** benzaldehyde **74a** and *p*-trifluoromethylbenzaldehyde **74b**, as depicted in scheme 12.

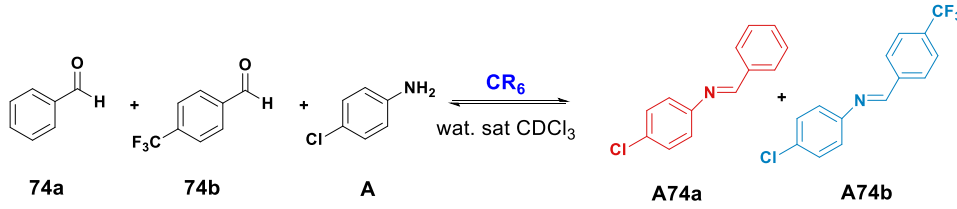

Scheme 12. Dynamic library formed by three components (**74a**/**74b**/**A**) and two constituents (**A74a**/**A74b**) in presence of **CR$_6$**.

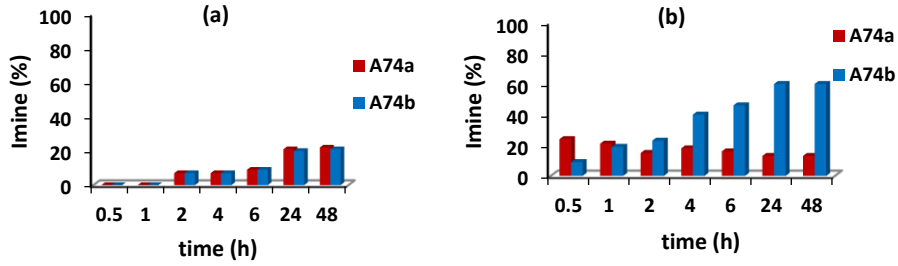

Figure 44. Distribution of imine **A74a** and **A74b** in the DCL in scheme 12 in absence (a) and in presence (b) of **CR$_6$.**

The experiments were carried out in water saturated $CDCl_3$ at 30°C using 42.3 mM of each components (**74a**, **74b**, **A** and **CR$_6$**). In absence of **CR$_6$**, the two imines **A74a** and **A74b** were formed in little and equal amount up to 48 h, fig. 44a. Interestingly, the DCL in scheme 12 can adapt its compositions to the presence of the capsule **CR$_6$,** fig. 44b. In fact, it is possible to detect both imines **A74a** and **A74b** already in the early stage of the reaction (30 min) with a conversion of 30% and 10%, respectively. The imine **A74a** was formed faster than **A74b**, but after 1 h **A74a** started to decrease while **A74b** increased until a constant **A74a**/**A74b** ratio (15/60) was reached after 24 h.

The results reported in fig. 44 showed that **A74a** was the kinetically favored product, while **A74b** was the thermodynamic one under these conditions.

At this point, in order to better understand our system, a new experiment was planned, depicted in scheme 13. According to this experiment, benzaldehyde **74a** and *p*-chloroaniline **A** were reacted in the presence of **CR$_6$** in order to form only imine **A74a**. After 24 h, when the conversion of **A74a** was 34%, **74b** (1 equiv.) was added to the mixture, fig. 45. Interestingly, 1 h later **A74b** started to form as **A74a** decreased until reaching the equilibrium 24 h later with a distribution pattern close to that achieved in the experiment in fig. 44b.

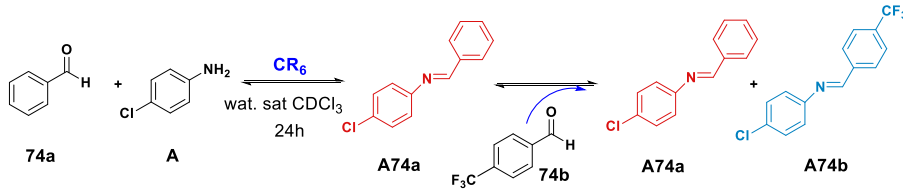

Scheme 13. DCL formed by three components (**74a**/**74b**/**A)** and two constituents (**A74a**/**A74b**) in presence of **CR$_6$**.

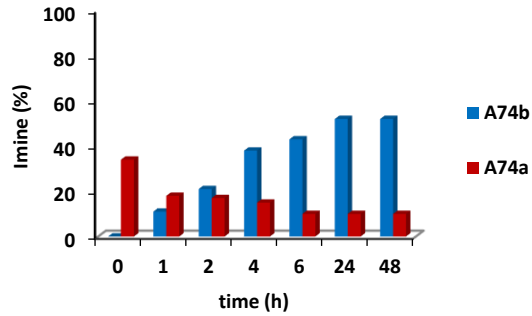

Figure 45. Distribution of imine **A74a** and **A74b** in the DCL in scheme 13 in presence of **CR$_6$**.

These results are remarkable: **CR_6** plays a dual role, in one hand thanks to its Brønsted acidity and ability to stabilize cationic intermediates, can accelerate the formation of imine and thus acting as catalyst; on the other hand **CR_6** acts as an external stimulus since the DCL composition of **A74a** and **A74b** adapts to its presence.

In order to find out the mechanism behind this modulation of the DCL, we evaluated the affinity **CR_6** for the substrates**,** carrying out an experiment in which **74a** and **74b** were in competition to occupy the inner cavity of **CR_6**, a value of 52% and 5% uptake[64] for **74a** and **74b** were measured after equilibration (1 h). These values indicated that **CR_6** shows a better affinity for the benzaldehyde **74a** and this is the reason why **A74a** is the preferred imine formed in the early stage of the reaction.

In addition to this experiment, further proofs of the encapsulation of benzaldehyde **A74a** inside **CR_6** came from NMR studies and in particular by DOSY and HSQC experiments (S29-S34, in the experimental section). In the same way, the encapsulation of the aldehyde **A74b** and **A** inside **CR_6** was supported by 1D and 2D NMR experiments. (S35-S41, in the experimental section).

The next step is to clarify the reason why **A74b** can be accumulated over the time while the **A74a** is suppressed and we evaluated the relative stability of both imines in water-saturated $CDCl_3$ in presence and in absence of **CR_6**, scheme 14.

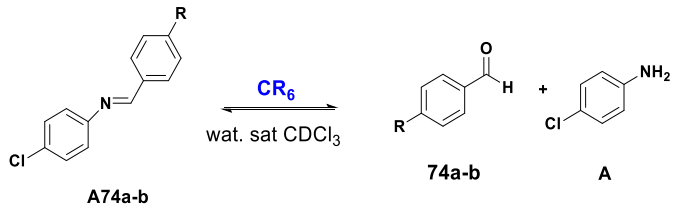

Scheme 14. Hydrolysis of imines **A74a-b** in presence **CR$_6$**

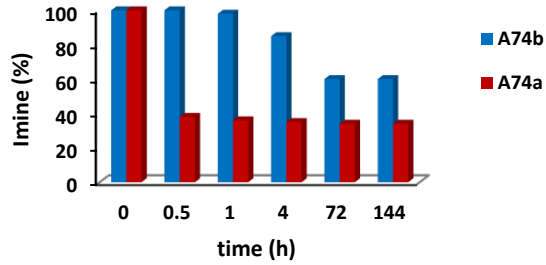

Figure 46. Hydrolysis of imines **A74a-b** in presence of **CR$_6$**.

When **A74a** was dissolved in water saturated $CDCl_3$ solution in presence of **CR$_6$** (1 equiv.), after 30 min a 62% of **A74a** was hydrolyzed into **74a** and **A,** and then, after 4 h the hydrolysis of **A74a** was close to the equilibrium with a 65% of conversion, fig. 46. Interestingly, a 29% uptake of **74a** inside **CR$_6$** was measured after 4h. This uptake of **74a** inside **CR$_6$** can suggest that probably, the benzaldehyde **74a** behaves like an inhibitor for the capsule **CR$_6$**, slowing down its catalytic activity. Under the same conditions but in the absence of **CR$_6$**, the imine **A74a** was stable over the reaction time and no hydrolysis products were detected (fig. S25, in the experimental section). These data clearly indicate that **CR$_6$** promotes the hydrolysis of **A74a** inside the cavity and this conclusion was also confirmed by another control experiments: when **A74a** was dissolved in water saturated $CDCl_3$ solution in presence of **CR$_6$** and DMSO, a solvent able to disaggregate the capsule, no

hint of **74a** and **A** was detected. Differently, the hydrolysis of **A74b** in the presence of **CR$_6$** was slower; in fact the equilibrium was reached after 72 h with a 40% of conversion of **A74b** into **74b** and **A**, fig 44. Considering these results, we proposed a mechanism for the kinetic and thermodynamic modulation of the DCL, depicted in fig. 47. The imine **A74a** is formed and accumulated preferentially during the early stage of the reaction, thanks to the better affinity of **74a** towards the encapsulation. Then, in presence of a significant amount of **A74a**, its hydrolysis starts quickly inside the capsule, catalyzed by its intrinsic Brønsted acidity, thus **CR$_6$** shows a remarkably predatory effect[106]. Differently, the formation of **A74b** is slower as well as its hydrolysis inside **CR$_6$** and for this reason it can be accumulated over long reaction time.

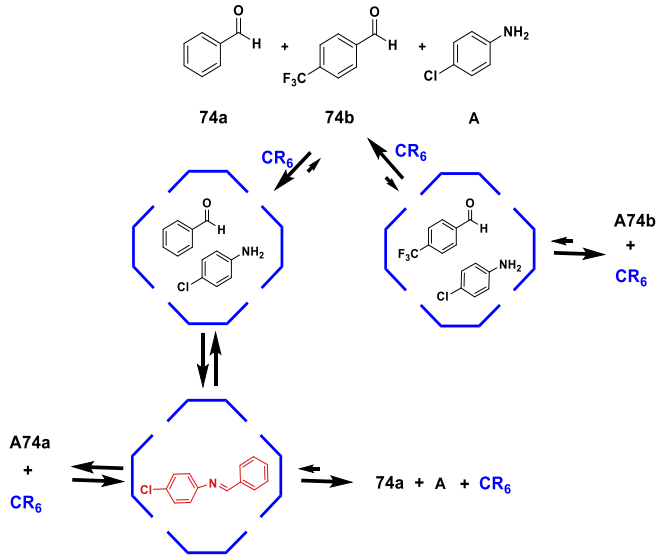

Figure 47. "Predatory" mechanism proposed for the adaptation of imine constituents in the DCL in scheme 12.

[106] a) T. Fujii, Y. Rondelez, *ACS Nano,* **2013**, *7*, 27; b) S. Dhers, J. Holub, J.-M. Lehn, *Chem. Sci.,* **2017**, *8*, 2125.

The difference in the hydrolysis reaction rate of **A74a** and **A74b** it is confirmed also by the uptake experiments: a very low-level of uptake of **A74b** inside **CR_6** was measured (<5%) while a bigger amount of **A74a** is encapsulated (45%). This means that **CR_6** has a very low affinity for **A74b** and this is also confirmed by QM calculations[107]: it was found an enthalpic stabilization of –22.14 kcal/mol and a Gibbs free energy stabilization of –8.08 kcal/mol for the formation of the **A74a⊂CR_6**[25] complex due to a strong H-bond interaction between the nitrogen atom of the imine moiety of **A74a** and a bridged water molecule of **CR_6**. Differently, the formation of the complex **A74b⊂CR_6** is unfavored: the presence of the more sterically demanding trifluoromethyl group forced **A74b** to stay on the axis that joins two vertexes of **CR_6** (fig. 48c-d) and the imine moiety of **A74b** is too far from the bridged water molecules of **CR_6** and cannot establish any H-bonding interactions.

[107] Quantum-mechanical studies were performed by Dr. Paolo Della Sala, Università degli studi di Salerno

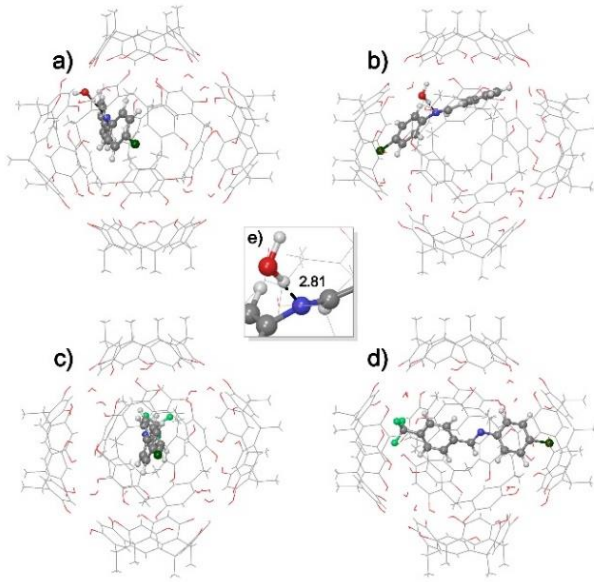

Figure 48. Different views of the optimized geometries of complexes: a) and b) **A74a⊂CR$_6$**; c) and d) **A74b⊂CR$_6$**; e) Particular of the H-bonding interaction of **A74a** with the bridged water molecule of **CR$_6$**.

Summarizing, the experimental and computational studies indicated that this is a rare case of kinetic and thermodynamic adaptation of an imine based DCL: **CR$_6$** can modulate the composition of a dynamic imine libraries by virtue the different affinity of the substrates and also thanks to a *predatory effect* on the imine products. A further proof of the *predator* role of **CR$_6$**, came from the modulation of the DCL in the presence of lower amount of **CR$_6$**. In presence of 0.5 equiv. of **CR$_6$** the kinetically favored imine **A74a** was prevalent up to 2h, fig. 49. Interestingly, working with 0.1 equiv. of **CR$_6$**, it was found that **A74a** is the predominant product to 20h, with a conversion of about 40%, higher than that detected in the presence of 0.5

equiv. (23%) and 1 equiv. (15%). These results indicated that the hydrolysis is promoted by **CR$_6$** and thus, supporting our hypothesis that the capsule **CR$_6$** acts as a predator for **A74a.**

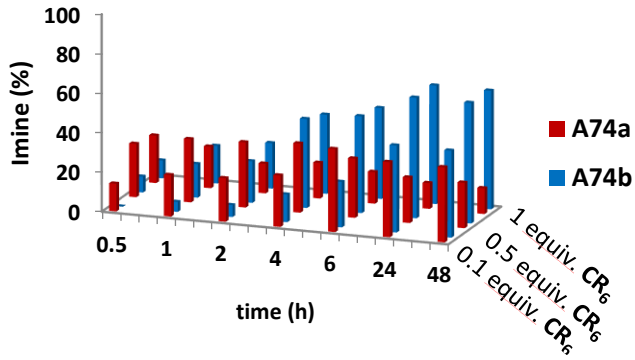

Figure 49. Evolution of the distribution of **A74a** and **A74b** with different amount of capsule **CR$_6$**.

Next, we turned our attention to study the effect of **CR$_6$** on different DCLs. In detail, replacing **74b** with *p*-nitrobenzaldehyde **74c** the DCL of three components **A**/**74a**/**74c** showed the same trend already observed for the first DCL: **CR$_6$** was able to thermodynamically drive the composition toward the formation of imine **A74c,** while the constituent **A74a** remained the kinetically favored one, fig. 50b. Interestingly, when the *p*-methoxybenzaldehyde **74d** was used instead of **74b**, the imine **A74a** was the preferred product during all the reaction time, even in low-moderate conversion. Probably, **A74d** acting as inhibitor, occupied the cavity of **CR$_6$** and prevented the hydrolysis of **A74a.**

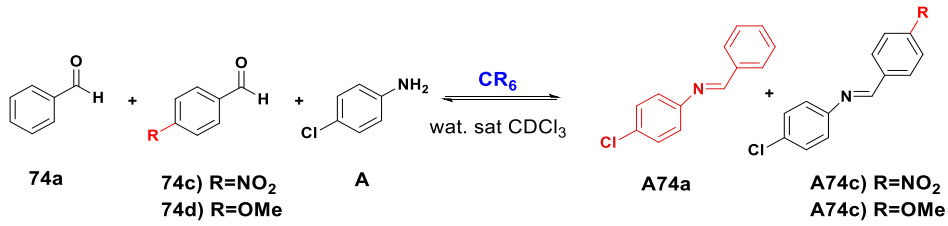

Scheme 15. DCLs formed by three components (**74a/74c-d/A**) and 2 constituents (**A74a/A74c-d**) in presence of **CR**$_6$.

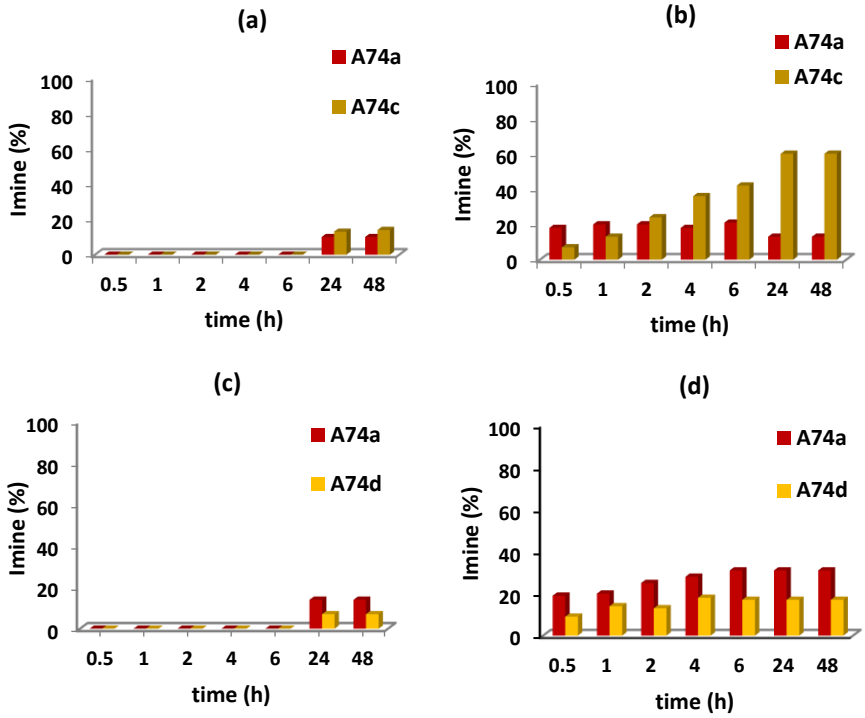

Figure 50. Distribution of imine constituents **A74a/A74c** (top) and **A74a/A74d** (bottom) in the DCL in presence (b, d) and in absence (a, c) of **CR**$_6$.

Next, we moved to study the behavior of DCLs formed by **74a, 74b** and different anilines, such as aniline **B** and *p*-methoxyaniline **C**, and an aliphatic one, *n*-butylammine **D**, Scheme 16.

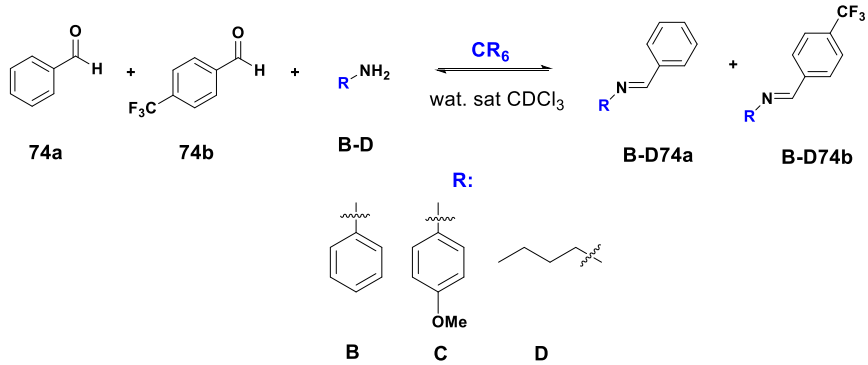

Scheme 16: DCL formed by three components **(74a/74b/B-E)** and two constituents (**B-D74a**/**B-D74b).**

When **A** was replaced by the aniline **B** in the three reaction components **74a/74b/B,** it was found that as well as the examples reported before, the reaction was faster in presence of **CR_6**: in 30 min it was possible already to detect the mixture of both imines with **B74a** as main product, while, in absence of **CR_6** the reaction was slower, fig. 51. Interestingly, over the reaction time **CR_6** exerts a predatory effect on **B74a**: after 1 h the amount of **B74a** started to decrease as **B74b** increased, reaching the equilibrium distribution of **B74b**/**B74a** ratio of 52/10 after 6h.

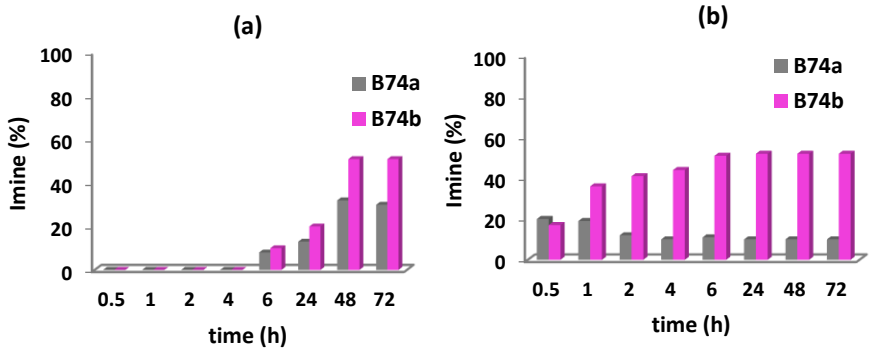

Figure 51. Distribution of imine constituents **B74a** and **B74b** in the DCL in absence (a) and in presence (b) of **CR$_6$**.

The predatory effect of **CR$_6$** on **B74a** was confirmed by the studies on the relative stability of the imine in presence and in absence of **CR$_6$**: as expected, **CR$_6$** promotes quickly the hydrolysis of the imine into **B** and **74a**, while it was found stable in water-saturated $CDCl_3$ after longer time, fig. 52.

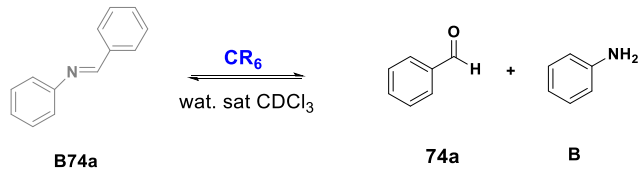

Scheme 17 Hydrolysis of the imine **B74a** in presence of **CR$_6$**.

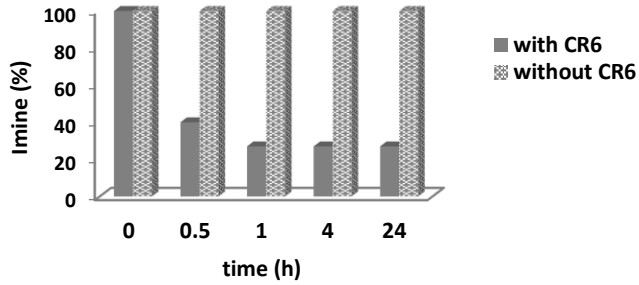

Figure 52. Hydrolysis of the imine **B74a** in presence **CR_6**.

These results suggested that, even changing the aniline from **A** to **B**, the benzaldehyde-based imines (**A74a** and **B74a**) are the kinetically favored products, while the imines obtained by **74b** (**A74b** and **B74b**) are the thermodynamic ones and the modulation in the composition of the DCLs is driven by the combination of the affinity of the **CR_6** for the substrates and an unusual predatory effect on one of the constituents.

When **A** was replaced by the *p*-methoxyaniline **C** in the three components reaction **74a/74b/C,** the capsule **CR_6** still promoted the formation of imines, even though little kinetic modulation was observed: for the whole reaction time **C74b** was the preferred product with a ratio **C74a/C74b** 32/67, while the reaction without **CR_6** proceeds slowly affording an equimolar amount of both imines, fig. 53.

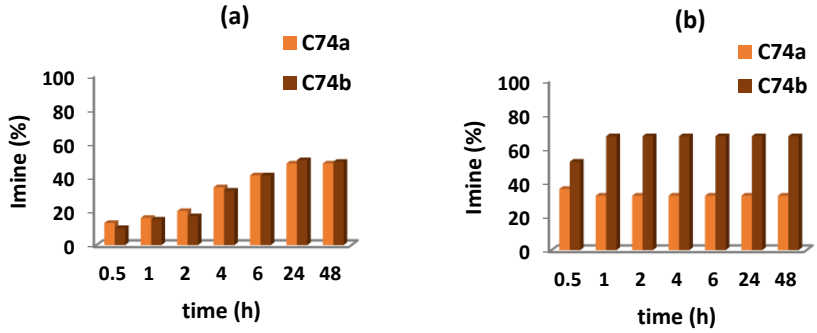

Figure 53. Distribution of imines **C74a** and **C74b** in the DCL in absence (a) and in presence (b) of **CR**$_6$.

Additionally, in presence of **CR**$_6$ a slight predatory effect was observed on the imine **C74a** that was confirmed by the study of the stability of **C74a** in water-saturated $CDCl_3$ with and without **CR**$_6$, scheme 14. It was found that **C74a** was rapidly hydrolyzed in the presence of capsule **CR**$_6$, while it was stable without **CR**$_6$, fig. 54.

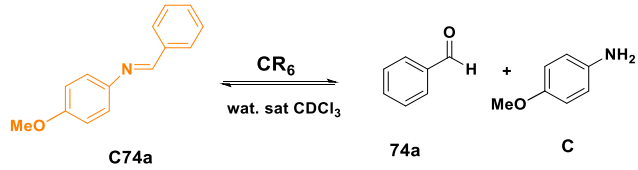

Scheme 14. Hydrolysis of imine **C74a** in presence **CR**$_6$.

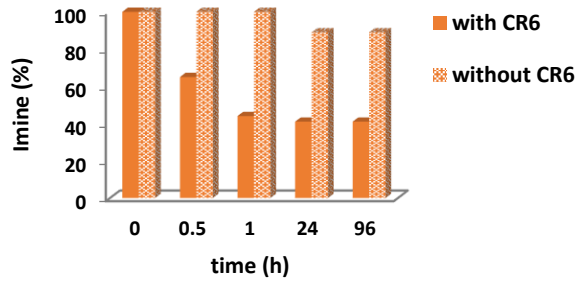

Figure 54. Hydrolysis of the imine **C74a** in presence **CR**$_6$**.**

Remarkably interesting results were observed when *n*-butylamine **D** was mixed with **74a** and **74b** in the three components reaction: the formation of

imines **D74a** and **D74b** was favored in the absence of **CR$_6$**, reaching a 17% and 40% conversion after 24h, respectively, while in presence of **CR$_6$**, they are detected in very small amount (3% and 13% conversion, respectively for **D74a** and **D74b**), fig. 55.

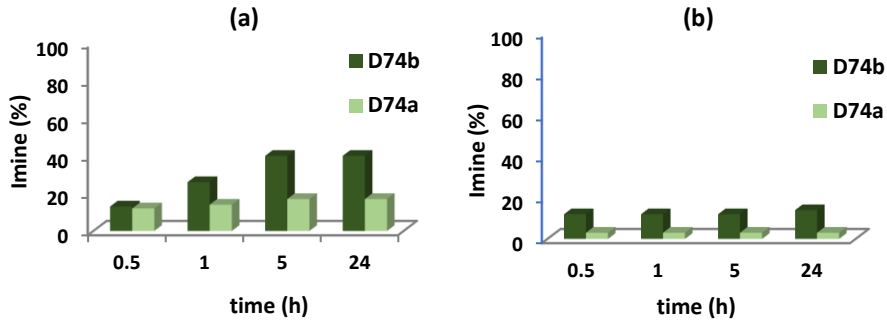

Figure 55. Distribution of imine constituents **D74a** and **D74b** in the DCL without (a) and with (b) the capsule **CR$_6$**.

This unusual trend can be explained in term of different basicity of the amines used in our study. In fact, according to Tiefenbacher[46], aliphatic amines such as **D**, were almost totally protonated by **CR$_6$** and thus encapsulated as cationic species. For this reason, only a low amount of **D** in neutral form can be converted into products inside the capsule. Differently, *p*-chloroaniline **A** was encapsulated as neutral form and consequently can react with aldehydes.

At this point, we wanted to investigate the behavior of the three components reaction in which **A** and **D** were in competition for the aldehyde **74a**, scheme 18. In absence of **CR$_6$**, the imines **D74a** and **A74a** were formed in 50% and 25% yield, respectively, fig. 56. Differently, in the presence of **CR$_6$**, **A74a** was favored, reversing the selectivity order to 15/25 **D74a**/**A74a**.

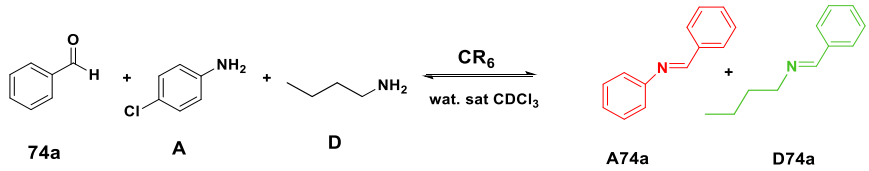

Scheme 18. DCL formed by three components (**74a/A/D)** and two constituents **(A74a/D74a)** in presence of **CR**$_6$.

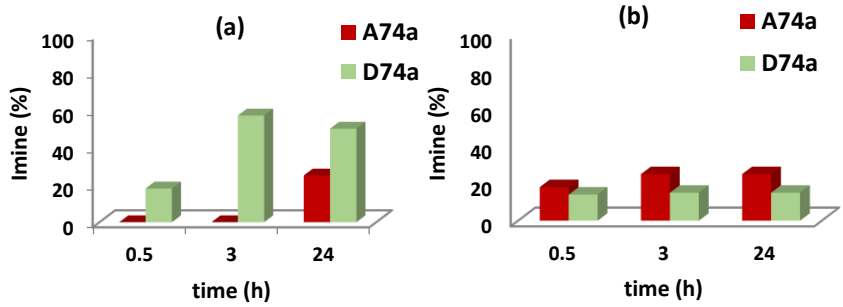

Figure 56. Distribution of imine **A74a** and **D74a** in absence (a) and in presence (b) of **CR**$_6$.

These results showed an interesting example of substrate selectivity driven by the different affinities for the protonation of **A** and **D** in presence of **CR**$_6$: while the more basic *n*-butylammine **D** is almost totally protonated and encapsulated as cationic form, preventing the conversion into imine **D74a**, the less basic *p*-chloroaniline **A** is encapsulated as free guest and can react with **74a** leading the selective formation of **A74a.**

4.2.2 Modulation of 2 x 2 DCLs in presence of CR_6

In comparison to the astonishing ability of natural enzymes to work in a very selective way even in complex mixtures of substrates, we wanted to investigate the ability of **CR_6** to control the distribution of DCLs derived by four components system. In this regard, we initially choose a four component system composed by **74a**, **74b**, **A** and **B**, scheme 19.

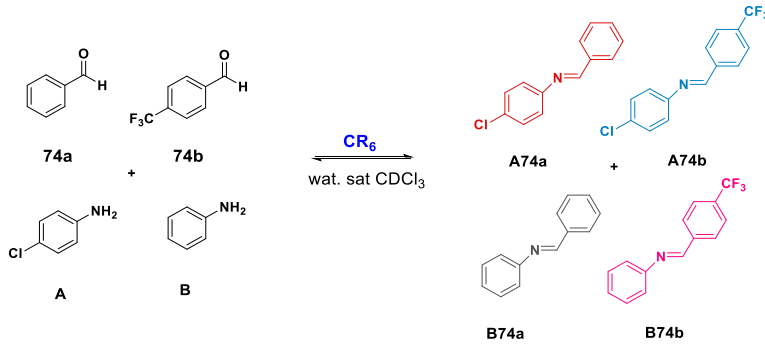

Scheme 19. DCL formed by four components (**74a/74b/A/B**) and four constituents (**A74a/A74b/B74a/B74b**) and in presence of **CR_6.**

In presence of **CR_6** the formation of imines was faster: a mixture of all four imines was detected in the early stage of the reaction with **A74a** and **B74b** as main components (25% and 20%). Over the reaction time, **A74b** and **B74b** were accumulated while **A74a** and **B74a** decreased because of the predatory effects of **CR_6** on both imines, until reaching the equilibrium distribution with **A74b** and **B74b** are the main products. In the absence of the capsule, the composition of the DCL showed no significant preference in the distribution of the imines, fig. 57.

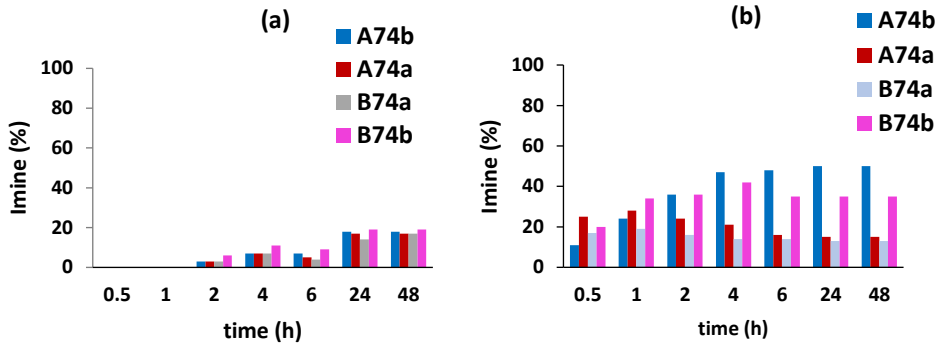

Figure 57. Distribution of imine constituents **A74a**, **A74b, B74a** and **B74b** in the DCL, without (a) and with (b) capsule **CR$_6$**.

Next, it was studied also the adaptation of a second DCL derived by the four components system **74d**/**74b**/**C**/**E**, scheme 20. The formation of imines was more efficient in the presence of **CR$_6$**, fig. 58: within the first 30 min of the reaction a mixture of all the possible imines was detected with **C74b** and **C74d** as main components, with a **C74b/C74d** ratio of 47/19, while the imines **E74b** and **E74d** were present in insignificant amounts. Over the reaction time the predatory effect on **C74d** forcing its hydrolysis into **74d** and **C**, led to the final imine distribution with a composition **C74b**, **E74b**, **C74d** and **E74d** of 66, 12, 5 and 5%, respectively, with **C74b** as main constituent.

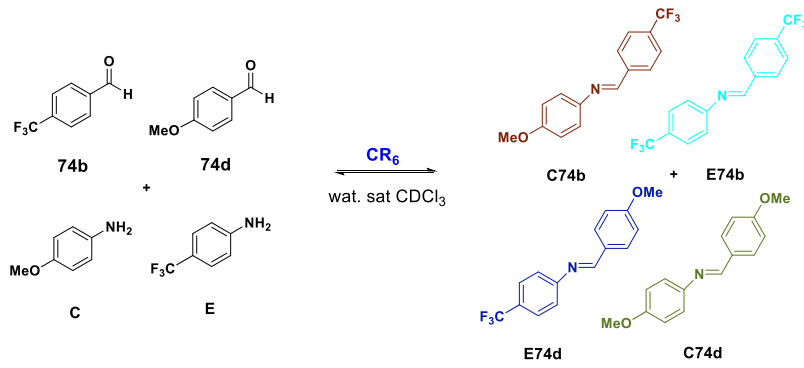

Scheme 20: DCL formed by four components (**74b/74d/C/E**) and four constituents **(C74b/C74d/E74b/E74d)** in presence of **CR$_6$.**

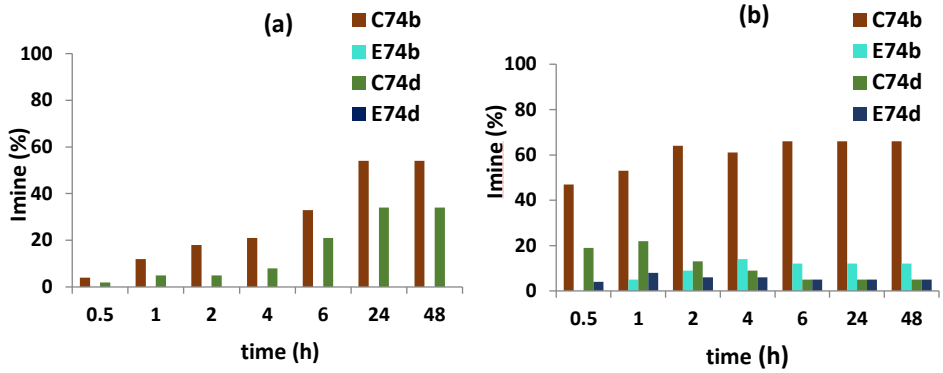

Figure 58 Distribution of imine constituents **C74b**, **E74b**, **C74d** and **E74d** in without (a) and with (b) capsule **CR$_6$**.

These results clearly showed that **CR$_6$** can exert a fine control over the distribution of imines even in a more complex DCLs, thus confirming the potentiality of **CR$_6$** as an artificial enzyme.

4.3 Conclusions

In conclusion, experimental and computational data have demonstrated that the hexameric resorcinarene capsule **CR_6** is able to control the composition of imine based dynamic covalent libraries. In detail, the DCL of imines **A74a** and **A74b** is influenced by the presence of **CR_6** showing a kinetic and thermodynamic preference for the products. The imine **A74a**, formed by reaction of benzaldehyde **74a** with and *p*-chloroaniline **A**, is the kinetically favored product and predominates the composition in the early stage of the reaction, thanks to the preferred encapsulation of **74a** inside the nanocavity of **CR_6**. Additionally, the capsule shows a *predator effect* on the imine **A74a**: after the formation, **CR_6** quickly promotes its hydrolysis in **74a** and **A**, avoiding the accumulation in the reaction mixture. On the contrary, thanks to its low affinity for the encapsulation, **A74b** is protected by the hydrolysis and can be accumulated in long reaction time. Finally, **CR_6** drives also more complex 2x2 DCL systems exerting a thermodynamic and kinetic modulation of the constituents with a good selectivity.

Chapter 5. Hexameric resorcinarene capsule in the promotion of Lewis-Acid catalysis by the in-situ generation of a carbocation

5.1 Introduction

Use of Lewis acids is one of the most common strategies for catalytic activation in organic chemistry. The most employed ones are based on metals (Al, Ti, Li, Mg, Cu, etc.) or metalloid compounds (B, Si) and they owe their reactivity to a low-lying LUMO that can accept an electron pair[108,109]. However, many metal-based Lewis acids suffer from several drawbacks, such as high costs, toxicity and waste treatment[110].

A potential Lewis acid that has been almost completely ignored in catalysis is the carbocation. They are in general considered unstable and not isolable intermediates in several reactions, but some of them are stable enough to be isolated and kept in air without any specific precautions[111]. The most common and quite stable carbocation is the triphenylmethylcation, called trityl cation (Try^+), because of the possibility to delocalize the positive charge on the three aromatic rings[112]. The trityl cation is characterized by a low-lying empty p orbital capable of accepting electrons and thereby

---

[108] S. Saito, Y. Motoyama, H. Nishiyama, *Lewis Acids in Organic Synthesis*, Yamamoto, H., Ed. Wiley-VCH: Weinheim, **2000**.
[109] a) K. Hara, R. Akiyama, M. Sawamura, *Org. Lett*., **2005**, *7*, 5621; b) R. Schmidt, K. Müther, C. Mück Lichtenfeld, S. Grimme, M. Oestreich*, J. Am. Chem. Soc*., **2012**, *134*, 4421; c) H. F. T. Klare, K. Bergander, M. Oestreich, *Angew.Chem*. **2009**, *121*, 9241.
[110] B.Fubini, C. Otero Areán, *Chem. Soc. Rev.,* **1999,** *28*, 373.
[111] G. A. Olah, G. K. S. Prakash, *Carbocation Chemistry* Wiley, Hoboken, **2004.**
[112] c) M. Horn, H. Mayr *Chem. Eur. J.* **2010,** *16*, 7469.

making, for example, an electrophile more susceptible to the nucleophilic attack, fig. 59.

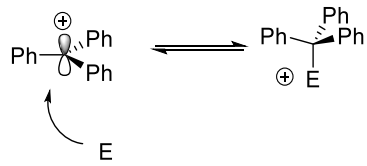

Figure 59. Carbocation activation of electrophiles.

Additionally, the Lewis acidity of the trityl cation can be modulated by variation of the electronic properties of the aromatic groups: the increase in the electron density of the aromatic rings further stabilizes the positive charge, thus leading to a decrease of Lewis acidity and, consequently, of reactivity, fig. 60. In fact, in the Mayr's scale[113], trityl cations display a wide range of reactivity towards water depending on the nature of groups on the aromatic rings: we pass from the simple high reactive trityl cation **C1** to the tris(*N,N*-dimethylaniline)methylium ion **C3** (crystal violet), stable in water.

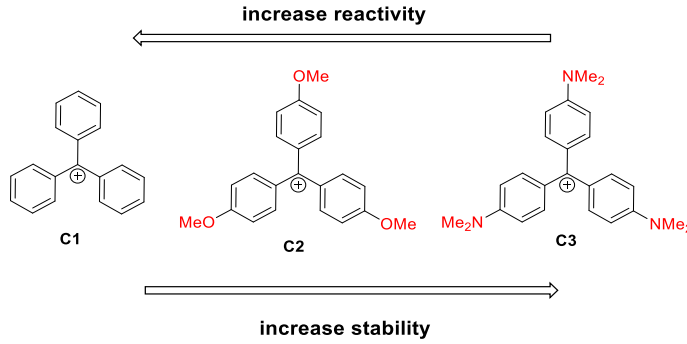

Figure 60. Electronic effects of the trityl cations on Lewis acidity and stability.

[113] a) H. Mayr, A. R. Ofial, *J. Phys. Org. Chem.*, **2008**, *21*, 584; b) M. Horn, H. Mayr, J. *Phys. Org. Chem.* **2012**, *25*, 979.

Thanks to their reactivity features, Franzén's group has demonstrated that **TryBF$_4$**, an inexpensive commercially available carbocation, stable enough to handle without any special precautions, is an efficient catalyst for several reactions[114], such as Diels–Alder, Aza-Diels-Alder, Michael Addition. In detail, very low catalyst loading (0.05-5mol%) is necessary to promote the reaction between several dienes and dienophile in an efficient and selective way, fig. 61.

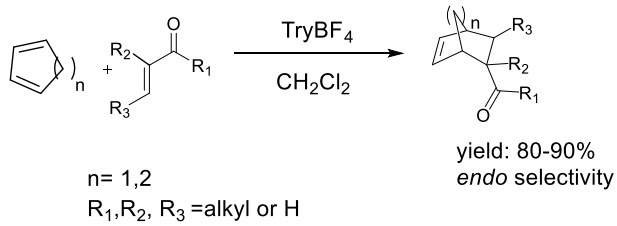

Figure 61. Diels-Alder reaction promoted by **TryBF$_4$**.

On the basis of these considerations and with the aim to further expand the application of **CR$_6$,** we wanted to investigate if a Diels-Alder reaction can occur inside the cavity of **CR$_6$** by Lewis acid activation mediated by a carbocation generated in situ.

Recently, our group has demonstrated that the bridging water molecules of **CR$_6$** play a catalytic role in the promotion of a Friedel Craft reaction between heteroarenes and benzyl chloride, polarizing the C-Cl bond through a H-bond interaction and thus facilitating the nucleophile attack[55]. Starting from this consideration, we envisioned that a similar interaction could occur with **TryCl.** In this case, the abstraction of chloride anion could lead to the Try$^+$ carbocation formation, which will be stabilized inside the electron rich

[114] V. R. Naidu, S. Ni, J.Franzén, *ChemCatChem* **2015**, *7*, 1896; b) J. Bah, V. R. Naidu, J. Teske, J. Franzén, *Adv. Synth. Catal.* **2015,** *357*, 48 c) J. Bah, J. Franzén, *Chem. Eur. J.* **2014,** *20*, 1066.

cavity of **CR$_6$** and, thus, it would be capable of activating the Diels-Alder reaction, Fig. 62b.

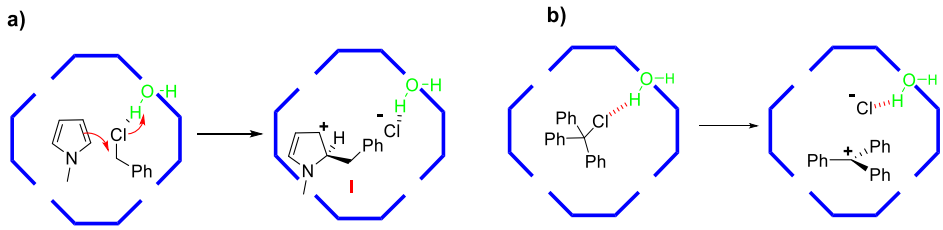

Figure 62. Two activation mechanisms proposed for a) Friedel-Craft and b) in situ generation of trityl cation.

5.2 Results and discussion

The study started with the investigation of a Diel-Alder (DS) reaction between cyclohexadiene **10** and crotonaldehyde **21a** in presence of **TryCl** and **CR$_6$**, scheme 21. At first, we performed the reaction using an equimolar amount of diene and dienophile in the presence of 26% of **CR$_6$** and 26% **TryCl** in water-saturated $CDCl_3$ at 30°C. Under these conditions (entry 1, Table 10), we obtained exclusively the *endo* product **78a** in 35% yield. When the reaction was performed under the same conditions but in the absence of **CR$_6$,** no conversion was observed. Interestingly, if the reaction was carried out in presence of **CR$_6$** but without **TryCl**, no products were detected. These initial studies supported the hypothesis that the synergistic combination of **CR$_6$** and **TryCl** played a key role in the efficiency of the reaction. Furthermore, if **TryCl** was not able to promote the reaction by itself, the presence of capsule **CR$_6$** probably promoted the generation of the Try$^+$ carbocation inside its own cavity and, thus, the real reaction catalyst.

Encouraged by these results, we performed a series of experiments playing with the reaction conditions in order to optimize the efficiency of the reaction.

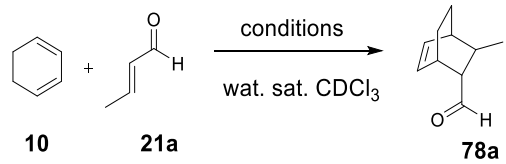

Scheme 21. DS reaction between cyclohexadiene **10** and crotonaldehyde **21a.**

Table 10: Optimization of the reaction condition for DS reaction between **10** and **21a**.

Entry [a]	CR_6 (mol%)	TryCl (mol%)	10:21a	T (°C)	Conv. [b] (%)	Yield (%)[c]	*Endo:exo*[d]
	26	26			40	35	>99:1
	26	--			--	--	--
1			**1:1**	**30**			
	--	26			--	--	--
	--	--			--	--	--
	26	26			60	50	>99:1
	26	--			--	--	--
2			**1:1**	**50**			
	--	26			--	--	--
	--	--			--	--	--
	26	26			quant	92	>99:1
	26	--			--	--	--
3			**3:1**	**50**			
	--	26			--	--	--
	--	--				--	--
					--		
	52	26			85	76	>99:1
4			**3:1**	**50**			
	52	--			--	--	--
5	26	52			quant	90	>99:1
			3:1	**50**			
	--	52			--	--	--

[a] 0.16 mmol of **21a** in 1.1 mL of wat. sat. $CDCl_3$. [b] Determinated by ^1H NMR analysis of the reaction mixture [c] Yields of the isolated products by chromatography on column. [d] Determined by ^1H NMR analysis of the isolated product.

Carrying out the reaction at 50°C in presence of **CR_6** and **TryCl**, adduct **78a** was obtained in 50% yield. Conversely, in the absence of **TryCl** or **CR_6** or both, no product was detected in the reaction mixture (entry 2, Table 10). Then, the influence of the **10/21a** ratio was also evaluated. When an excess of **10** with respect to **21a** was used, we observed an increase of the reaction efficiency in terms of conversion into **78a**, preserving the high level of *endo* selectivity (entry 3, Table 10). Additionally, we studied the effect of molar ratio of **CR_6/TryCl** on the reaction efficiency: with 2/1 ratio, we observed a decrease in term of conversion (entry 4, Table 10). This behavior could be explained by the presence of individual diene, dienophile or **TryCl** complexes with the capsule preventing the reactants to come in direct contact in the same nanocontainer. When the reaction was performed with **CR_6/TryCl** in 1/2 ratio, there was no influence on the conversion (entry 5, Table 10), this clearly indicated that **TryCl** did not act as inhibitor for the reaction.

At this point, to confirm that the reaction took place inside **CR_6**, we carried out some control experiments according to protocol previously reported[46,47]. In detail, one reaction was run in presence of the cationic competitive Et_4NBF_4 guest that, showing a high affinity for **CR_6,** occupied its cavity (entry 1, Table 11) and the second one in presence of DMSO, a H-bond solvent competitor able to disaggregate the capsule (entry 2, Table 11). In both cases, any product was observed, thus confirming that the reaction took place inside the cavity. Other evidence came from the NMR

study regarding the proofs of the encapsulation of the reagents **10, 21a** and **TryCl** inside the nanoconfined space of **CR_6**. My research group have previously reported a detailed 2D NMR study which demonstrated the encapsulation of **21a** inside **CR_6**[47]**.** In the same manner, we studied the encapsulation of **TryCl** inside **CR_6:** in the DOSY experiment of the mixture **TryCl**/**CR_6**, the diffusion coefficient of incapsulated **TryCl** was aligned with those of the capsule, thus probing its internalization in **CR_6** (fig. S45, in the experimental section). Unfortunately, in the case of **10,** the signals of the encapsulated species were overlapped with those of **CR_6**, making the study not useful.

Table 11: Control experiments of **DS** reaction between **10** and **21a**

Entry[a]	CR_6	TryX	Additive (equiv.)[b]	Conv.[c] (%)	Yield (%)[d]	*Endo:exo*[e]
1	yes	-Cl	Et_4NBF_4 (10)	--	--	--
2	yes	-Cl	DMSO (30)	--	--	--
3	yes	$-BF_4$	--	quant.	90	>99:1
4	no	$-BF_4$	--	50	43	>99:1
5	yes	-OH	--	--	--	--
6	no	-OH	--	--	--	--
7	yes	-Br	--	75	68	>99:1
8	no	-Br	--	--	--	--

[a]Reaction conditions: **10** (0.45 M), **21a** (0.15 M), **CR_6** and **TryX** (0.039M) in 1.1 mL of water-saturated $CDCl_3$ at 50 °C for 16h. [b] Amount of additive respect to **CR_6**. [c] Determinated by ^1H NMR analysis of the reaction mixture. [d] Yields of the isolated products by chromatography on column. [e] Determined by ^1H NMR analysis of the isolated product.

Next, in order to prove that the activation of the carbonyl group of the crotonaldehyde **21a** was mediated by trityl cation Try^+, generated in situ inside the cavity from **TryCl**, we carried out the reaction replacing **TryCl** with trityl tetrafluoroborate **$TryBF_4$,** a typical carbocation Lewis acid catalyst. When the reaction was performed in the presence of both **CR_6** and **$TryBF_4$**, a total conversion into **78a** was observed. Conversely, in the absence of **CR_6, 78a** was obtained in only 43% yield, (entries 3 and 4, Table 11). These results suggest that the reaction is Try^+ cation promoted and the capsule **CR_6** induces the generation of the carbocation through the cleavage of the C-Cl bond mediated by an H-bond interaction with a bridging water molecule of the **CR_6** structure. Furthermore, the π-electron rich aromatic walls of **CR_6** stabilize the incipient trityl cation suppressing uncontrolled catalyst interceptions.

At this point, we investigated the possibility to use different precursors of the carbocation Try^+ in combination with capsule **CR_6** and to evaluate the influence on the DS reaction outcome. When the reaction was carried out replacing **TryCl** with **TryOH**, no conversion was observed, either in the absence and in the presence of **CR_6** (entries 5 and 6, Table 11), indicating that **CR_6** was unable to stimulate the formation of the trityl cation from **TryOH.** Insterestingly, using **TryBr**, the product **78a** was obtained with 68% of yield, while, in absence of **CR_6**, no product was observed (entries 7 and 8, Table 11). Thus, **TryCl** shows itself to be a better carbocation Try^+ precursor than **TryBr** within the cavity, despite bromine being reported as a better leaving group than chlorine. The highest conversion observed with **TryCl** compared to **TryBr** could be explained by the fact that **CR_6** would promote more efficiently the abstraction of Cl^- (and then also a better stabilization)

than Br^-. Based on these considerations, we have proposed the mechanism depicted in fig. 63 for the in situ-formation of Try^+ carbocation and the reaction outcome. **CR_6** is capable of hosting **TryCl** followed by crotonaldehyde **21a** and cyclohexadiene **10**. After the encapsulation of **TryCl**, the formation of a hydrogen-bonding interaction between a bridging water molecule in **CR_6** structure and the chlorine atom promotes the heterolytic carbon-chloride bond cleavage and, thus, the generation of Try^+ carbocation. At this point, the Try^+ carbocation, stabilized inside the electron-rich cavity of **CR_6**, interacts with the carbonyl group of crotonaldehyde **21a** causing a lowering of its LUMO and, thus, making **21a** more susceptible towards the attack of the cyclohexadiene **10**.

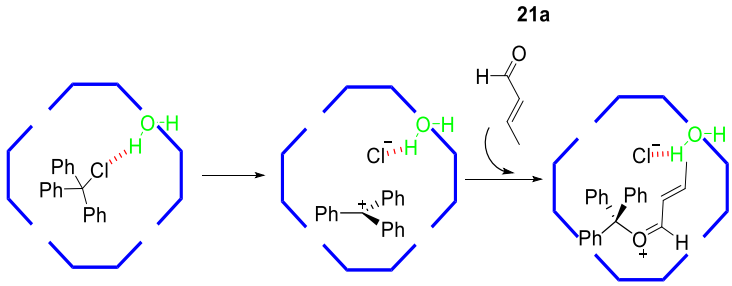

Figure 63. Proposed mechanism for the abstraction of chloride anion inside **CR_6**.

Further evidence that the catalysis arises from in situ formation of the trityl cation by abstraction of chloride anion inside the cavity was probed by UV-VIS spectroscopy. The UV-Vis spectra of a free trityl ion, such as **$TryBF_4$**, shows the characteristic twin absorption at λ = 425 and 405 nm. After mixing **CR_6** and **$TryBF_4$**, the typical orange solution of **CR_6** became dark red and the characteristic UV-Vis absorption of the trityl cation is still present even if the twin band is less defined (S46-S47, in the experimental section). Conversely, UV-Vis spectra of the single **CR_6** shows an absorption at λ = 290

while the free **TryCl** exhibits no significant absorption. When **CR_6** and **TryCl** were mixed, the typical orange solution turns into dark red and in the UV-Vis spectra a new band appeared at the same wavelength of those observed for the solution **$TryBF_4$/CR_6**, thus this new absorption can be attributed to the trityl ion generated in situ.

With these results in the hand and with the optimized reaction conditions illustrated in entry 3, Table 10, we decided to investigate the scope of the DS reaction promoted by the combined action of **CR_6** and **TryCl** exploring different dienophiles.

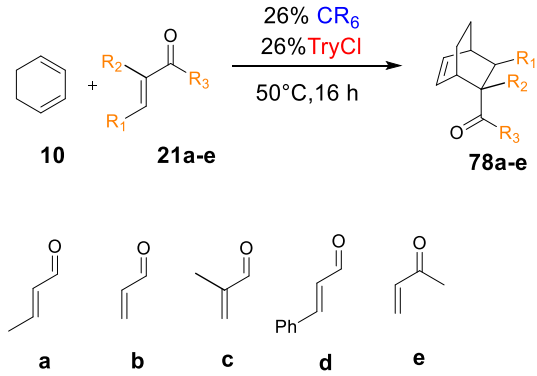

Scheme 22. Scope study for the DS reaction between diene **10** and dienophiles **21a-e.**

Table 12: Control experiments of DS reaction between **10** and **21a-f.**

Entry[a]	21	Conv.(%)[b]	Yield(%)[c]	*Endo*:*exo*[d]
1	21a	quant.	92	>99:1
2	21b	quant.	85	>99:1

3	21c	quant.	88	>99:1
4	21d	50	47	>99:1
5	21e	quant.	87	>99:1

[a]Reaction conditions: **10** (0.45 M), **21a-e** (0.15 M), **CR_6** and **TryCl** (0.039M) in 1.1 mL of water-saturated $CDCl_3$ at 50 °C for 16h. [b] Determinated by ^1H NMR analysis of the reaction mixture. [c]Yields of the isolated products by chromatography on column. [d]Determined by ^1H NMR analysis of the isolated product.

The DS reaction was found to be tolerant for all the dienophiles used. Interestingly, the use of smaller ones (**21a-c** and **21e**) leads to the corresponding DS products in high yields, while for bigger aldehyde such as *trans*-cinnamaldehyde **21d** only 50% of conversion was observed. These results suggested a substrate-selection ability of **CR_6** which exerts a control over the reaction efficiency: after the encapsulation of **TryCl** within the cavity of **CR_6**, the residual space available allows for selective access to the confined space of only dienophiles of appropriate size, thus activating them towards the DS reaction.

5.3 Conclusions

We have demonstrated that the hexameric resorcinarene capsule **CR_6** is able to promote the conversion of **TryCl** into Try^+, which represents the real catalyst for the Diels-Alder reaction between cyclohexadiene and α/β insaturated carbonyl compounds.

It is plausible that the activation of the pre-catalyst is achieved thanks to a H-bond interaction involving the bridging water molecule of **CR_6** and the chlorine atom, which favours the abstraction of Cl^-. Additionally, the big electron rich cavity of **CR_6** is perfect to stabilize Try^+ and most of all to prevent its quench. In this case, **CR_6** does not act as catalyst itself, but it plays a crucial role for the promotion of the DS reaction, exerting also a control over the reaction thanks to the substrate selectivity.

Chapter 6. Summary

6.1 Final conclusions

With this phD research project, it was confirmed the importance of carrying out organic reactions in a nanoconfined space. In detail, the synergic interplay between the nano-confinement effect with the catalytic features of the self-assembled resorcin[4]arene **CR_6** makes it a powerful and versatile biomimetic catalyst. In fact, it was proved that **CR_6** promotes type Friedel-Craft reaction in very efficient and selective way in mild conditions thanks to its H-bonding ability and its intrinsic Brønsted acidity, leading the formation of significant building blocks for the synthesis of more complex structures with pharmaceutical and biological activity.

Additionally, an interesting behavior was observed in dynamic covalent libraries (DCLs) in the presence of **CR_6**: the capsule drives the composition of DCLs by virtue of substrate selectivity and an unusual predatory effect on one of the constituents.

In the end, it was demonstrated **CR_6** was able to generate in situ a tritylium carbocation by halide abstraction mediated by the bridging water molecules in the structure of the capsule, and thus promoting a Diels-Alder reaction inside the cavity.

Chapter 7. Experimental Section

7.1 General Remarks

All chemicals were reagent grade and were used without further purification. Solvents were purchased from Aldrich. Reaction temperatures were measured externally; reactions were monitored by ^{1}H NMR spectroscopy and by TLC on Merck silica gel plates (0.25 mm) and visualized by UV light. Flash chromatography was performed on Merck silica gel (60, 40-63 µm). NMR spectra were recorded on Bruker Avance-600 spectrometer [600.13 MHz (^{1}H) and 150.03 MHz (^{13}C)], Bruker Avance-400 spectrometer [400 (^{1}H) and 100.57 MHz (^{13}C)], Bruker Avance-300 spectrometer [300 (^{1}H) and 75.48 MHz (^{13}C)]; chemical shifts are reported relative to the residual solvent peak ($CHCl_3$: δ 7.26, $CDCl_3$: δ 77.23). DOSY experiments were performed on a Bruker Avance-600 spectrometer equipped with 5 mm PABBO BB|19F-1H\D Z-GRD Z114607/0109. The standard Bruker pulse program, ledbpgp2s, employing a double stimulated echo sequence and LED, bipolar gradient pulses for diffusion, and two spoil gradients were utilized. Diffusion times were 150 ms, eddy current delay was 5 ms, gradient recovery delays were 0.2 ms, and gradient pulse was 1400 ms. Individual rows of the quasi-2D diffusion databases were phased and baseline corrected. $CDCl_3$ used for experiments was passed through activated 3Å molecular sieves and alumina basic oxide to remove water and DCl traces and was preserved in a brown glass vial to keep out of the light. The quantitative ^{1}H NMR analysis was performed by using TCE (tetrachloroethane) as internal standard, the optimisation of NMR

parameters were performed according to literature data[115]. High-resolution mass spectra (HRMS) were acquired using a Bruker Solaris XR Fourier transform ion cyclotron resonance mass spectrometer equipped with a 7 T refrigerated actively-shielded superconducting magnet. The samples were ionized in positive ion mode using the ESI ion source (Bruker Daltonik GmbH, Bremen, Germany). The mass spectra were calibrated externally using a NaTFA solution in positive ion mode. Low resolution mass spectral analyses were carried out using an electrospray spectrometer Waters 4 micro quadrupole. A linear calibration was applied. Water saturated deuterated chloroform was prepared as reported in the literature[116]. Resorcinarene **16** was synthesized according to literature procedures[117] *N*-benzylpirrole[118], *N*-phenylpyrrole[119] were synthesized according to literature procedures.

7.2 General Procedures for the Alkylation of Heteroarenes by nitrostyrene and carbonyl compounds inside CR_6

7.2.1 General procedure in presence of $\boldsymbol{CR_6}$

Resorcinarene **16** (281.6 mg, 254.7 µmol, 1.56 equiv.) was weighed in a 4 mL vial. Then, 1.1 mL of water-saturated chloroform was added, and the mixture was homogenized in an ultrasonic water bath at 40 °C for 10 min. To this clear yellow solution, the nucleophile (654.4 µmol, 4 equiv.) was

---

[115]Osypenko, A.; Dhers, S.; Lehn, J.-M. *J. Am. Chem. Soc*. **2019**, *141*, 12724.

[116] a) T.M. Bruer, Q. Zhang, K. Tiefenbacher, *Angew. Chem. Int. Ed.* **2016**, *55*, 7698; b) Q. Zhang, K. Tiefenbacher, L. Catti, J. Pleiss, *J. Am. Chem. Soc.*, **2017**, *139*, 11482

[117]G. La Sorella, L. Sperni, G. Strukul, A. Scarso, *Adv. Synth. Catal*. **2016**, *358*, 3443

[118] W. R. Scaggs, T. D. Scaggs, T. N. Snaddon, *Org. Biomol. Chem*, **2019**, *17*, 1787.

[119] X. Hong, Q. Tan, B. Liu, B. Xu, . *Angew. Chem. Int. Ed*., 2017, 56, 39615

added, and the solution was stirred at 50 °C for 10 minutes. Later, the electrophile (162.6 µmol, 1.0 equiv.) was added, and the reaction system was vigorously stirred (1400 rpm) at 50 °C for the appropriate time. The reaction was monitored by ^{1}H NMR analysis taking aliquots of the reaction mixture (50 µL) at various time intervals and diluting with chloroform-d. The reaction was stopped pouring the solution in a 50 mL Eppendorf conical tube and diluting with 0.13% (v/v) DMSO in *n*-hexane (35 mL). The tube was placed in a freezer at −20 °C for 3 h and successively centrifugated for 10 minutes. The diluted reaction mixture was subjected three times to this process of centrifugation/dilution with *n*-hexane. Finally, the clear solution was concentrated under reduced pressure. The crude was purified by flash chromatography on silica gel to afford the desired title compounds. Regioisomeric ratios were determined by ^{1}H NMR analysis via integration of proton signals of the title compounds in comparison with literature data.

The compounds ***α*-63a(a-e)**[120], ***β*-63aa**[77], α-**64**[76], ***β*-66**[76], ***β*-67**[76], **69aa**[121], **69ab**[121],**71ae**[122], **71be**[122],**73(a-d)b**[123], **75a(a-h)**[124],**75ba**[125], **77ba**[124] were previously described.

7.2.2 Reaction in presence of competitive guest

To a solution of resorcinarene **16** (281.6 mg, 254.7 µmol, 1.56 equiv.) in water saturated chloroform-d (1.1 mL), hexamethonium iodide or tetrabutylammonium tetrafluoroborate (763.8 µmol, 18 equiv. respect to

---

[120] M. De Rosa, A, Soriente, *Tetrahedron,* **2010**, *66,* 2981
[121] J. M. Brittain, R. A. Jones, J. S. Arques, T. A. Saliente, *Synthetic Communications*, **1982**, *12*, 2318
[122] J.-L. Zhao, L. Liu, H.-B. Zhang, Y.-C. Wu, D. Wang, Y. J. Chen, *Tetrahedron Lett.*, **2006**, *47*, 25114
[123] S. Lucarini, M. Mari, G. Piersanti, G. Spadoni, *RSC Adv.*, **2013**, *3*, 19135.
[124] K. Singh, S. Sharma, A. Sharma, *Molecular Catalysis*, **2011**, *347*, 34
[125] K. Singh, S. Behal and M. S. Hundal, *Tetrahedron*, **2005**, *61*, 6614

CR_6) was added. Then, the nucleophile (654.4 µmol, 4 equiv.) and electrophile (162.6 µmol, 1.0 equiv.) were added to the solution. The reaction system was kept under stirring (1400 rpm) at 50 °C for 16 h. No formation of product was observed.

7.2.3 *Reaction in presence of DMSO*

To a resorcinarene **16** (281.6 mg, 254.7 µmol, 1.56 equiv.) solution in water saturated chloroform-d (1.1 mL), 90 µl of DMSO (1.27 mmol) were added. Next, nucleophile (654.4 µmol, 4 equiv.) and electrophile (162.6 µmol, 1.0 equiv.) were added. The reaction vial was kept stirring at 50°C for 16 h. No formation of products was observed.

7.2.4 General procedure in absence of ***CR_6***

The nucleophile (650.4 µmol, 4 eq) and the electrophile (162.6 µmol, 1 eq) were dissolved in 1.1 mL of water saturated chloroform-d. The reaction mixture was vigorously stirred at 50°C for the appropriate time. No formation of product was observed.

7.2.5 Reaction without capsule in presence of Brønsted acids and monomeric unit

To a solution of nucleophile (654.4 µmol, 4 equiv.) and electrophile (162.6 µmol, 1 equiv.) in 1.1 mL of water saturated chloroform-d, Brønsted acid (1equiv.) or monomeric unit 4-dodecyl resorcinol (24 equiv.) was added. The reaction system was kept under stirring (1400 rpm) at 50 °C for 16 h.

*7.2.6 NMR experiments as evidence of encapsulation of nitrostyrene **59a** and ethylpiruvate **68a** inside **CR$_6$***

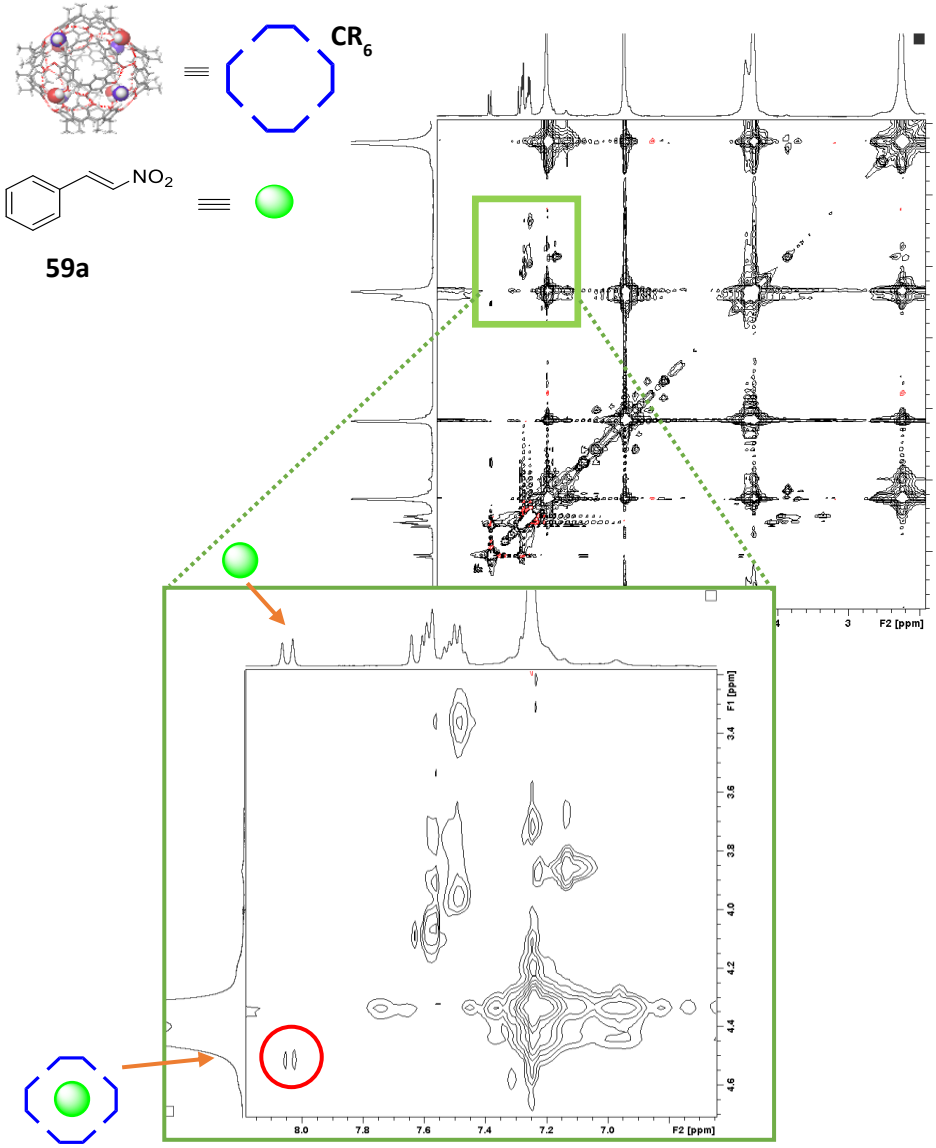

Figure S1. Relevant region of 2D EXSY experiment (400 MHz, $CDCl_3$, 298 K, mixing time 250 ms) of the mixture of **CR$_6$** (21 mM) and nitrostyrene **59a** (82 mM).

Exchange cross-peaks for free and encapsulated vinyl proton at 8.00 ppm of **59a** are marked.

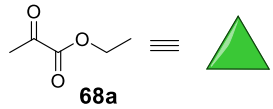

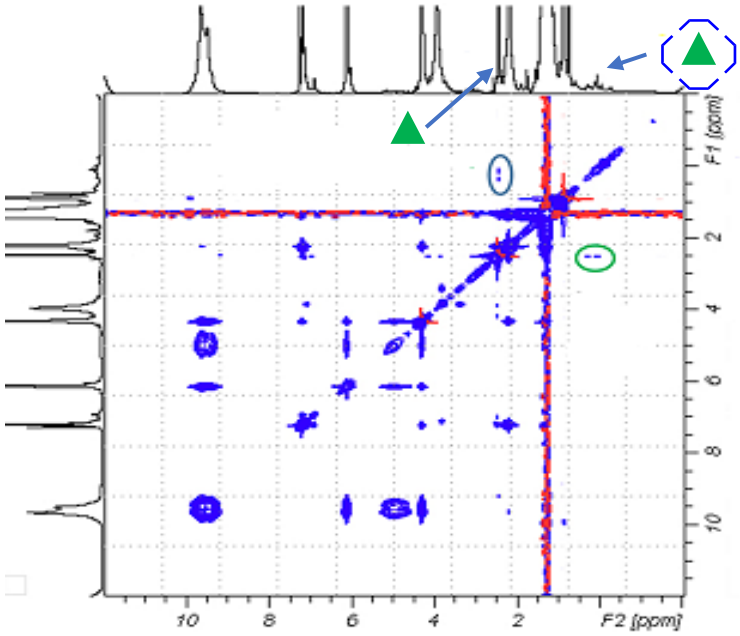

Figure S2. 2D EXSY experiment (400 MHz, $CDCl_3$, mixing time 400 ms) of the mixture of **68a** and **CR$_6$**. Exchange cross-peaks for free and encapsulated ethylpiruvate **68a** are marked.

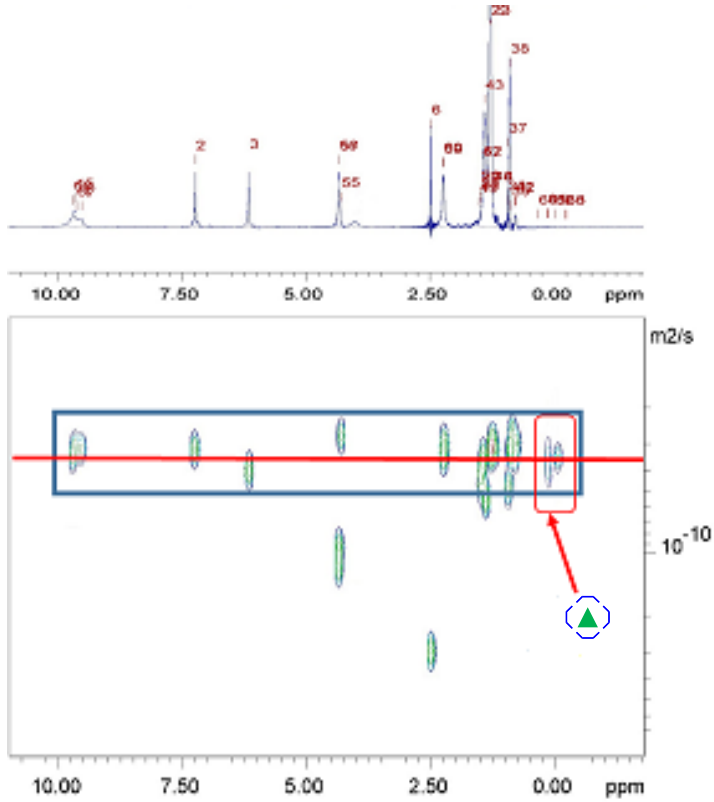

Figure S3. DOSY NMR (600 MHz, $CDCl_3$, 298 K) of the mixture of **68a** and **CR_6**. the signals pattern associated to **68a** inside the capsule **CR_6** are aligned with the capsule diffusion coefficient.

7.2.7 Computational Studies

The computations studies were performed by Prof. A. Rescifina and co-workers from University of Catania.

Due to the high computational cost derived from the large number of atoms involved, an *in silico* investigation was conducted using the ONIOM method upon a reduced model of (**16**)·$8H_2O$, namely $\mathbf{C_R}$ substituting the undecylic residues (the so-called "feet") present in the hexameric capsule with the methyl ones.

The calculations have been performed using the ONIOM method incorporated in the Gaussian16 package, for the reaction between the *N*-methylpyrrole **54a** and the nitrostyrene **59a**. The reactive species (**54a** and **59a**) together with one of the four acidic molecules of water directly involved in the supramolecular assembly and the corresponding three phenolic hydroxyl groups surrounding it were modeled using the M06-2X DFT functional, employing the cc-pVDZ basis set, while the semiempirical method PM6 was employed for all the other atoms.

In order to determine the activation energy barrier of each step and the reaction energy profile, reactant complex, transition state and product complex structures were optimized. All transition structures were characterized by only one imaginary frequency in normal mode analysis and further supported by Intrinsic Reaction Coordinate (IRC) calculations. Other stationary points (reactant complex, intermediates, and product complex) were characterized by all real frequencies and by IRC calculations. Thermodynamic corrections were calculated at 298.15 K and 1 atm for the optimized geometries. All the relative energies presented are referred to

the sum of electronic and thermal free energies calculated at the ONIOM[M06-2X/cc-pVDZ:PM6] level (zero-point energy-corrected ONIOM values). The optimizations were carried out using the Berny analytical gradient optimization method. All calculations were carried out with the Gaussian 16 suite of programs.

Table S1. Relative enthalpies (ΔH), Gibbs free energies (ΔG), and direct ($\Delta G^{\ddagger}$) and inverse inv-($\Delta G^{\ddagger}$) activation Gibbs free energies (in kcal/mol) of the stationary (S) and transition state (TS) points involved in the MTFC reaction in the absence and in the presence of the capsule.

S or TS point	ΔH^{a}	ΔG^{a}	$\Delta G^{\ddagger}$	inv-$\Delta G^{\ddagger}$
MC	0.00	0.00	—	—
α-TS1	23.77	38.32	38.32	n.d.[b]
β–TS1	26.31	39.61	39.61	n.d.
MC-TFA	0.00	0.00	—	—
α-TS1-TFA	19.99	23.84	23.84	n.d.
β-TS1-TFA	22.85	25.34	25.34	n.d.
[**54a**+**59a**]@$\mathbf{C_R}$	0.00	0.00	—	—
α-TS1@$\mathbf{C_R}$	27.05	29.93	29.93	1.19
α–I1@$\mathbf{C_R}$	24.41	28.74	—	—
α–TS2@$\mathbf{C_R}$	23.89	28.99	0.20	29.30
α-I2@$\mathbf{C_R}$	−3.75	−0.31	—	—
α–**63aa**@$\mathbf{C_R}$	−12.08	−10.46	—	—
β-TS1@$\mathbf{C_R}$	26.04	31.10	31.10	0.62
β-I1@$\mathbf{C_R}$	23.58	30.48	—	—
β-TS2@$\mathbf{C_R}$	24.57	30.75	0.27	30.05
β-I2@$\mathbf{C_R}$	−4.46	0.70	—	—
β-**63aa**@$\mathbf{C_R}$	−11.33	−9.95	—	—

[a]Referred to **54a**+**59a**,**54a**+**59a**+TFA, or[**54a+59a**]@C_R. [b] Not done

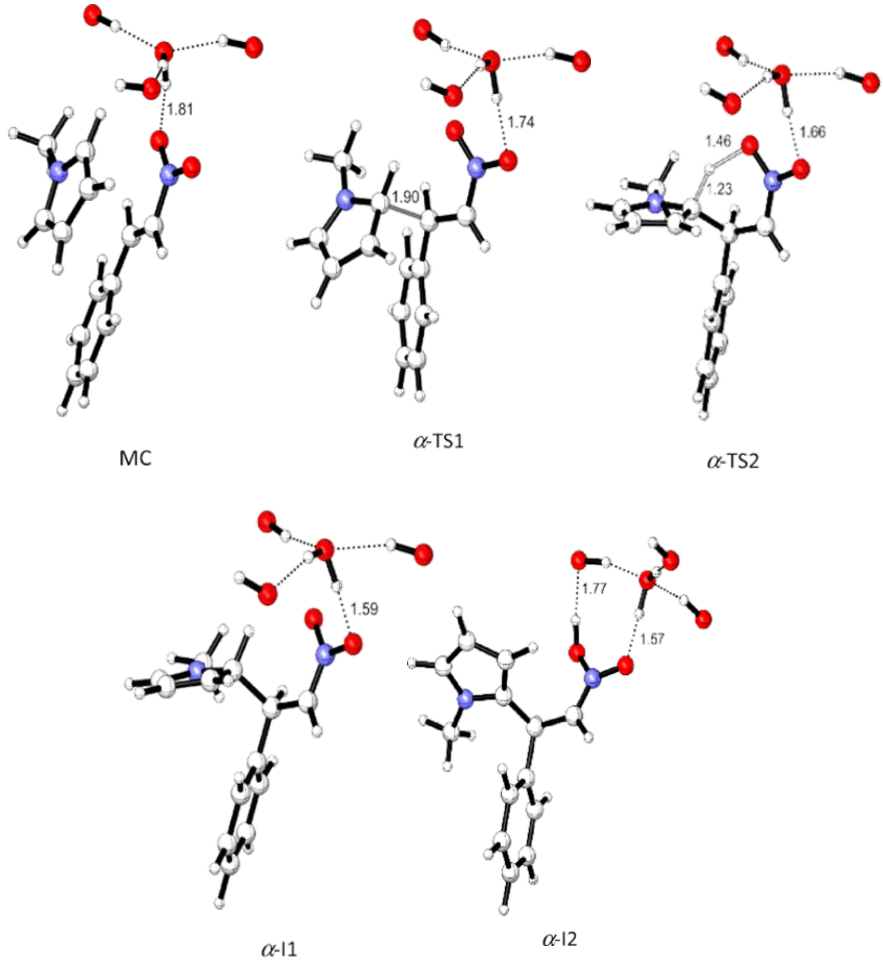

Figure S4. Geometries for the all S and TS points associated with the path ongoing to the **α–63aa** product for the MTFC reaction. Only the atoms of the ONIOM high layer have been represented; the capsule has been omitted for clarity. Along the path, one oxygen atom of the nitro group present in **59a** is always engaged in a hydrogen bond with a water molecule of **CR_6.** The distances are given in Å.

7.2.8 Characterization data of new compounds

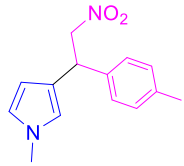

***1-methyl-3-(2-nitro-1-(p-tolyl)ethyl)-1H-pyrrole* (*β* 63ab**): brown oil; ^{1}H-NMR (300 MHz, $CDCl_3$, 298 K): δ 2.32 (s,3H; CH_3), 3.58 (s, 3H; CH_3), 4.70-4.89 (m, 3H;CH_2 overlapped with CH), 5.97-5.98 (m, 1H, ArH_{pyrr}), 6.35-6.36 (m, 1H, ArH_{pyrr}), 6.52-6.54 (m, 1H, ArH_{pyrr}), 7.11-7.19 (m, 4H; ArH); ^{13}C NMR (75 MHz, $CDCl_3$, 298 K): δ= 21.4, 36.5, 42.7, 80.9, 107.4, 119.8, 122.5, 122.6, 127.3 (2C), 129.7 (2C), 137.2, 137.5. HRMS (MALDI-FT ICR): exact mass $[M+H]^+$ calculated for $C_{14}H_{17}N_2O_2$: 245.12845, found 245.12795.

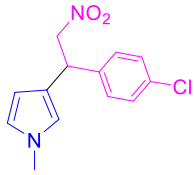

***3-(1-(4-chlorophenyl)-2-nitroethyl)-1-methyl-1H-pyrrole* (*β*-63ac):** brown oil; ^{1}H-NMR (300 MHz, $CDCl_3$, 298K): δ 3.60 (s, 3H; CH_3), 4.73- 4.91 (m, 3H; CH_2 overlapped with CH), 5.96-5.98 (m, 1H, ArH_{pyrr}), 6.36-6.37 (m, 1H, ArH_{pyrr}), 6.55-6.57 (m, 1H, ArH_{pyrr}), 7.22-7.33 (m, 4H, ArH); ^{13}C NMR (75 MHz, $CDCl_3$, 298 K): δ 36.4, 42.2, 80.4, 107.3, 119.7,121.8, 122.7, 129.1, 129.2, 133.3, 139.0. HRMS (MALDI-FT ICR): exact mass $[M+H]^+$ calculated for $C_{13}H_{14}ClN_2O_2$: 265.07382, found 265.07440.

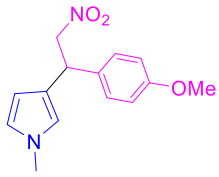

***3-(1-(4-methoxyphenyl)-2-nitroethyl)-1-methyl 1H-pyrrole* (*β*–63ad**): brown oil; ^{1}H-NMR (300 MHz, $CDCl_3$, 298 K): δ 3.59 (s, 3H; CH_3), 3.80 (s, 3H; CH_3), 4.71- 4.91 (m, 3H; CH_2 overlapped with CH),

5.98-5.99 (m, 1H, ArH_{pyrr}), 6.35-6.37 (m, 1H, ArH_{pyrr}), 6.55-6.57 (m, 1H, ArH_{pyrr}), 6.87 (d, *J*= 8.6 Hz, 2H, ArH), 7.22 (d, *J*= 8.6 Hz, 2H, ArH); ^{13}C NMR (75 MHz, $CDCl_3$, 298 K): δ 36.4, 42.2, 55.4, 80.8, 107.3, 114.3, 119.7, 122.6, 122.7, 128.9, 132.5, 158.9. HRMS (MALDI-FT ICR): exact mass $[M+H]^+$ calculated for $C_{14}H_{17}N_2O_3$: 261.12337, found 261.12287.

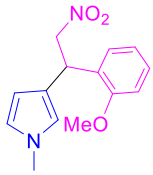

***3-(1-(2-methoxyphenyl)-2-nitroethyl)-1-methyl-1H-pyrrole* (*β*-63ae)**: yellow oil; ^{1}H-NMR (300 MHz, $CDCl_3$, 298 K): δ 3.60 (s, 3H; CH_3), 3.89 (s, 3H; CH_3), 4.81 (dd,^2J = 12.3 Hz, ^3J = 9.2 Hz, 1H, CH), 4.90 (dd, ^2J = 12.3 Hz, ^3J = 6.7 Hz, 1H, CH), 5.19 (dd, ^2J = 9.2 Hz, ^3J = 6.7 Hz, 1H, CH), 6.04-6.05 (m, 1H, ArH_{pyrr}), 6.44-6.46 (m, 1H, ArH_{pyrr}), 6.52-6.55 (m, 1H, ArH_{pyrr}), 6.89-6.94 (m, 2H, ArH), 7.17-7.28 (m, 2H, ArH); ^{13}C NMR (75 MHz, $CDCl_3$, 298 K): □ 36.0, 36.6, 55.3, 79.1, 107.5,, 110.6, 119.7, 120.5, 121.3, 121.9, 128.1, 128.4, 128.7, 156.6. HRMS (MALDI-FT ICR): exact mass $[M+H]^+$ calculated for $C_{14}H_{17}N_2O_3$: 261.12337, found 261.12475.

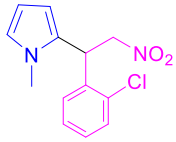

***2-(1-(2-chlorophenyl)-2-nitroethyl)-1-methyl-1H pyrrole* (*α*-63af)**: brown oil; ^{1}H-NMR (300 MHz, $CDCl_3$, 298 K): δ= 3.36 (s, 3H; CH_3), 4.76 (dd, ^2J = 13.2 Hz, ^3J = 5.6 Hz, 1H, CH), 4.85 (dd, ^2J = 13.2 Hz, ^3J = 9.8 Hz, 1H, CH), 5.48 (dd, J=9.8, J=5.6 Hz, 1H, CH), 6.13-6.15 (m, 1H, ArH_{pyrr}), 6.21-6.23 (m, 1H, ArH_{pyrr}), 6.60-6.62 (m, 1H, ArH_{pyrr}), 6.97-7.00 (m, 1H, ArH), 7.18-7.28 (m, 2H, ArH), 7.43-7.46 (m, 1H, ArH); ^{13}C NMR (75 MHz, $CDCl_3$, 298 K): □= 33.8, 38.2, 77.1, 107.0, 107.3, 123.4, 127.9, 128.7, 129.4, 130.0, 130.2, 133.5, 135.4. HRMS (MALDI-FT ICR): exact mass $[M+H]^+$ calculated for $C_{13}H_{14}N_2O_2$: 265.07385, found 265.07385.

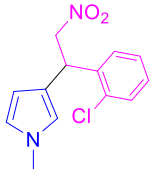

3-(1-(2-chlorophenyl)-2-nitroethyl)-1-methyl-1H pyrrole* (*β*-63af)*: yellow oil; ^{1}H NMR (300 MHz, $CDCl_3$, 298 K): δ 3.60 (s, 3H; CH_3), 4.79-4.92 (m, 2H, CH_2), 5.33-5.39 (m, 1H, CH), 6.02 (m, 1H, = ArH_{pyrr}), 6.45 (m, 1H, ArH_{pyrr}), 6.55-6.57 (m, 1H, ArH_{pyrr}), 7.18-7.42 (m, 4H, ArH); ^{13}C NMR (75 MHz, $CDCl_3$, 298 K): δ 36.4, 39.2, 79.0, 107.6, 120.2, 120.7, 122.7, 127.4, 128.7, 128.8, 130.3, 133.9, 138.0. HRMS (MALDI-FT ICR): exact mass $[M+H]^+$ calculated for $C_{13}H_{14}N_2O_2$: 265.07385, found 265.07385.

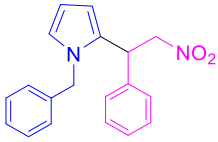

1-benzyl-2-(2-nitro-1-phenylethyl)-1H-pyrrole (α-65)*:* colourless oil; ^{1}H NMR (600 MHz, $CDCl_3$, 298 K): δ 4.67-4.93 (m, 5H, CH_2, CH, CH_2Ph overlapped), 6.21-6.22 (m, 2H, ArH_{pyrr}), 6.67-6.68 (m, 1H, ArH_{pyrr}), 6.88-6.89 (m, 2H, ArH), 7.10-7.12 (m, 2H, ArH), 7.24-7.31 (m, 7H, ArH); ^{13}C NMR (150 MHz, $CDCl_3$, 298 K): δ 41.8, 50.7 79.5, 107.7 107.0, 123.2, 126.6, (2C), 127.8, 128.0, 128.1 (2C), 129.0 (2C), 129.3 (2C), 129.6, 137.6, 138.4. HRMS (MALDI-FT ICR): exact mass $[M+H]^+$ calculated for $C_{19}H_{19}N_2O_2$: 307.14410 , found 307.14415.

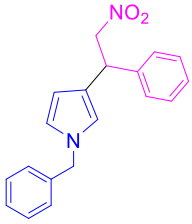

1-benzyl-3-(2-nitro-1-phenylethyl)-1H-pyrrole (β-65)*:* brown oil; ^{1}H NMR (400 MHz, $CDCl_3$, 298 K): δ 4.78-4.93 (m, 3H, CH_2 and CH overlapped), 5.00 (s, 2H, N*CH_2*Ph), 6.04-6.06 (m, 1H, ArH_{pyrr}), 6.48-6.50 (m, 1H, ArH_{pyrr}), 6.63-6.65 (m, 1H, ArH_{pyrr}), 7.08-7.11. (m, 2H, ArH), 7.27-7.37 (m, 8H, ArH); ^{13}C NMR (150 MHz, $CDCl_3$, 298 K):

43.0, 53.6, 80.8, 107.9, 119.3, 122.1, 122.6, 127.2 (2C), 127.5, 127.9 (2C), 128.0 (2C), 128.9, 129.0, 137.9, 140.5. HRMS (MALDI-FT ICR): exact mass $[M+H]^+$ calculated for $C_{19}H_{19}N_2O_2$: 307.14410 , found 307.14413.

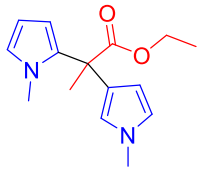

ethyl 2-(1-methyl-1H-pyrrol-2-yl)-2-(1-methyl-1H-pyrrol-3-yl)propanoate (70aa)*:* yellow oil. ^{1}H NMR (600 MHz, $CDCl_3$, 298 K): δ 1.26 (t, *J* = 7.2 Hz, 3H, -OCH_2*CH_3*), 1.86 (s, 3H, CH_3), 3.33 (s, 3H, NCH_3), 3.59 (s, 3H, NCH_3), 4.19-4.25 (m, 2H, -O*CH_2*CH_3), 5.98-6.07 (m, 3H, ArH), 6.42-6.56 (m, 3H, ArH). ^{13}C NMR (150 MHz, $CDCl_3$, 298 K): δ 14.4, 28.5, 35.3, 36.4, 46.9, 61.3, 106.1, 107.4, 108.4, 120.0, 121.4, 123.3, 126.8, 136.0, 175.4. HRMS (MALDI-FT ICR) exact mass $[M+H]^+$ calculated for $C_{15}H_{20}N_2O_2$: 261.17540, found: 261.17527.

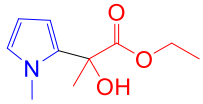

ethyl 2-hydroxy-2-(1-methyl-1H-pyrrol-2yl)propanoate (71aa)*:* yellow oil, ^{1}H NMR (600 MHz, $CDCl_3$, 298 K): δ 1.26 (t, *J* = 7.2 Hz, 3H, -OCH_2*CH_3*), 1.82 (s, 3H, -*CH_3*), 3.52 (s, 1H, -*OH*), 3.59 (s, 3H, -N*CH_3*), 4.20-4.33 (m, 2H,-O*CH_2*CH_3), 6.03-6.04 (m, 2H, ArH), 6.19-6.20 (m, 2H, ArH), 6.56-6.57 (m, 2H, ArH). ^{13}C NMR (150 MHz, $CDCl_3$, 298 K): δ 14.3, 26.9, 35.2, 62.7, 72.2, 106.5, 108.6, 124.7, 131.9, 176.3. HRMS (MALDI-FT ICR) exact mass $[M+H]^+$ calculated for $C_{10}H_{15}NO_3$: 198.11247, found: 198.11242.

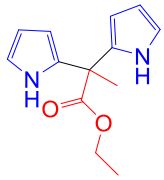

ethyl 2,2-di(1H-pyrrol-2-yl)propanoate (69ba): yellow oil, ^{1}H NMR (600 MHz, $CDCl_3$, 298 K): δ 1.29 (t, J = 7.2 Hz, 3H, -OCH_2*CH_3*), 1.91 (s, 3H, CH_3), 4.24 (q, *J* = 7.2 Hz, 2H, -

OCH_2CH_3), 6.07-6.08 (m, 2H, ArH), 6.14-6.16 (m, 2H, ArH), 6.70-6.71 (m, 2H, ArH), 8.46 (s, 2H, NH). ^{13}C NMR (150 MHz, $CDCl_3$, 298 K): δ 14.3, 25.1, 47.2, 62.1, 106.1, 108.4, 117.8, 132.8, 173.9. HRMS (MALDI-FT ICR) exact mass $[M+H]^+$ calculated for $C_{13}H_{16}N_2O_2$: 233.12845, found: 233.12867.

***ethyl 2-hydroxy-3-methyl-2-(1-methyl-1H-pyrrol-2-yl)butanoate* (71ac)**: yellow oil. ^1H NMR (600 MHz, $CDCl_3$, 298 K): δ 0.89 (d, *J* = 5.9 Hz, 3H, $CH(CH_3)_2$), 1.06 (d, *J* = 6.7 Hz, 3H, $CH(CH_3)_2$), 1.26 (t, *J* = 7.2 Hz, 3H, $-OCH_2CH_3$), 2.62 (sept, *J* = 6.8 Hz, 1H, $CH(CH_3)_2$), 3.59 (s, 1H, OH), 3,66 (s, 3H, NCH_3), 4.15-4.32 (m, 2H, $-OCH_2CH_3$), 6.04 (dd, *J* = 2.7 Hz, 3.7 Hz, 1H, ArH), 6.18 (dd, J = 1.8 Hz, 3.7 Hz, 1H ArH), 6.50-6.51 (m, 1H, ArH). ^{13}C NMR (150 MHz, $CDCl_3$, 298 K): δ 14.1, 17.0, 17.1, 34.4, 36.1, 62.4, 78.4, 106.3, 109.4, 124.4, 130.4, 175.3. HRMS (MALDI-FT ICR) exact mass $[M+H]^+$ calculated for $C_{12}H_{19}NO_3$: 226.14377, found: 226.14400.

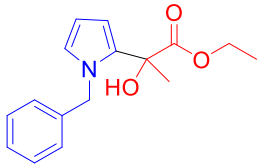

***ethyl 2-(1-benzyl-1H-pyrrol-2-yl)-2 hydroxypropanoate (71ca)*:** colourless oil. ^1H NMR (600 MHz, $CDCl_3$, 298 K): δ 1.11 (t, *J* = 7.1 Hz, 3H, $-OCH_2CH_3$), 1.81 (s, 3H, CH_3), 3.54 (s, 1H, OH), 3.58 (dq, *J* = 7.1 Hz, 10.7 Hz, 1H, $-OCH_2CH_3$), 3.97 (dq, *J* = 7.1 Hz, 10.6 Hz, 1H, $-OCH_2CH_3$), 5.15 (d, *J* = 16.5 Hz, 1H, NCH_2-Ar), 5.25 (d, *J* = 16.5 Hz, 1H, NCH_2-Ar), 6.14 (dd, *J* = 2.9 Hz, 3.6 Hz, 1H, ArH_{pyrr}), 6.28 (dd, *J* = 1.8 Hz, 3.7 Hz, 1H, ArH_{pyrr}), 6.62 (dd, *J* = 2.6 Hz, 2.7 Hz, 1H, ArH_{pyrr}), 6.99 (d, *J* = 7.3 Hz, 2H, ArH), 7.21-7.23 (m, 2H, ArH), 7.27-7.29 (m, 1H, ArH). ^{13}C NMR (150 MHz, $CDCl_3$, 298 K): δ 14.1, 27.5, 51.1, 62.5, 72.2, 107.3, 108.9, 124.5, 126.8, 127.4, 128.6, 132.1, 138.7, 176.1. HRMS (MALDI-FT ICR) exact mass $[M+Na]^+$ calculated for $C_{16}H_{19}NO_3$: 296.12571, found: 296. 12571.

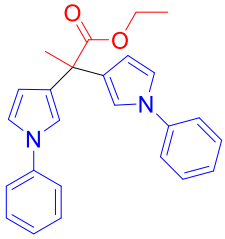

***ethyl 2,2-bis(1-phenyl-1H-pyrrol-3-yl)propanoate* (72da):** colourless oil. ^{1}H NMR (600 MHz, $CDCl_3$, 298 K): δ 1.29 (t, *J* = 7.2 Hz, 3H, $-OCH_2CH_3$), 1.93 (s, 3H, CH_3), 4.23 (q, *J* = 7.2 Hz, 2H, $-OCH_2CH_3$), 6.37 (dd, *J* = 1.8 Hz, 2.9 Hz, 2H, ArH_{pyrr}), 7.00-7.01 (m, 2H, ArH_{pyr}), 7.04-7.05 (m, 2H, ArH_{pyrr}), 7.19-7.22 (m, 2H, ArH), 7.36-7.40 (m, 8H, ArH). ^{13}C NMR (150 MHz, $CDCl_3$, 298 K): δ 14.4, 26.9, 46.3, 61.2, 110.7, 117.3, 119.0, 120.3, 125.5, 129.7, 130.7, 140.9, 175.8. HRMS (MALDI-FT ICR) exact mass $[M+Na]^+$ calculated for $C_{25}H_{24}N_2O_2$: 407.17300, found: 407.17279.

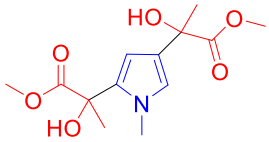

***dimethyl 2,2'-(1-methyl-1H-pyrrole-2,4-diyl)bis(2-hydroxypropanoate)*:** colourless oil. ^{1}H NMR (600 MHz, $CDCl_3$, 298 K): δ 1.72 (s, 3H, CH_3), 1.74 (s, 3H, CH_3), 3.77-3.81 (overlapped, 11H, NCH_3, OCH_3, OH), 6.11 (s, 1H, ArH), 6.16 (s, 1H, ArH). ^{13}C NMR (150 MHz, $CDCl_3$, 298 K): δ 23.3, 23.4, 53.5, 58.5, 58.6, 82.4, 82.7, 116.7, 116.8, 147.8, 166.4, 169.7, 172.4. HRMS (MALDI-FT ICR) exact mass $[M]^+$ calculated for $C_{13}H_{19}NO_6$: 285.12069, found: 285.12072.

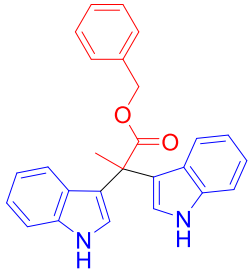

***benzyl 2,2-di(1H-indol-3-yl)propanoate* (73ad):** a yellow solid m.p: 153.2-154.1 °C. ^{1}H NMR (600 MHz, $CDCl_3$, 298 K): δ 2.15 (s, 3H, CH_3), 5.15 (s, 2H, CH_2), 6.91-6.95 (overlapped, 4H, ArH_{ind}), 7.10 (d, *J* = 6.6 Hz, 2H, ArH), 7.14 (t, *J* = 7.8 Hz, 2H, ArH_{ind}), 7.18-7.23 (overlapped, 3H, ArH), 7.33 (d, *J* = 8.1 Hz, 2H, ArH_{ind}), 7.44, (d, *J* = 8.1 Hz, 2H, ArH_{ind}), 8.00 (s, 2H, NH). ^{13}C NMR (150 MHz, $CDCl_3$, 298 K): δ 26.0, 46.7, 67.0, 111.4, 119.2, 119.4, 121.6, 121.9, 123.1, 126.2, 128.0, 128.3, 128.4, 136.1, 136.9, 175.3. HRMS (MALDI-FT ICR)

exact mass $[M+Na]^+$ calculated for $C_{26}H_{22}N_2O_2$: 417.15735, found: 417.15705.

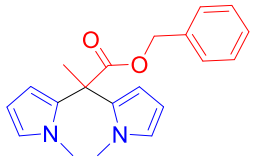

***benzyl 2,2-bis(1-methyl-1H-pyrrol-2-yl)propanoate* (69ad):** colourless oil. ^{1}H NMR (600 MHz, $CDCl_3$, 298 K): δ 1.89 (s, 3H, CH_3), 3.00 (s, 6H, $N(CH_3)$), 5.14 (s, 2H, $-CH_2$), 5.92 (dd, J_1 = 1.9 Hz, J_2 = 3.7 Hz, 2H, ArH_{pyrr}), 5.95 (dd, J_1 = 2.8 Hz, J_2 = 3.7 Hz, 2H, ArH_{pyrr}), 6.44 (t, J = 2.2 Hz, 2H, ArH_{pyrr}), 7.18-7.25 (overlapped, 5H, ArH). ^{13}C NMR (150 MHz, $CDCl_3$, 298 K): δ 25.8, 34.8, 48.3, 67.3, 106.6, 108.2, 124.2, 128.2, 128.3, 128.7, 132.5, 135.9, 172.8. HRMS (MALDI-FT ICR) exact mass $[M+H]^+$ calculated for $C_{20}H_{22}N_2O_2$: 323.16890, found: 323.16889.

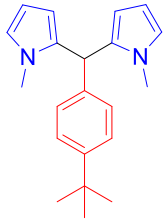

***2,2'-((4-(tert-butyl)phenyl)methylene)bis(1-methyl-1H-pyrrole)* (75ai)**: brown solid, mp 95-97 °C**.** ^{1}H NMR (600 MHz, $CDCl_3$, 298 K): δ 1.32 (s, 9H, CH_3), 3.40 (s, 6H, $N(CH_3)$), 5.25 (bs, 1H, CH), 5.53-5.23 (m, 2H, ArH_{Pyr}), 6.03 (t, J = 3.2 Hz, 2H, ArH_{Pyr}), 6.58 (t, J = 2.2 Hz, 2H, ArH_{Pyr}), 7.07 (d, J = 8.2 Hz, 2H, ArH), 7.31 (d, J = 8.2 Hz, 2H, ArH). ^{13}C NMR (150 MHz, $CDCl_3$, 298 K): δ 31.6, 34.1, 34.6, 41.7, 106.6, 109.0, 122.0, 125.4, 128.5, 134.0, 138.3, 149.6. ESI m/z calcd for $C_{21}H_{26}N_2$ $[M]^+$: 306.20905, found: 306.20450.

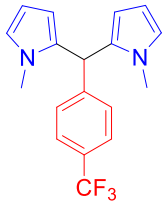

***2,2'-((4-(trifluoromethyl)phenyl)methylene)bis(1-methyl-1H-pyrrole)* (75ab):** brown solid, mp 103.4-105.5°C. ^{1}H NMR (400 MHz, $CDCl_3$, 298 K): δ 3.42 (s, 6H, $N(CH_3)$), 5.36 (s, 1H, CH), 5.51 (bs, 2H, ArH_{Pyr}), 6.06 (t, J = 3.1 Hz, 2H, ArH_{Pyr}), 6.63 (bs, 2H, ArH_{Pyr}), 7.29 (d, J = 7.6 Hz, 2H, ArH), 7.69 (d, J = 7.6Hz, 2H, ArH). ^{13}C NMR (100 MHz, $CDCl_3$, 298 K): δ 34.0, 41.9,

106.7, 109.3, 122.4, 124.4 (q, $^{1}J_{CF}$ = 272.2 Hz), 125.5 (q, $^{3}J_{CF}$ = 3.8 Hz), 129.3 (q, $^{2}J_{CF}$ = 32.1 Hz), 129.2, 132.6, 154.1. HRMS (MALDI-FT ICR) exact mass $[M+H]^+$ calculated for $C_{18}H_{17}F_3N_2$: 319.14166, found: 319.14491.

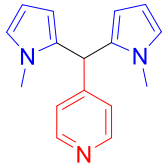

4-(bis(1-methyl-1H-pyrrol-2-yl)methyl)pyridine **(75aj):** brown solid, ^{1}H NMR (400 MHz, $CDCl_3$, 298 K) : δ 3.38 (s, 6H, $N(CH_3)$), 5.26 (s, 1H, CH), 5.50 (bs, 2H, ArH_{Pyr}), 6.03 (bs, 2H, ArH_{Pyr}), 6.61 (bs, 2H, ArH_{Pyr}), 7.08 (d, J = 5.3 Hz, 2H, ArH), 8.54 (d, J = 5.3, 2H, ArH). ^{13}C NMR (100 MHz, $CDCl_3$, 298 K): δ 34.1, 41.6, 106.9, 109.6, 122.7, 124.2, 131.8, 150.2, 150.6. HRMS (MALDI-FT ICR) exact mass $[M+H]^+$ calculated for $C_{16}H_{17}N_3$: 252.14952, found: 252.14968.

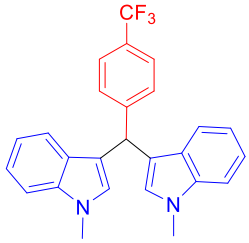

3,3'-((4(trifluoromethyl)phenyl)methylene)bis(1-methyl-1H-indole) **(77bb) :** Obtained as pink solid, mp 157.1-158.3. ^{1}H NMR (400 MHz, $CDCl_3$, 298 K) : δ 3.74 (s, 6H, $N(CH_3)$), 6.00 (s, 1H, CH), 6.58 (s, 2H, ArH_{Ind}), 7.07 (t, J = 7.8, 2H, ArH_{Ind}), 7.27 (t, J = 7.8, 2H, ArH_{Ind}),7.36 (d, J = 7.8 Hz, 2H, ArH_{Ind}), 7.40 (d, J =7.8, 2H, ArH_{Ind}), 7.50 (d, J = 8.1, 2H, ArH), 7.58 (d, J = 8.1, 2H, ArH). ^{13}C NMR (100 MHz, $CDCl_3$, 298 K): δ 32.9, 40.2, 109.4, 119.1, 120.0, 121.9, 124.6 (q, $^{1}J_{CF}$ = 271.9 Hz), 125.4 (q, $^{3}J_{CF}$ = 3.5 Hz), 125.4, 127,4, 128.5 (q, $^{2}J_{CF}$ = 32.1 Hz), 128.5, 129.2, 137.6, 148.8. ESI (m/z) calcd for $C_{26}H_{21}N_2$ $[M]^+$: 418.16513, found: 418.16052

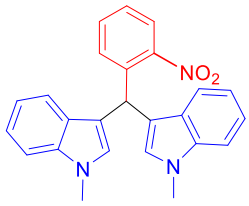

3,3'-((2-nitrophenyl)methylene)bis(1-methyl-1H-indole) **(77bf):** orange solid, mp> 242°C decomp^{1}H NMR (600 MHz, $CDCl_3$, 298 K) : δ 3.68 (s, 6H, $N(CH_3)$), 6.54 (s, 2H, ArH_{Ind}), 6.67 (s, 1H, CH), 7.02 (t, J = 7.8, 2H, ArH_{Ind}), 7.21 (t, J = 7.8, 2H, ArH_{Ind}), 7.30 (d, J = 7.8 Hz, 2H, ArH_{Ind}), 7.34

(t, J= 7.9, 1H, ArH), 7.38 (d, J = 7.9, 2H, ArH_{Ind}), 7.41 (t, J=7.9, 1H, ArH), 7.46 (d, J =7.9, 1H, ArH), 7.85 (d, J = 7.9, 1H, ArH). ^{13}C NMR (150 MHz, $CDCl_3$, 298 K): δ 33.0, 40.2, 109.4, 116.5, 119.2, 120.1, 122.0, 124.6, 127.3, 127.4, 128.8, 131.4, 132,5, 137.7, 138,7, 150.0. ESI (m/z) calcd for $C_{25}H_{21}N_3O_2$ $[M]^+$: 395.16283, found: 395.15819

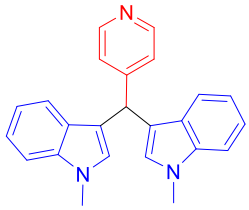

***3,3'-(pyridin-4-ylmethylene)bis(1-methyl-1H-indole)* (77bj):** pink solid, mp 164.6-165.4. ^1H NMR (600 MHz, $CDCl_3$, 298 K) : δ 3.72 (s, 6H, $N(CH_3)$), 5.98 (s, 1H, CH), 6.57 (s, 2H, ArH_{Ind}), 7.04 (t, J = 7.3, 2H, ArH_{Ind}), 7.25 (t, J = 7.3, 2H, ArH_{Ind}), 7.29 (d, J = 6.5 Hz, 2H, ArH), 7.34 (d, J=7.3, 1H, ArH_{Ind}), 7.37 (d, J =7.3 , 2H, ArH_{Ind}), 8.5 (d, J = 6.5, 2H, ArH). ^{13}C NMR (150 MHz, $CDCl_3$, 298 K): δ 32.9, 39.7, 109.4, 116.5, 119.1, 119.8, 121.9, 124.2, 127.3, 128.4, 137.6, 149.8, 153.7. ESI (m/z) calcd for $C_{24}H_{21}N_3$ $[M+H]^+$: 352.18082, found: 352.18439.

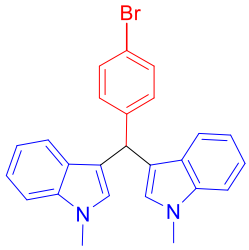

***3,3'-((4-bromophenyl)methylene)bis(1-methyl-1H indole)* (77be):** red solid, mp 202.3-203.5. ^1H NMR (400 MHz, $CDCl_3$, 298 K) : δ 3.70 (s, 6H, $N(CH_3)$), 5.86 (s, 1H, CH), 6.53 (s, 2H, ArH_{Ind}), 7.03 (t, J = 7.7, 2H, ArH_{Ind}), 7.21-7.24 (m, 4H, overlapped ArH_{ind}), 7.32 (d, J = 7.7Hz, 2H, ArH_{Ind}), 7.38 (d, J=7.7, 1H, ArH), 7.41 (d, J =7.9 , 2H, ArH). ^{13}C NMR (75 MHz, $CDCl_3$, 298 K): δ 32.8, 39.7, 109.3, 117.8, 118.9, 119.9, 120.1, 121.7, 127.4, 128.4, 130.6, 131.4, 137.6, 143.7. ESI (m/z) calcd for $C_{25}H_{21}BrN_2$ $[M]^+$: 428.08826, found: 428.08363.

7.3 General procedures for the modulation of imine-based DCLs

7.3.1 General procedures for the synthesis of imines

Imines were independently prepared by condensation of the aldehydes and amines according to the following procedure. A mixture of the selected aniline (2 mmol) and aldehyde (2 mmol) in ethanol (12 mL) was refluxed upon stirring for 8 h. Then, the reaction mixture was refrigerated and the desired imine was obtained as solid, after filtration. Spectroscopic data of imines **A74a**[126], **A74c**[127], **A74d**[128], **B74a**[126], **B74b**[129], **C74a**[130], **C74b**[131], **C74d**[132], **D74a**[133], **D74b**[133] matched with that reported in literature.

7.3.2 Characterization data of new imines

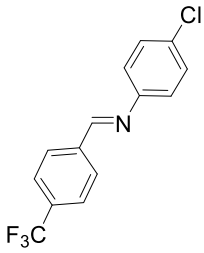

***N*-(4-chlorophenyl)-1-(4-(trifluoromethyl)phenyl) methanimine (A74b)** : yellow solid (95% yield), mp 80.1-81.5. ^{1}H NMR (400 MHz, $CDCl_3$, 298 K): δ 7.17 (d, J = 8.5 Hz, 2H, ArH), 7.38 (d, J = 8.5 Hz, 2H, ArH), 8.01 (d, J = 8.3 Hz, 2H, ArH), 7.73 (d, J = 8.3 Hz, 2H, ArH), 8.48 (s, 1H, CH). ^{13}C NMR (75 MHz, $CDCl_3$, 298 K): δ 122.4, 124.1 (q, $^{1}J_{CF}$ = 271.7 Hz), 125.8 (q, $^{3}J_{CF}$ = 3.7 Hz), 129.3, 129.6, 132.4, 133.1 (q, $^{2}J_{CF}$ = 32.4 Hz), 139.3,

---

[126] L. Liu, S. Zhang, X. Fu, C.-H., Yan, *Chem. Commun.,* **2011**, *47*, 10148
[127] A. Iqbal, H. L. Siddiqui, C. M. Ashraf, *Chem. Pharm. Bull.,* **2007**, *55*, 1070.
[128] H. Miyamura, M. Morita, T. Inaasaki, S. Kobayashi, *Bull. Chem. Soc. Jpn.,* **2011**, *84*, 588
[129] A. Hasegawa, Y. Naganawa, M. Fushimi, K. Ishihara, H. Yamamoto, *Org. Lett.,* **2006**, *8*, 3175
[130] R. Torregrosa, I. M. Pastor, M. Yus, *Tetrahedron,* **2005**, *61*, 11148
[131] J.-T. Lai, Y.-J. Yang, J.-H. Lin, D.-Y. Yang, *Synlett.,* **2010**, *1*, 111
[132] J. S. Bennett, K. L. Charles, M. R. Miner, C. F. Heuberger, E. J. Spina, M. F. Bartels, T. Foreman, *Green Chem.,* **2009**, *11*, 166
[133] P. Zhou, L. Jiang, S. Wang, X. Hu, H. Wang, Z. Yuan, Z. Zhang, *ACS Catal.,* **2019**, *9*, 8413

150.1, 159.0. HRMS (MALDI-FT ICR) exact mass $[M+H]^+$ calculated for $C_{14}H_9ClF_3N$ $[M+H]^+$: 284.04484, found: 284.04479.

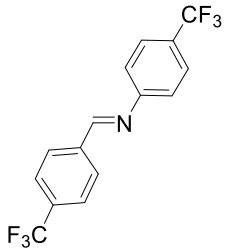

1-bis(4-(trifluoromethyl)phenyl)methanimine (C74b): yellow solid (85% yield) mp 87.5-88.2. ^{1}H NMR (400 MHz, $CDCl_3$, 298 K): δ 7.28 (d, J = 8.4, 2H, ArH), 7.67 (d, J = 8.4, 2H, ArH), 7.76 (d, J = 8.3, 2H, ArH), 8.04 (d, J = 8.3, 2H, ArH), 8.48 (s, 1H, CH). ^{13}C NMR (100MHz, $CDCl_3$, 298 K): δ 121.0, 123.8 (q, $^1J_{CF}$ = 270.0 Hz), 124.2 (q, $^1J_{CF}$ = 271.1 Hz), 125.8 (q, $^3J_{CF}$ = 3.5 Hz), 126.4 (q, $^3J_{CF}$ = 3.4 Hz), 128.3 (q, $^2J_{CF}$ = 30.6 Hz), 129.2, 133.29 (q, $^2J_{CF}$ = 34.7 Hz), 138.8, 154.57, 160.3. HRMS (MALDI-FT ICR) exact mass $[M+H]^+$ calculated for $C_{15}H_9F_6N$: 318.07119, found: 318.07130.

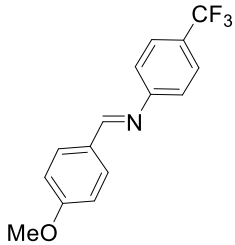

1-(4-methoxyphenyl)-N-(4-(trifluoromethyl)phenyl)methanimine (D74d): yellow solid (92%yield), mp 84.5-85.5. ^{1}H NMR (300 MHz, $CDCl_3$, 298 K): δ 3.89 (s, 3H, OCH_3), 7.01 (d, J =8.4, 2H, ArH), 7.24 (d, J =8.1, 2H, ArH), 7.63 (d, J =8.1, 2H, ArH), 7.86 (d, J =8.4, 2H, ArH), 8.35 (s, 1H, CH). ^{13}C NMR (100MHz, $CDCl_3$, 298 K): δ 55.6, 114.2, 121.0, 124.6 (q, $^1J_{CF}$ = 271.8), 126.5 (q, $^3J_{CF}$ = 3.9 Hz), 127.4 (q, $^2J_{CF}$ = 32.3 Hz), 128.9, 131.0, 155.4, 161.1, 162.6. Elemental analysis calculated (%) for $C_{15}H_{12}F_3NO$: C, 64.51; H, 4.33; N, 5.02; found: C, 64.45; H, 4.28; N, 5.10.

7.3.3 General procedure for self-sorting system without capsule ***CR₆***

Resorcinarene **16** (281.6 mg, 254.7 µmol, 6 eq.) was weighed in a 4 ml vial. Then, 1 mL of water saturated deuterated chloroform was added and the

mixture was warmed at 50°C until clarification (ca 5 min). Next, the components of the system, aldehydes and anilines, were added simultaneously in the same equivalent (0.0423 mmol, 1 equiv.). The reaction mixture was vigorously stirred (1400 rpm) at the reported temperature T and the evolution of the system composition was monitored by ^{1}H NMR as a function of time.

7.3.4 General procedure for self-sorting system without capsule ***CR_6***

The components of the DCL system were dissolved in equimolar amounts (0.0423 mmol) in water saturated deuterated chloroform (1mL) and stirred (1400 rpm) at the reported temperature T. The distribution of the DCL components was monitored by ^{1}H NMR until no change in composition was detected.

7.3.5 Reaction Monitoring

Aliquots of the reaction mixture (30 µL) were taken at different times and diluted with 470 µL of $CDCl_3$. After adding TCE (1 µL) as internal standard, the reaction mixture was monitored by ^{1}H NMR spectroscopy. d1 parameter was set to 3 x T1. The ratios of the DCL components were determined by integration of the corresponding resonance signals in the spectrum by comparison with the internal standard TCE. For the reaction in the presence of **CR_6**, the ratios were determined after addition of DMSO (2 µL) to the reaction aliquot, in order to disaggregate the capsule.

7.3.6 Two – component reactions

Formation of A74a by aldehyde 74a and aniline A

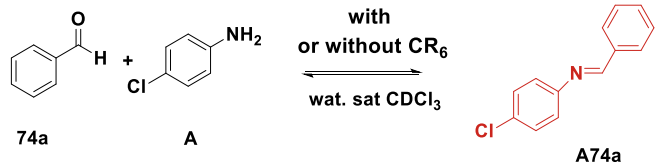

Scheme S1. Synthesis of **A74a** in presence or in absence of capsule **CR_6**.

Table S2. Time-dependent conversion in **A74a** of an equimolar mixture of **A** and **74a** in presence and in absence of **CR_6** [a]

Time[b] (h)	A74a (%)[c] in absence of CR_6	A74a (%)[c,d] in presence of CR_6
0.5	-[e]	24
1	-[e]	26
2	-[e]	34
4	-[e]	34
6	-[e]	34
24	12	34
48	12	34

[a] Reaction conditions: **74a** (0.0423 mmol, 42.3 mM), **A** (0.0423 mmol, 42.3 mM), water-saturated $CDCl_3$ (1 mL), rt. [b] Time at which an aliquot (30 µL) of the reaction mixture was taken and monitored via ^{1}H-NMR spectrum. [c] Conversion was calculated using TCE as internal standard. [d] Conversion was calculated after addition of DMSO (2 µL) to a reaction aliquot, in order to disaggregate the capsule. [e] Below the limit of detection. Error in ^{1}H-NMR signal integration was ± 5%.

Formation of A74a by aldehyde 74b and aniline A

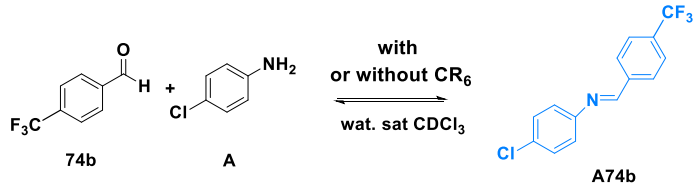

Scheme S2. Synthesis of **A74b** in presence or in absence of capsule **CR$_6$**.

Table S3. Time-dependent conversion in **A74b** of an equimolar mixture of **A** and **74b** in presence and in absence of **CR$_6$** [a]

	in absence of CR$_6$	**in presence of CR$_6$**
Time[b] (h)	**A74b (%)[c]**	**A74b (%)[c,d]**
0.5	-[e]	10
1	-[e]	20
2	-[e]	27
4	5	39
6	11	47
24	11	60
48	11	60

[a] Reaction conditions: **74b** (0.0423 mmol, 42.3 mM), **A** (0.0423 mmol, 42.3 mM), water-saturated $CDCl_3$ (1 mL), rt. [b] Time at which an aliquot (30 µL) of the reaction mixture was taken and monitored via ^{1}H-NMR spectrum. [c] Conversion was calculated using TCE as internal standard. [d] Conversion was calculated after addition of DMSO (2 µL) to a reaction aliquot, in order to disaggregate the capsule. [e] Below the limit of detection. Error in ^{1}H-NMR signal integration was ± 5%.

7.3.7 Evolution of dynamic imine libraries as a function of time

Competitive reaction between equivalent amounts of 74a, 74b and A with and without capsule CR_6

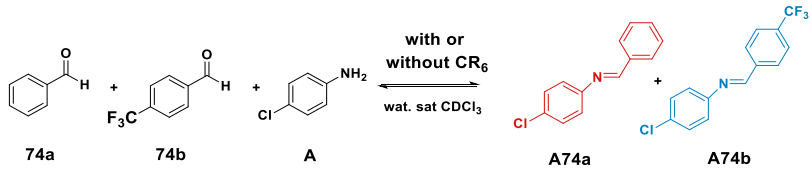

Scheme S3. Synthesis of **A74a** and **A74b** in absence or in presence of capsule **CR_6**.

Table S4. Time-dependent conversion in **A74b** of an equimolar mixture of **A** and **74b** in absence of **CR_6** [a].

	in absence of CR_6	
Time[b] (h)	**A74a (%)[c]**	**A74b (%)[c]**
0.5	-[d]	-[d]
1	-[d]	-[d]
2	7	7
4	7	7
6	9	9
24	21	21
48	21	21

[a] Reaction conditions: **74a**, **74b** (0.0423 mmol, 42.3 mM), **A** (0.0423 mmol, 42.3 mM) water-saturated $CDCl_3$ (1 mL), rt. [b] Time at which an aliquot (30 µL) of the reaction mixture was taken and monitored via ^{1}H-NMR spectrum. [c]Conversion was calculated using TCE as internal standard. [e]Below the limit of detection. Error in ^{1}H-NMR signal integration was ± 5 %.

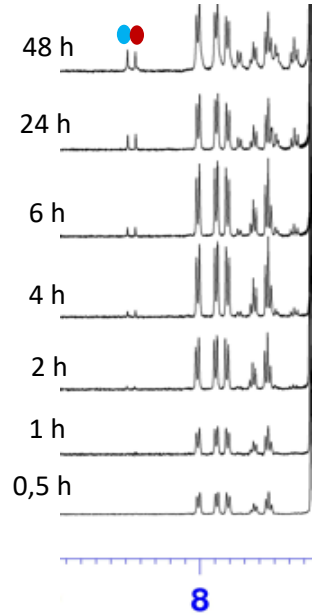

Figure S5 Selected region of ^{1}H NMR (400 MHz, $CDCl_3$, 298 K) spectra of an equimolar mixture of **A, 74a and 74b** (42.3 mM each, water-saturated $CDCl_3$, rt) after 0.5, 1, 2, 4, 6 and 24 h.

Table S5. Time-dependent conversion in **A74b** of an equimolar mixture of **A** and **74b** in presence of **CR_6**[a].

	in presence of CR_6	
Time[b] (h)	**A2a (%)[c,d]**	**A2b (%)[c,d]**
0.5	30	10
1	21	19
2	15	23
4	18	40
6	16	46
24	15	60
48	15	60

[a] Reaction conditions: **74a**, **74b** (0.0423 mmol, 42.3 mM), **A** (0.0423 mmol, 42.3 mM) and CR_6 (42.3 mM) in water-saturated $CDCl_3$ (1 mL), rt. [b] Time at which an aliquot (30 µL) of the reaction mixture was taken and monitored via ^{1}H-NMR spectrum. [c] Conversion was calculated using TCE as internal standard. [d] Conversion was calculated after addition of DMSO (2 µL) to a reaction aliquot, in order to disaggregate the capsule. [e] Below the limit of detection. Error in ^{1}H-NMR signal integration was ± 5 %.

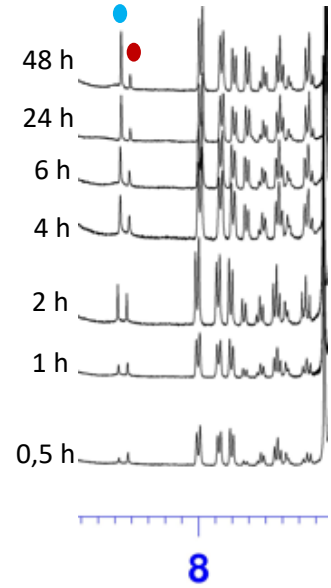

Figure S6. Selected region of ^{1}H NMR (400 MHz, $CDCl_3$, 298 K) spectra of an equimolar mixture of **A, 74a, 74b** and **CR_6** (42.3 mM each, water-saturated $CDCl_3$, r.t.) after 0.5, 1, 2, 4, 6, 24 and 48 h. The spectra are recorded after addition of DMSO (2 µL) to the reaction aliquot, in order to disaggregate the capsule.

Competitive reaction between equivalent amounts of 74a, 74b and A, in presence of 0.5 and 0.1 equiv of capsule CR_6

Table S6. Time-dependent conversion in **A74a** and **A74b** of an equimolar mixture of **A, 74a** and **74b** in presence of 0.5 equiv. of **CR_6** [a]**.**

	in presence of 0.5 equiv CR_6	
Time[b] (h)	**A74a (%)[c]**	**A74b (%)[c]**
0.5	27	8
1	32	17
2	33	21
4	35	45
6	30	49
24	23	61
48	23	61

[a] Reaction conditions: **74a**, **74b** (0.0423 mmol, 42.3 mM), **A** (0.0423 mmol, 42.3 mM), capsule **CR_6** (21.2 mM), water-saturated $CDCl_3$ (1.0 mL), rt. [b] Time at which an aliquot (30 µL) of the reaction mixture was taken and monitored via ^{1}H-NMR spectrum. [c] Conversion was calculated using TCE as internal standard. [d]Conversion was calculated after addition of DMSO (2 µL) to a reaction aliquot, in order to disaggregate the capsule. [e]Below the detection limit. Error in ^{1}H-NMR signal integration was ± 5%.

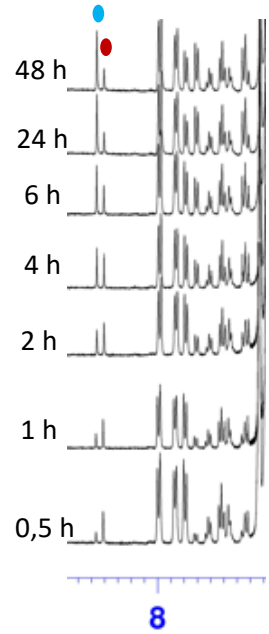

Figure S7. Selected region of ^{1}H NMR (400 MHz, $CDCl_3$, 298 K) spectra of an equimolar mixture of **A, 74a** and **74b** (42.3 mM each, water-saturated $CDCl_3$, r.t.) in presence of **CR_6** (21.2 mM) after 0.5, 1, 2, 4, 6, 24 and 48 h. The spectra are recorded after addition of DMSO (2 µL) to the reaction aliquot, in order to disaggregate the capsule.

Table S7. Time-dependent conversion in **A74a** and **A74b** of an equimolar mixture of **A, 74a** and **74b** in presence of 0.1 equiv. of **CR_6** [a].

	in presence of 0.1 equiv CR_6	
Time[b] (h)	**A74a (%)[c]**	**A74b (%)[c]**
0.5	14	-[e]
1	21	5
2	22	6
4	28	14
6	42	23
24	38	44
48	38	44

[a] Reaction conditions: **74a**, **74b** (0.0423 mmol, 42.3 mM), **A** (0.0423 mmol, 42.3 mM), capsule **CR_6** (4.2 mM), water-saturated $CDCl_3$ (1.0 mL), rt. [b] Time at which an aliquot (30 µL) of the reaction mixture was taken and monitored via ^{1}H-NMR spectrum. [c] Conversion was calculated using TCE as internal standard. [d]Conversion was calculated after addition of DMSO (2 µL) to a reaction aliquot, in order to disaggregate the capsule. [e]Below the detection limit. Error in ^{1}H-NMR signal integration was ± 5%.

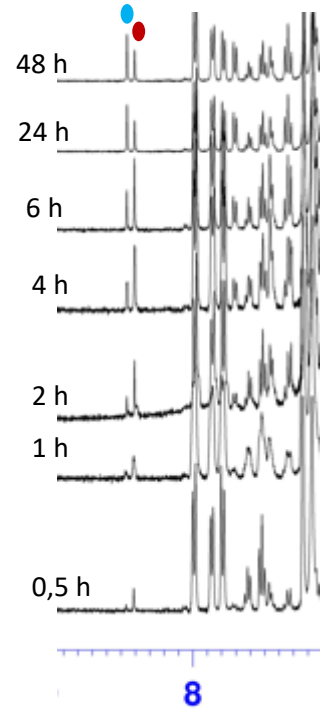

Figure S8. Selected region of ^{1}H NMR (400 MHz, $CDCl_3$, 298 K) spectra of an equimolar mixture of **A, 74a** and **74b** (42.3 mM each, water-saturated $CDCl_3$, r.t.) in presence of **CR_6** (4.2 mM) after 0.5, 1, 2, 4, 6, 24 and 48 h. The spectra are recorded after addition of DMSO (2 µL) to the reaction aliquot, in order to disaggregate the capsule.

Evidence of the capsule effect on the imine distribution in DCL 2a, 2b and A

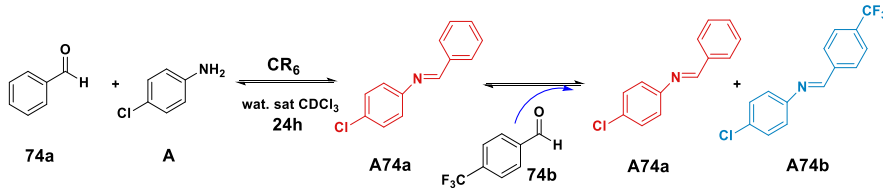

Scheme S4. Competition experiment of **A74a** and **A74b** in presence of capsule **CR6**.

Resorcinarene **16** (281.6 mg, 254.7 µmol, 6 equiv) was weighed in a 4 mL vial and 1 mL of water saturated deuterated chloroform was added. The mixture was warmed at 50 °C until clarification (ca 5 min). Then, **74a** and **A** (0.0423 mmol, 1 equiv) were added simultaneously, and the reaction mixture was vigorously stirred (1400 rpm) at 30 °C. After 24 h was added of **74b** (0.0423 mmol, 1 equiv) and the evolution of the system composition was monitored by ^{1}H NMR as a function of time.

Table S8. Time-dependent modulation of **A74a** by adding after 24h **74b** in presence of **CR$_6$** [a]

	in presence of CR$_6$	
Time[b] (h)	**A74a (%)[c]**	**A74b (%)[c]**
0	34	0
1	18	11
2	17	21
4	15	38
6	10	43
24	10	52
48	10	52

[a] Reaction conditions: **74a**, **74b** (0.0423 mmol, 42.3 mM), **A** (0.0423 mmol, 42.3 mM), capsule **CR$_6$** (4.2 mM), water-saturated $CDCl_3$ (1.0 mL), rt. [b] Time at which an aliquot (30 µL) of the reaction mixture was taken and monitored via ^{1}H-NMR spectrum. [c] Conversion was calculated using TCE as internal standard. [d] Conversion was calculated after addition of DMSO (2 µL) to a reaction aliquot, in order to disaggregate the capsule. [e] Below the detection limit. Error in ^{1}H-NMR signal integration was ± 5%.

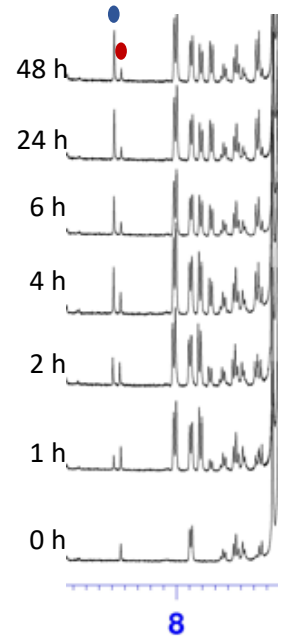

Figure S9. Selected region of ^{1}H NMR (400 MHz, $CDCl_3$, 298 K) spectra of an equimolar mixture of **A, 74a** and **CR$_6$** (42.3 mM each, water saturated $CDCl_3$, r.t.) after 1, 2, 4, 6, 24 and 48 h by the addition of **74b** (0.0423 mmol) respectively.

Competitive reaction between equivalent amounts of 74a, 74c and A with and without capsule CR_6

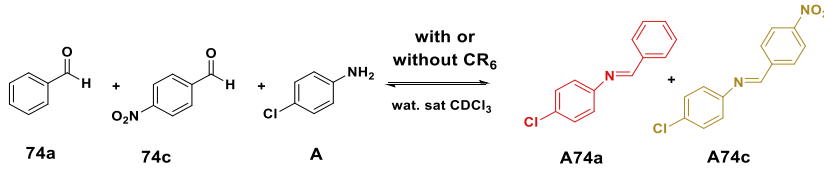

Scheme S7. Competition experiment of **A74a** and **A74c** in presence and in absence of capsule **CR_6**.

Table S9. Time-dependent conversion in **A74a** and **A74c** of an equimolar mixture of **A, 74a** and **74c** in absence of **CR_6**

	in absence of CR_6	
Time[b] (h)	**A74a (%)[c]**	**A74c (%)[c]**
0.5	-[e]	-[e]
1	-[e]	-[e]
2	-[e]	-[e]
4	-[e]	-[e]
6	-[e]	-[e]
24	10	13
48	10	13

[a] Reaction conditions: **74a**, **74c** (0.0423 mmol, 42.3 mM), **A** (0.0423 mmol, 42.3 mM) in water-saturated $CDCl_3$ (1.0 mL), rt. [b] Time at which an aliquot (30 µL) of the reaction mixture was taken and monitored via ^{1}H-NMR spectrum. [c]Conversion was calculated using TCE as internal standard.

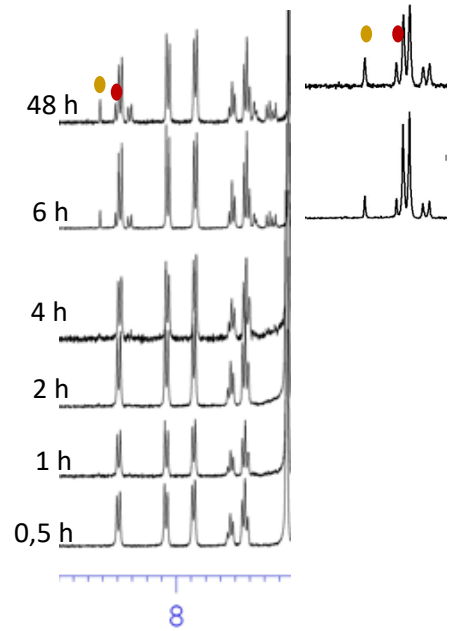

Figure S10. Seelcted region of ^{1}H NMR (400 MHz, $CDCl_3$, 298 K) spectra of an equimolar mixture of **A, 74a** and **74c** (42.3 mM each, water saturated $CDCl_3$, r.t.) after 0.5, 1, 2, 4, 6, 24 and 48 h.

Table S10. Time-dependent conversion in **A74a** and **A74c** of an equimolar mixture of **A, 74a** and **74c** in presence of **CR_6**

	in presence of CR_6	
Time[b] (h)	**A74a (%)[c,d]**	**A74c (%)[c,d]**
0.5	18	7
1	20	13
2	20	24
4	20	36
6	21	42
24	13	60
48	13	60

[a] Reaction conditions: **74a**, **74c** (0.0423 mmol, 42.3 mM), **A** (0.0423 mmol, 42.3 mM), capsule **CR_6** (42.3 mM), water-saturated $CDCl_3$ (1.0 mL), rt. [b] Time at which an aliquot (30 µL) of the reaction mixture was taken and monitored via ^{1}H-NMR spectrum. [c] Conversion was calculated using TCE as internal standard. [d] Conversion was calculated after addition of DMSO (2 µL) to a reaction aliquot, in order to disaggregate the capsule. [e] Below the detection limit. Error in ^{1}H-NMR signal integration was ± 5%.

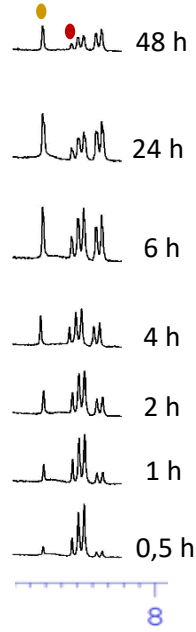

Figure S11. Selected region of ^{1}H NMR (400 MHz, $CDCl_3$, 298 K) spectra of an equimolar mixture of **A, 74a, 74c and CR_6**(42.3 mM each, water saturated $CDCl_3$, r.t.) after 0.5, 1, 2, 4, 6, 24 and 48 h.

Competitive reaction between equivalent amounts of 74a, 74d and A with and without capsule CR_6.

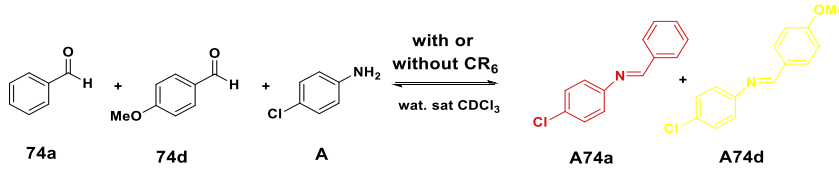

Scheme S8. Competition experiment of **A74a** and **A74d** in presence and in absence of capsule **CR_6**.

Table S11. Time-dependent conversion in **A74a** and **A74d** of an equimolar mixture of **A, 74a** and **74d** in absence of **CR_6**.

	in absence of CR_6	
Time[b] (h)	**A74a (%)[c]**	**A74d (%)[c]**
0.5	-[e]	-[e]
1	-[e]	-[e]
2	-[e]	-[e]
4	-[e]	-[e]
6	-[e]	-[e]
24	14	7
48	14	7

[a] Reaction conditions: **74a**, **74d** (0.0423 mmol, 42.3 mM), **A** (0.0423 mmol, 42.3 mM) in water-saturated $CDCl_3$ (1.0 mL), rt. [b] Time at which an aliquot (30 µL) of the reaction mixture was taken and monitored via ^{1}H-NMR spectrum. [c] Conversion was calculated using TCE as internal standard.

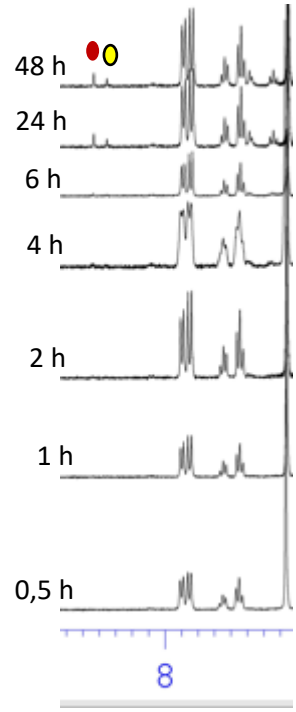

Figure S12. Selected region of ^{1}H NMR (400 MHz, $CDCl_3$, 298 K) spectra of an equimolar mixture of **A, 74a and 74d** (42.3 mM each, water saturated $CDCl_3$, r.t.) after 0.5, 1, 2, 4, 6, 24 and 48 h.

Table S12. Time-dependent conversion in **A74a** and **A74d** of an equimolar mixture of **A, 74a** and **74d** in presence of **CR$_6$**.

	in presence of CR$_6$	
Time[b] (h)	**A74a (%)[c,d]**	**A74d (%)[c,d]**
0.5	19	9
1	20	14
2	25	13
4	28	18
6	31	17
24	31	17
48	31	17

[a] Reaction conditions: **74a**, **74d** (0.0423 mmol, 42.3 mM), **A** (0.0423 mmol, 42.3 mM), capsule **CR$_6$** (42.3 mM), water-saturated $CDCl_3$ (1.0 mL), rt. [b] Time at which an aliquot (30 µL) of the reaction mixture was taken and monitored via ^{1}H-NMR spectrum. [c] Conversion was calculated using TCE as internal standard. [d] Conversion was calculated after addition of DMSO (2 µL) to a reaction aliquot, in order to disaggregate the capsule. [e] Below the detection limit. Error in ^{1}H-NMR signal integration was ± 5%.

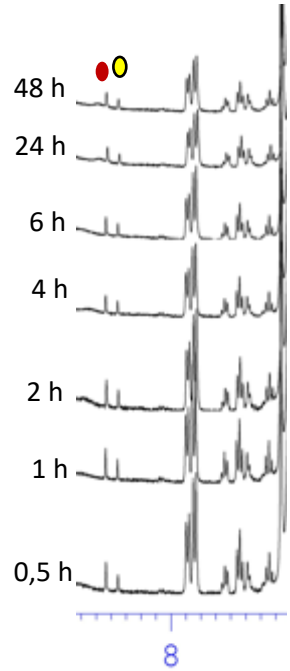

Figure S13. Selected region of ^{1}H NMR (400 MHz, $CDCl_3$, 298 K) spectra of an equimolar mixture of **A, 74a, 74d** and **CR$_6$** (42.3 mM each, water saturated $CDCl_3$, r.t.) after 0.5, 1, 2, 4, 6, 24 and 48 h.

Competitive reaction between equivalent amounts of 74a, 74b and B with and without capsule CR_6

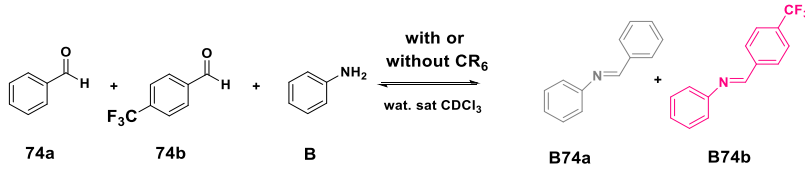

Scheme S9. Competition experiment of **B74a** and **B74b** in presence and in absence of capsule **CR_6**.

S13. Time-dependent conversion in **B74a** and **B74a** of an equimolar mixture of **B, 74a** and **74b** in absence of **CR_6**.

	in absence of CR_6	
Time[b] (h)	**B74a (%)[c]**	**B74b (%)[c]**
0.5	-[e]	-[e]
1	-[e]	-[e]
2	-[e]	-[e]
4	-[e]	-[e]
6	8	10
24	13	20
48	32	51
72	32	51

[a] Reaction conditions: **74a**, **74b** (0.0423 mmol, 42.3 mM), **B** (0.0423 mmol, 42.3 mM) in water-saturated $CDCl_3$ (1.0 mL), rt. [b] Time at which an aliquot (30 µL) of the reaction mixture was taken and monitored via ^{1}H-NMR spectrum.[c] Conversion was calculated using TCE as internal standard. [e]Below the detection limit. Error in ^{1}H-NMR signal integration was ± 5%.

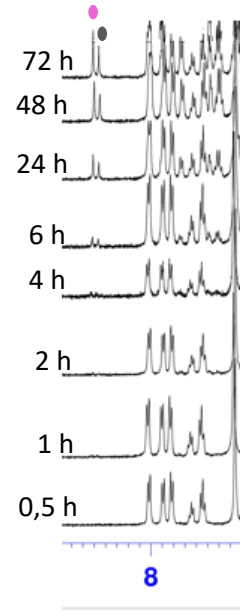

Figure S14. Selected region of ^{1}H NMR (400 MHz, $CDCl_3$, 298 K) spectra of an equimolar mixture of **74a, 74b** and **B,** (42.3 mM each, water saturated $CDCl_3$, r.t.) after 0.5, 1, 2, 4, 6, 24, 48 and 72 h.

Table S14. Time-dependent conversion in **A74a** and **A74b** of an equimolar mixture of **B, 74a** and **74b** in presence of **CR**$_6$.

	in presence of CR$_6$	
Time[b] (h)	**B74a (%)[c,d]**	**B74b (%)[c,d]**
0.5	20	17
1	19	36
2	12	41
4	10	44
6	11	51
24	10	52
48	10	52
72	10	52

[a] Reaction conditions: **74a**, **74b** (0.0423 mmol, 42.3 mM), **B** (0.0423 mmol, 42.3 mM), capsule **CR$_6$** (42.3 mM), water-saturated $CDCl_3$ (1.0 mL), rt. [b] Time at which an aliquot (30 µL) of the reaction mixture was taken and monitored via ^{1}H-NMR spectrum. [c] Conversion was calculated using TCE as internal standard. [d] Conversion was calculated after addition of DMSO (2 µL) to a reaction aliquot, in order to disaggregate the capsule. [e] Below the detection limit. Error in ^{1}H-NMR signal integration was ± 5%.

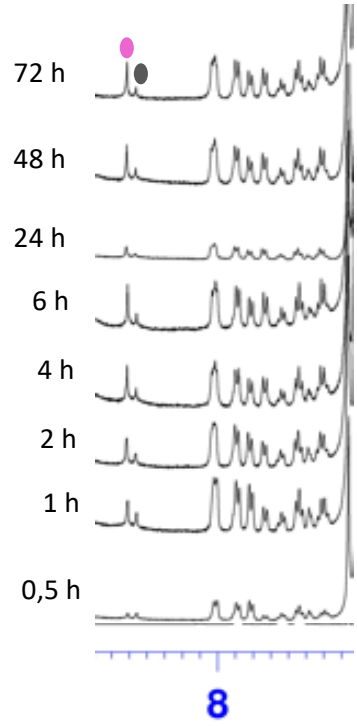

Figure S15. Selected region of ^{1}H NMR (400 MHz, $CDCl_3$, 298 K) spectra of an equimolar mixture of **B, 74a, 74b** and **CR$_6$** (42.3 mM each, water saturated $CDCl_3$, r.t.) after 0.5, 1, 2, 4, 6, 24, 48 and 72 h.

Competitive reaction between equivalent amounts of 74a, 74b and C with and without capsule CR_6

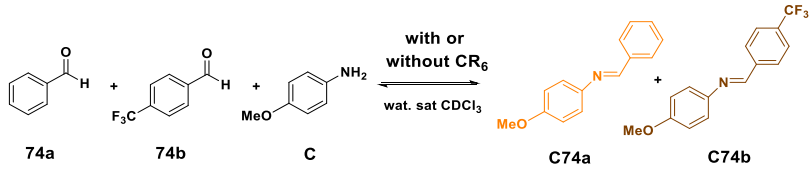

Scheme S10. Competition experiment of **C74a** and **C74b** in presence and in absence of capsule **CR_6**.

Table S15. Time-dependent conversion in **C74a** and **C74d** of an equimolar mixture of **C, 74a** and **74b** in absence of **CR_6**.

	in absence of CR_6	
Time[b] (h)	**C74a (%)[c]**	**C74b (%)[c]**
0.5	13	10
1	16	15
2	20	17
4	34	32
6	41	41
24	48	50
48	48	49

[a] Reaction conditions: **C**, **74a**, **74b** (0.0423 mmol, 42.3 mM), **CR_6** (0.0423 mmol, 42.3 mM) in water-saturated $CDCl_3$ (1.0 mL), rt. [b] Time at which an aliquot (30 μL) of the reaction mixture was taken and monitored via ^{1}H-NMR spectrum. [c] Conversion was calculated using TCE as internal standard. [e]Below the detection limit. Error in ^{1}H-NMR signal integration was ± 5%.

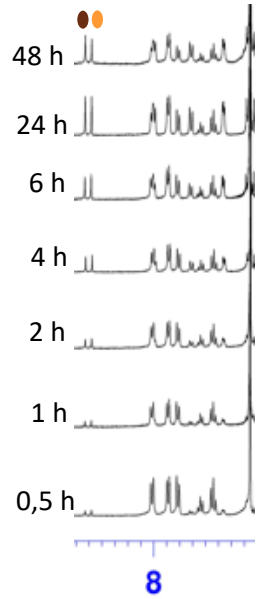

Figure S16. Selected region of ^{1}H NMR (400 MHz, $CDCl_3$, 298 K) spectra of an equimolar mixture of **C**, **74a, 74b** and **CR_6** (42.3 mM each, water saturated $CDCl_3$, r.t.) after 0.5, 1, 2, 4, 6, 24 and 48 h.

Table S16. Time-dependent conversion in **C74a** and **C74b** of an equimolar mixture of **C, 74a** and**74b** in presence of **CR_6**

	in presence of CR_6	
Time[b] (h)	**C74a (%)[c,d]**	**C74b (%)[c,d]**
0.5	36	52
1	32	67
2	32	67
4	32	67
6	32	67
24	32	67
48	32	67

[a] Reaction conditions: **74a**, **74b** (0.0423 mmol, 42.3 mM), **C** (0.0423 mmol, 42.3 mM), capsule **CR_6** (42.3 mM), water-saturated $CDCl_3$ (1.0 mL), rt. [b] Time at which an aliquot (30 µL) of the reaction mixture was taken and monitored via ^{1}H-NMR spectrum. [c] Conversion was calculated using TCE as internal standard. [d] Conversion was calculated after addition of DMSO (2 µL) to a reaction aliquot, in order to disaggregate the capsule. [e] Below the detection limit. Error in ^{1}H-NMR signal integration was ± 5%.

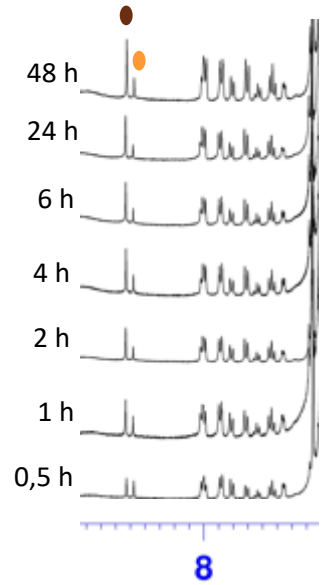

Figure S17. Selected region of ^{1}H NMR (400 MHz, $CDCl_3$, 298 K) spectra of an equimolar mixture of **C, 74a, 74b** and **CR_6** (42.3 mM each, water saturated $CDCl_3$, r.t.) after 0.5, 1, 2, 4, 6, 24 and 48 h.

Competitive reaction between equivalent amounts of 74a, 74b and D with and without capsule CR_6

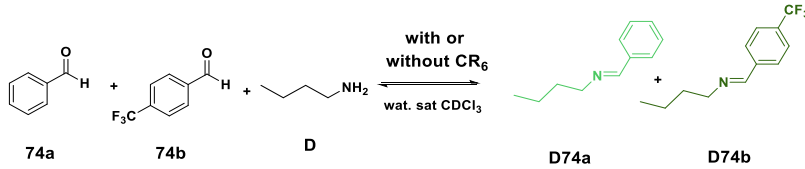

Scheme S11. Competition experiment of **D74a** and **D74b** in presence and in absence of capsule **CR_6**.

Table S17. Time-dependent conversion in **A74a** and **A74b** of an equimolar mixture of **D, 74a** and **74b** with and without **CR_6**.

	in absence of CR_6		*in presence of CR_6*	
Time[b] (h)	**D74a (%)[c]**	**D74b (%)[c]**	**D74a (%)[c,d]**	**D74b (%)[c,d]**
0.5	12	13	3	12
1	14	26	3	12
5	17	40	3	12
24	17	40	3	13

[a] Reaction conditions: **74a**, **74c** (0.0423 mmol, 42.3 mM), D (0.0423 mmol, 42.3 mM), with and without capsule **CR_6** (42.3 mM), water-saturated $CDCl_3$ (1.0 mL), rt. [b] Time at which an aliquot (30 µL) of the reaction mixture was taken and monitored via ^{1}H-NMR spectrum. [c] Conversion was calculated using TCE as internal standard. [d]Conversion was calculated after addition of DMSO (2 µL) to a reaction aliquot, in order to disaggregate the capsule. [e]Below the detection limit. Error in ^{1}H-NMR signal integration was ± 5%.

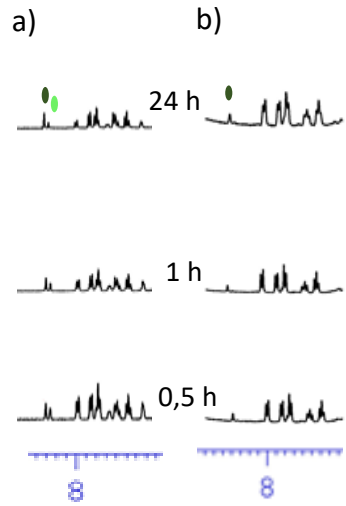

Figure S18. Selected region of ^{1}H NMR (400 MHz, $CDCl_3$, 298 K) spectra of an equimolar mixture of **D, 74a, 74b** (42.3 mM each, water saturated $CDCl_3$, r.t.) after 0,5 and 24 h in absence (a) or in presence (b) of **CR_6**.

Competitive reaction between equivalent amounts of 74a, A and D with and without capsule CR_6

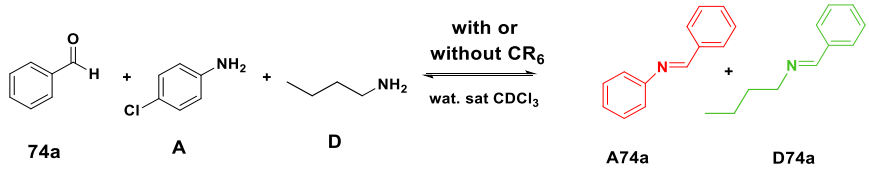

Scheme S12. Competition experiment of **D74a** and **A74a** in presence and in absence of capsule **CR_6**.

Table S18. Time-dependent conversion in **A74a** and **D74a** of an equimolar mixture of **A, D** and **74a** in presence and in absence of **CR_6**.

	in absence of CR_6		*in presence of CR_6*	
Time[b] (h)	**A74a (%)[c]**	**D74a (%)[c]**	**A74a (%)[c,d]**	**D74a (%)[c,d]**
0.5	-[e]	18	18	14
3	-[e]	57	25	15
24	25	50	25	15

[a] Reaction conditions: **74a**, **A** (0.0423 mmol, 42.3 mM), **D** (0.0423 mmol, 42.3 mM), capsule **CR_6** (42.3 mM), water-saturated $CDCl_3$ (1.0 mL), rt. [b] Time at which an aliquot (30 μL) of the reaction mixture was taken and monitored via ^{1}H-NMR spectrum. [c] Conversion was calculated using TCE as internal standard. [d]Conversion was calculated after addition of DMSO (2 μL) to a reaction aliquot, in order to disaggregate the capsule. [e]Below the detection limit. Error in ^{1}H-NMR signal integration was ± 5%.

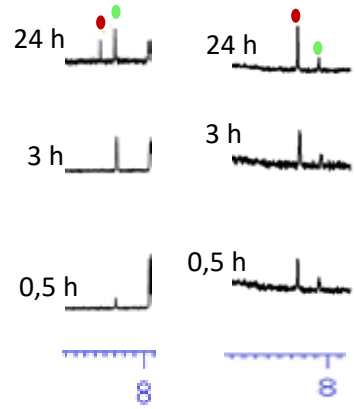

Figure S19. Selected region of ^{1}H NMR (400 MHz, $CDCl_3$, 298 K) spectra of an equimolar mixture of **A, D** and **74a** (42.3 mM each, water saturated $CDCl_3$, r.t.) after 0,5 and 24 h in absence (a) or in presence (b) of **CR_6**.

Competitive reaction between equivalent amounts of 74a, 74b, A and B with and without capsule CR_6

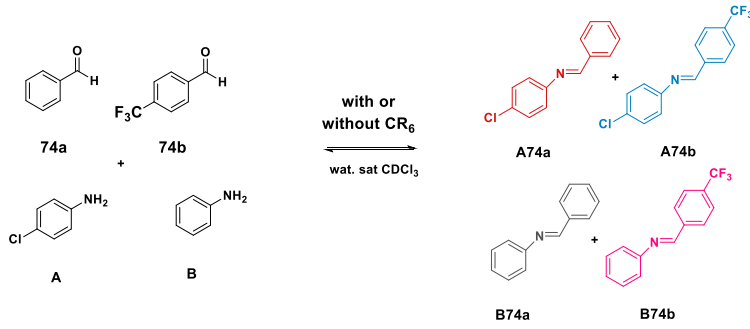

Scheme S13. Competition experiment of **A74a, A74b, B74a** and **B74b** in presence and in absence of capsule **CR_6**.

Table S19. Time-dependent conversion in imines **A74a, A74b, B74a** and **B74b** of an equimolar mixture of **74a, 74b, A** and **B** in absence of **CR_6**

	in absence of CR_6			
Time[b] (h)	**A74a (%)[c]**	**A74b (%)[c]**	**B4a (%)[c]**	**B74b b(%)[c]**
0.5	-[e]	-[e]	-[e]	-[e]
1	-[e]	-[e]	-[e]	-[e]
2	3	3	3	6
4	7	7	7	11
6	5	7	4	9
24	17	18	14	19
48	17	18	14	19

[a] Reaction conditions: **74a**, **74b, A and B** (0.0423 mmol, 42.3 mM) in water-saturated $CDCl_3$ (1.0 mL), rt. [b] Time at which an aliquot (30 μL) of the reaction mixture was taken and monitored via ^{1}H-NMR spectrum. [c] Conversion was calculated using TCE as internal standard. [e]Below the detection limit. Error in ^{1}H-NMR signal integration was ± 5%.

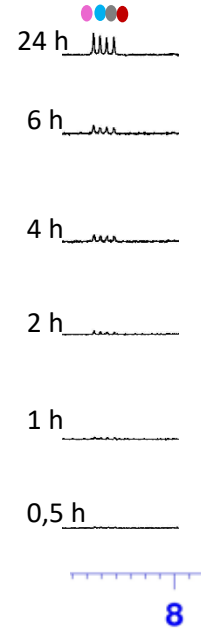

Figure S20. Selected region of ^{1}H NMR (400 MHz, $CDCl_3$, 298 K) spectra of an equimolar mixture of **A, B, 74a and 74b** (42.3 mM each, water saturated $CDCl_3$, r.t.) after 0.5, 1, 2, 4, 6 and 24 h in absence of CR_6.

Table S20. Time-dependent conversion in imines **A74a, A74b, B74a** and **B74b** of an equimolar mixture of **74a, 74b, A** and **B** in presence of **CR_6**.

	in presence of CR_6			
Time[b] (h)	**A74a (%)[d]**	**A74b (%)[d]**	**B4a (%)[d]**	**B4b (%)[d]**
0.5	25	11	17	20
1	28	24	19	34
2	24	36	16	36
4	21	47	14	42
6	16	48	14	35
24	15	50	13	35
48	15	50	13	35

[a] Reaction conditions: **74a, 74b, A** and **B** (0.0423 mmol, 42.3 mM) in water-saturated $CDCl_3$ (1.0 mL), rt. [b] Time at which an aliquot (30 µL) of the reaction mixture was taken and monitored via ^{1}H-NMR spectrum. [c] Conversion was calculated using TCE as internal standard. [d]Conversion was calculated after addition of DMSO (2 µL) to a reaction aliquot, in order to disaggregate the capsule. [e]Below the detection limit. Error in ^{1}H-NMR signal integration was ± 5%.

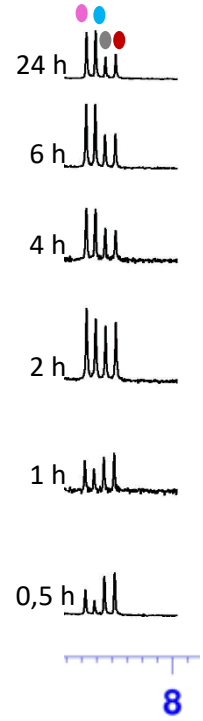

Figure S21. Selected region of ^{1}H NMR (400 MHz, $CDCl_3$, 298 K) spectra of an equimolar mixture of **74a, 74b, A** and **B** (42.3 mM each, water saturated $CDCl_3$, r.t.) after 0.5, 1, 2, 4, 6 and 24 H in absence of **CR_6**

Competitive reaction between equivalent amounts of 74b, 74d, C and E with and without capsule CR_6

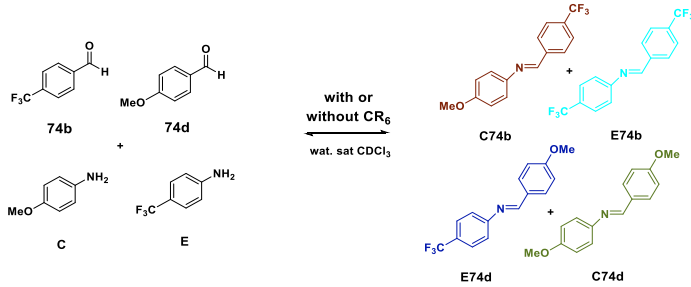

Scheme S14. Competition experiment of **C74b, C74d, E74b** and **E74d** in presence and in absence of capsule **CR_6**.

Table S21. Time-dependent conversion in **C74b, C74d, E74b** and **E74d** of an equimolar mixture of **74b, 74d, C** and **D** in absence of **CR_6**

	in absence of CR_6			
Time[b] (h)	**C74b (%)[c]**	**C74d (%)[c]**	**D74b (%)[c]**	**D74d (%)[c]**
0.5	4	2	-[e]	-[e]
1	12	5	-[e]	-[e]
2	18	5	-[e]	-[e]
4	21	8	-[e]	-[e]
6	33	21	-[e]	-[e]
24	54	34	-[e]	-[e]
48	54	34	-[e]	-[e]

[a] Reaction conditions: **74b, 74d, C** and **D** (0.0423 mmol, 42.3 mM), in water-saturated $CDCl_3$ (1.0 mL), rt. [b] Time at which an aliquot (30 μL) of the reaction mixture was taken and monitored via ^{1}H-NMR spectrum. [c] Conversion was calculated using TCE as internal standard. [e] Below the detection limit. Error in ^{1}H-NMR signal integration was ± 5%.

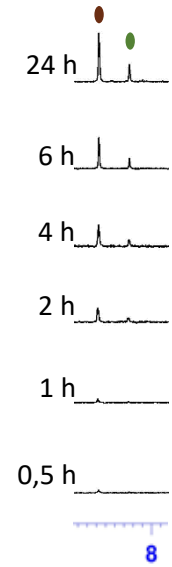

Figure S22. Selected region of ^{1}H NMR (400 MHz, $CDCl_3$, 298 K) spectra of an equimolar mixture of **74b, 74d, C** and **D** (42.3 mM each, water saturated $CDCl_3$, r.t.) after 0.5, 1, 2, 4, 6 and 24 H in absence of **CR_6**

Table S22. Time-dependent conversion in **C74b, C74d, E74b** and **E74d** of an equimolar mixture of **74b, 74d, C** and **D** in presence of **CR_6**

	in presence of CR_6			
Time[b] (h)	**C74b (%)[d]**	**C74d (%)[d]**	**D74b (%)[d]**	**D74d (%)[d]**
0.5	47	19	-[e]	4
1	53	22	5	8
2	64	13	9	6
4	61	9	14	6
6	66	7	12	3
24	66	5	12	5
48	66	5	12	5

[a] Reaction conditions: **74b, 74d, C** and **D** (0.0423 mmol, 42.3 mM), in water-saturated $CDCl_3$ (1.0 mL), rt. [b] Time at which an aliquot (30 μL) of the reaction mixture was taken and monitored via ^{1}H-NMR spectrum. [c] Conversion was calculated using TCE as internal standard. [d]Conversion was calculated after addition of DMSO (2 μL) to a reaction aliquot, in order to disaggregate the capsule. [e]Below the detection limit. Error in ^{1}H-NMR signal integration was ± 5%.

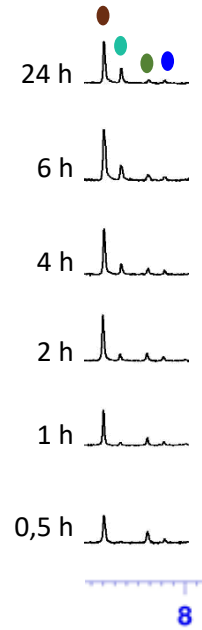

Figure S23. Selected region of ^{1}H NMR (400 MHz, $CDCl_3$, 298 K) spectra of an equimolar mixture of **74b, 74d, C** and **D** (42.3 mM each, water saturated $CDCl_3$, r.t.) after 0.5, 1, 2, 4, 6 and 24h in presence of CR_6

7.3.8 Uptake experiments

General experimental conditions in presence of CR_6

Resorcinarene **16** (281.6 mg, 254.7 µmol, 6 equiv) was weighed in a 4 mL vial and 1 mL of water saturated deuterated chloroform was added. The mixture was warmed at 50 °C until clarification (ca 5 min). To this solution the substrate (0.0423 mmol, 1 equiv) was added at 30 °C under stirring. An aliquot portion of this mixture (500 µL) was taken and monitored by ^{1}H NMR spectroscopy after an appropriate time. The spectra were recorded before and after addition of DMSO (35 µL). The uptakes of the substrates within **CR_6** were measured by quantitative ^{1}H NMR experiments using the equation $([G]_0 - [G]_t)/ [G]_0$[64], where the terms $[G]_0$ indicates the total concentration of **G** and $[G]_t$ the remaining free **G** after the sample was equilibrated for the appropriate time.

Competitive uptake experiment of 74a/74b within CR_6

A competition experiment was performed in which aldehydes **74a** and **74b** were in competition to occupy the cavity of capsule **CR_6**. Resorcinarene **16** (281.6 mg, 254.7 µmol, 6 equiv.) was weighed in a 4 mL vial and 1mL of water saturated $CDCl_3$ was added. The mixture was warmed at 50 °C until clarification (ca 5 min). To this solution, aldehydes **74a** (0.0423 mmol, 1 equiv) and **74b** (0.0423 mmol, 1 equiv.) were added simultaneously and the mixture was kept at 30 °C under stirring for 1 h before being subjected to ^{1}H-NMR spectroscopy. An aliquot portion of this mixture (500 µL) was taken and monitored by ^{1}H NMR spectroscopy. The spectra were recorded before and after addition of DMSO (35 µL), fig S24. The ^{1}H NMR signals of free the

aldehydes (7.51 ppm for **74a** and 7.89 ppm for **74b**) were integrated with respect to the signal of TCE (5.97 ppm, 2H, 0.019 mmol).

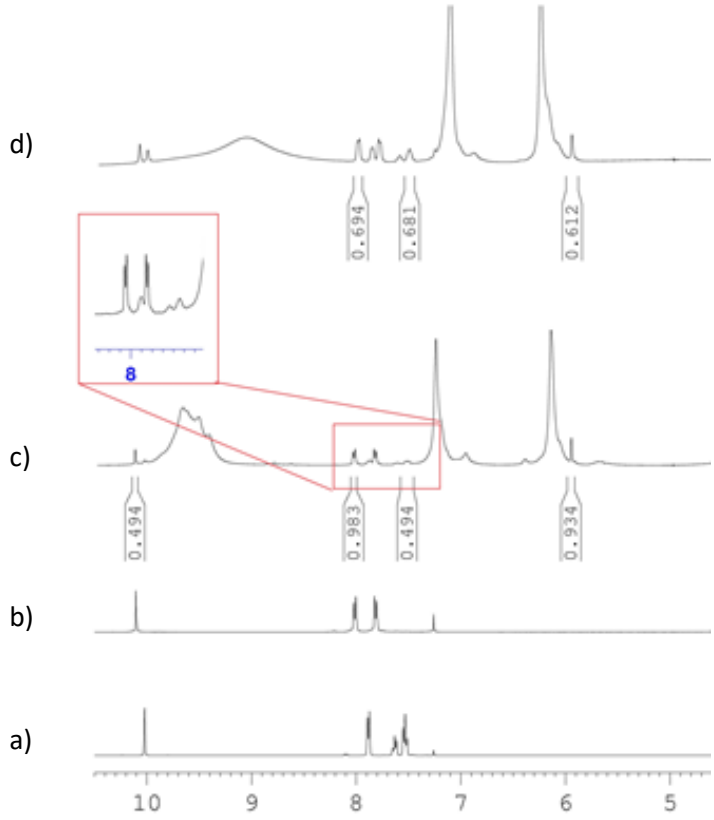

Figure S24. Selected region of ^{1}H NMR (400 MHz, $CDCl_3$, 298 K) spectra of: a) free 74a; b) free 74b; c) an equimolar mixture of **74a**, **74b** and **CR_6** (42.3 mM each, water saturated $CDCl_3$, r.t.) and d) an equimolar mixture of **74a**, **74b** and **CR_6** (42.3 mM each, water saturated $CDCl_3$, r.t.) after addition of DMSO.

Uptake of imines A74a and A74b inside the capsule

Resorcinarene **16** (281.6 mg, 254.7 µmol, 6 equiv.) was weighed in a 4 mL vial and 1mL of water saturated $CDCl_3$ was added. The mixture was warmed at 50 °C until clarification (ca 5 min). To this solution, the imine (0.0423 mmol, 1 equiv) was added. Immediately after the mixing, an aliquot portion of this mixture (500 µL) was taken and monitored by ^{1}H NMR spectroscopy. The spectra were recorded before and after addition of DMSO (35 µL). The quantity of encapsulated imine was obtained by difference between the concentration of the free imine in solution with **CR_6** and that measured after disassembly of the hexameric capsule by adding DMSO. The ^{1}H NMR signals of free imines (8.46 ppm for **A74a** and 8.51 ppm for **A74b**) were integrated with respect to the signal of TCE (5.97 ppm, 2H, 0.019 mmol).

Table S23. Uptake of imines **A74a and A74b** inside **CR_6**.

Imine	Integral [a] (before adding DMSO)	mmol of free imine (**before adding DMSO**)	Integral [a] (after addition DMSO)	mmol free imine (**after addition DMSO**)	Uptake (%)
A74a	0.6012	0.0114	1.1123	0.0211	45
A74b	1.0523	0.0199	1.1035	0.0209	5

[a] Integral of free imine proton signal at 8.46 ppm for **A74a** and 8.51 ppm for **A74b**.

7.3.9 Predatory effect of CR_6: Stability of imines in presence of CR_6

General experimental conditions in presence of CR_6

Resorcinarene **16** (281.6 mg, 254.7 µmol, 6 equiv) was weighed in a 4 mL vial and 1 mL of water saturated deuterated chloroform was added. The

mixture was warmed at 50 °C until clarification (ca 5 min). To this solution the appropriate imine (0.0423 mmol, 1 equiv) was added at 30 °C under stirring. The mixture was monitored by taking aliquots over time and recording ^{1}H-NMR spectra. An aliquot portion of the mixture (30 µL) was taken and diluted with 470 µL of $CDCl_3$ (freshly filtered through activated 3Å molecular sieves and basic aluminium oxide) and, after by adding TCE (1 µL) as internal standard, the mixture was monitored by ^{1}H NMR spectroscopy. The spectra were recorded before and after addition of DMSO (2 µL) to the aliquot.

Control experiment in presence of CR_6 and DMSO

Resorcinarene **16** (281.6 mg, 254.7 µmol, 6 equiv) was weighed in a 4 mL vial and 1 mL of water saturated deuterated chloroform was added. The mixture was warmed at 50 °C until clarification (ca 5 min). To this solution DMSO (300 µL, 100 eq. respect capsule **CR_6**) was added, followed by imine **A74a** (0.0423 mmol). The mixture was monitored by taking aliquots over time and recording ^{1}H-NMR spectra. An aliquot portion of the mixture (30 µL) was taken and diluted with 470 µL of $CDCl_3$ (freshly filtered through activated 3Å molecular sieves and basic aluminium oxide) and, after by adding TCE (1 µL) as internal standard, the mixture was monitored by ^{1}H NMR spectroscopy.

General experimental conditions in absence of CR_6

Imines were dissolved in 1 mL of water-saturated $CDCl_3$. The mixture was monitored by taking aliquots over time and recording ^{1}H-NMR spectra. An aliquot portion of the mixture (30 µL) was taken and diluted with 470 µL of $CDCl_3$ (freshly filtered through activated 3Å molecular sieves and basic

aluminium oxide) and, after by adding TCE (1 µL) as internal standard, the mixture was monitored by ^{1}H NMR spectroscopy.

Stability of imine A74a in absence and in presence of CR_6

Table S24. Hydrolysis of **A74a** in presence of **CR_6**.[a]

	In presence of CR_6	
Time[a] (h)	**A74a (%)[b]**	**74a (%)[b]**
0	100	-[c]
0.5	38	62
1	36	64
4	35	65
72	34	66
144	34	66

[a] Time at which an aliquot (30 µL) of the mixture was taken and monitored via ^{1}H-NMR spectrum. [b]Conversion calculated after addition of DMSO. [c]Below the limit of detection. Error in ^{1}H-NMR signal integration was ± 5%.

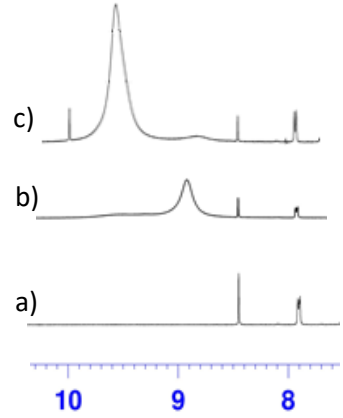

Figure S25. Selected region of ^{1}H NMR (400 MHz, $CDCl_3$, 298 K) of **A74a** (0.0423 mmol) (a) in water saturated $CDCl_3$ (1.0 mL), (b) the presence of **CR_6** (0.0423 mmol) and DMSO (0.3 mL) and c) in presence of **CR_6** (0.0423 mmol) after 4h.

Uptake of 74a inside the capsule after hydrolysis of A74a in presence of CR_6.

With respect to the total quantity of aldehyde **74a** obtained by hydrolysis of **A74a**, the uptake of aldehyde **74a** within **CR_6** was measured by quantitative ^{1}H NMR experiments following the experimental conditions reported in paragraph *7.3.8.* The quantity of encapsulated aldehyde was obtained by difference between the concentration of the free aldehyde in solution with **CR_6** and that measured after disassembly of the hexameric

capsule by adding DMSO. The ^{1}H NMR signal of the free aldehyde was integrated with respect to the signal of the internal standard (TCE).

Table S25. Uptake of aldehyde 74a inside CR_6.

time (h)	Integral [a] (before adding DMSO)	mmol of free aldehyde (**before adding DMSO**)	Integral [a] (after addition DMSO)	mmol free aldehyde (**after addition DMSO**)	Uptake (%)
0.5	0.0589	0.0187	0.0825	0.0261	28
1	0.0610	0.0193	0.0853	0.0270	29
4	0.0603	0.019	0.0866	0.0270	29

[a] Integral of free aldehyde proton signal at 10.0 ppm.

Stability of imine A74b in absence and in presence of CR_6

Table S26. Hydrolysis of **A74b** in presence of **CR_6**.

Time[a] (h)	**A74b (%)[b]**	**74b (%)[b]**
0	100	-[c]
0.5	100	-[c]
1	98	2
4	85	15
72	60	40
144	60	40

[a] Time at which an aliquot (30 µL) of the mixture was taken and monitored via ^{1}H-NMR spectrum. [b]Conversion calculated after addition of DMSO. [c]Below the limit of detection. Error in ^{1}H-NMR signal integration was ± 5%.

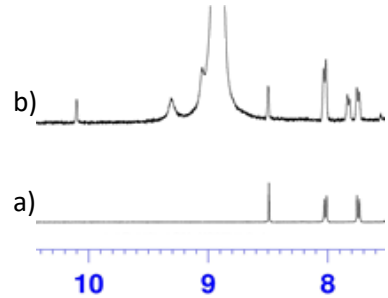

Figure S26. Selected region of ^{1}H NMR (400 MHz, $CDCl_3$, 298 K) of **A74b** (0.0423 mmol) (a) in water saturated $CDCl_3$ (1.0 mL); (b) in the presence of **CR_6** (0.0423 mmol) after 4h.

Uptake of 74b inside the capsule after hydrolysis of A74b in presence of CR_6.

With respect to the total quantity of aldehyde **74b** obtained by hydrolysis of **A74b**, the uptake of aldehyde **74b** within **CR_6** was measured by quantitative ^{1}H NMR experiments following the experimental conditions reported in paragraph *7.3.8.* The quantity of encapsulated aldehyde was obtained by difference between the concentration of the free aldehyde in solution with **CR_6** and that calculated after disassembly of the hexameric capsule by adding DMSO. The ^{1}H NMR signal of the free aldehyde was integrated with respect to the signal of the internal standard (TCE). Come sopra.

Table S27. Uptake of aldehyde **74b** inside **CR_6**.

time (h)	Integral[a] (before adding DMSO)	mmol free aldehyde **(before adding DMSO)**	Integral[a] (after addition DMSO)	mmol free aldehyde **(after addition DMSO)**	Uptake (%)
4	0.0199	0.006	0.0199	0.006	-
72	0.0534	0.0169	0.0534	0.0169	-

[a] Integral of free aldehyde proton signal at 10.1 ppm

Stability of imine B74a in presence and in absence of CR_6

Table S28. Hydrolysis of **B74a** in presence of $\mathbf{CR_6}$.[a]

Time[a] (h)	B74a (%)[b]	74a (%)[b]
0	100	-[c]
0.5	40	60
1	27	73
4	27	73
24	27	73

[a] Time at which an aliquot (30 µL) of the mixture was taken and monitored via ^{1}H-NMR spectrum. [b] Conversion calculated after addition of DMSO. [c]Below the limit of detection. Error in ^{1}H-NMR signal integration was ± 5%.

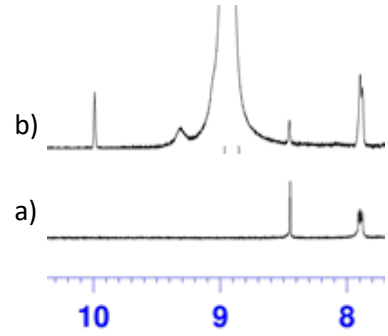

Figure S27. Selected region of ^{1}H NMR (400 MHz, $CDCl_3$, 298 K) of **B74a** (0.0423 mmol) (a) in water saturated $CDCl_3$ (1.0 mL), (b) in the presence of $\mathbf{CR_6}$ (0.0423 mmol) after 24h

Stability of imine C74a in presence and in absence of CR_6

Table S29. Hydrolysis of **C74a** with and without **CR_6**.

	with CR_6		without CR_6	
Time[a] (h)	**C74a (%)[b]**	**74a (%)[b]**	**C74a (%)**	**74a (%)**
0	100	-[c]	100	-[c]
0.5	65	35	100	-[c]
1	41	59	100	-[c]
24	41	59	89	11
96	41	59	89	11

[a] Time at which an aliquot (30 μL) of the mixture was taken and monitored via ^{1}H-NMR spectrum. [b] Conversion calculated after addition of DMSO. [c]Below the limit of detection. Error in ^{1}H-NMR signal integration was ± 5%.

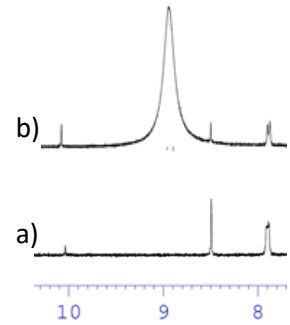

Figure S28. Selected region of ^{1}H NMR (400 MHz, $CDCl_3$, 298 K) of **C74a** (0.0423 mmol) (a) in water saturated $CDCl_3$ (1.0 mL), (b) in the presence of **CR_6** (0.0423 mmol) after 24h.

7.3.10 NMR experiments as evidence of encapsulation

-Encapsulation of benzaldehyde

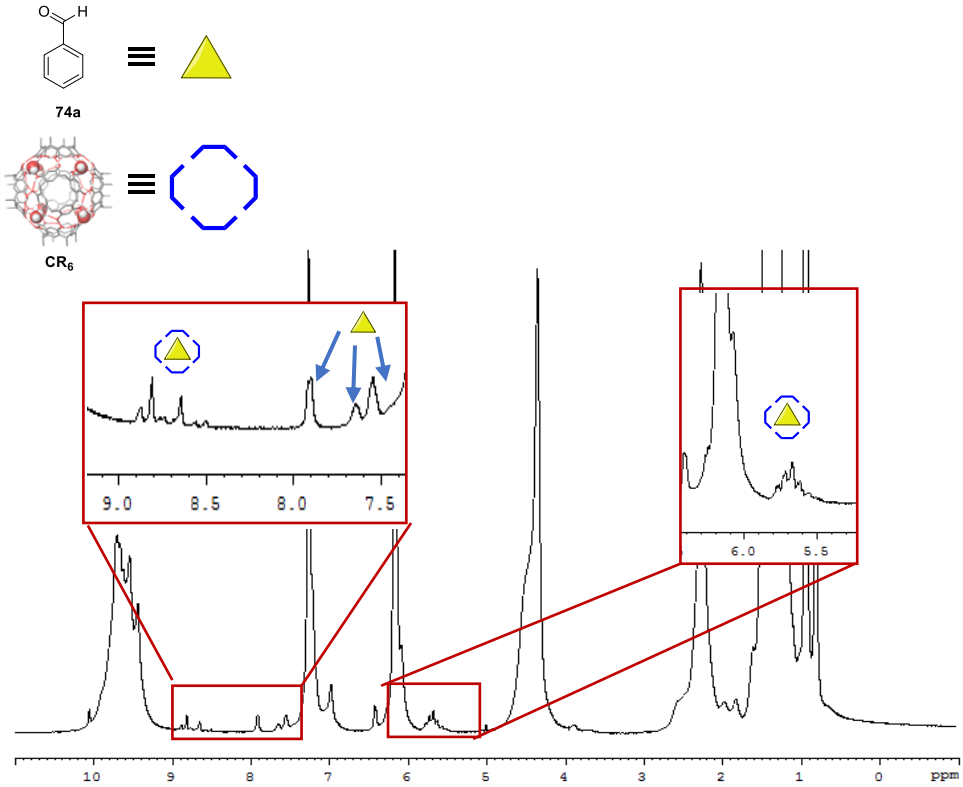

Figure S29. ^{1}H NMR spectrum (400 MHz, $CDCl_3$, 298 K) of the mixture of benzaldehyde **74a** and **CR$_6$** (42.3 mM of each component). The ^{1}H NMR signals of the encapsulated aldehyde **74a** are very complex, and in accord with the data previously reported by Cohen[134] and by Neri[55] which indicates that the molecules of **74a** are encapsulated in slightly different nanocontainers.

[134] L. Avram, Y. Cohen, *Org. Lett*. **2006**, *8*, 219.

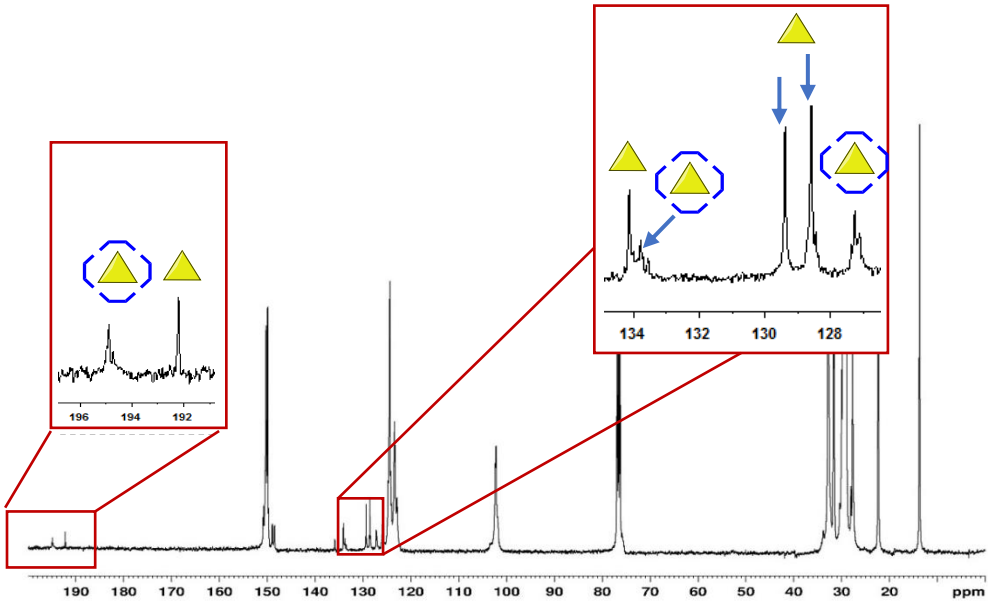

Figure S30. ^{13}C NMR spectrum (100 MHz, $CDCl_3$, 298 K) of the mixture of benzaldehyde **74a** and **CR_6**, 42.3 mM each component.

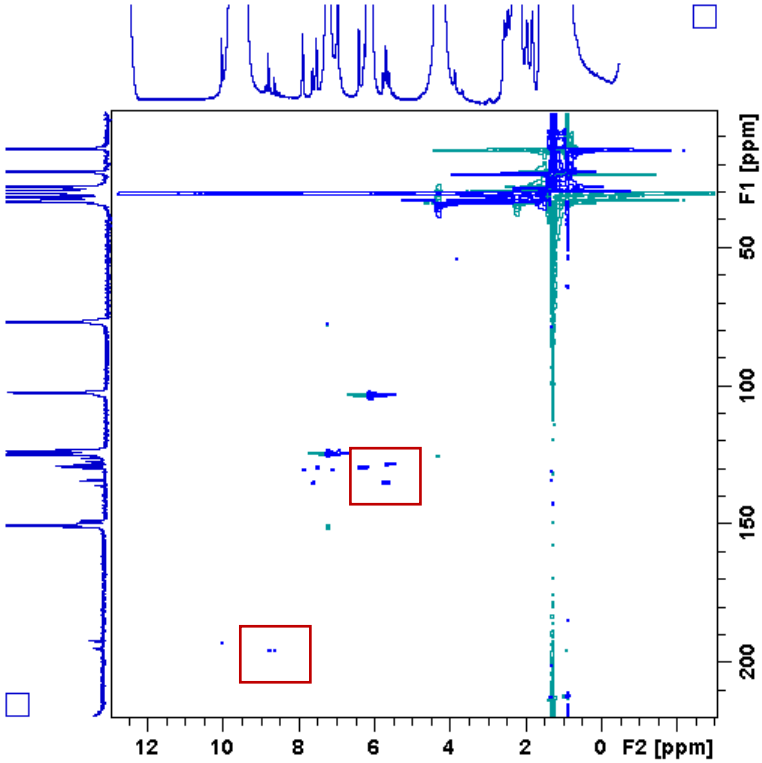

Figure S31. HSQC NMR spectrum (400 MHz, $CDCl_3$, 298 K) of the mixture of benzaldehyde **74a** and capsule **CR$_6$**, 42.3 mM each component.

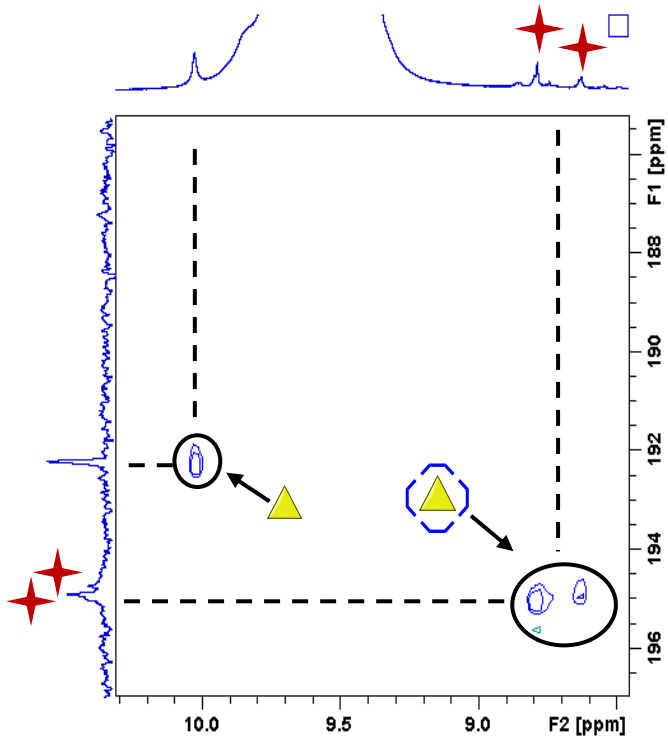

Figure S32. Selected region of the HSQC NMR spectrum in Figure S31. ^{1}J correlations between hydrogen and carbon of the aldehyde group of **74a** attributable to free and encapsulated **74a**.

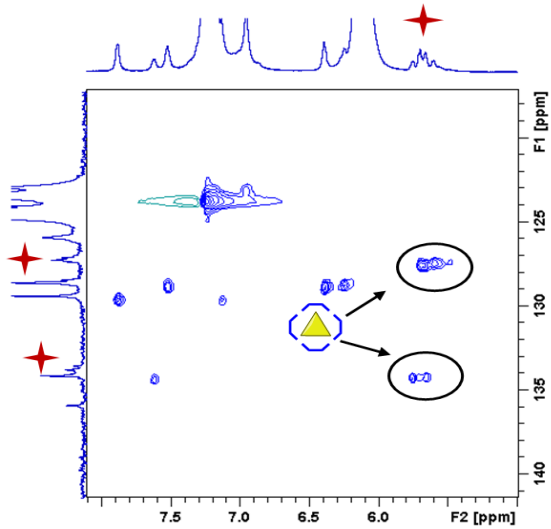

Figure S33. Selected region of the HSQC NMR spectrum in Figure S51. ^{1}J correlations attributable to the aromatic protons of the benzaldehyde **74a** inside the nanocontainer **CR$_6$** are marked.

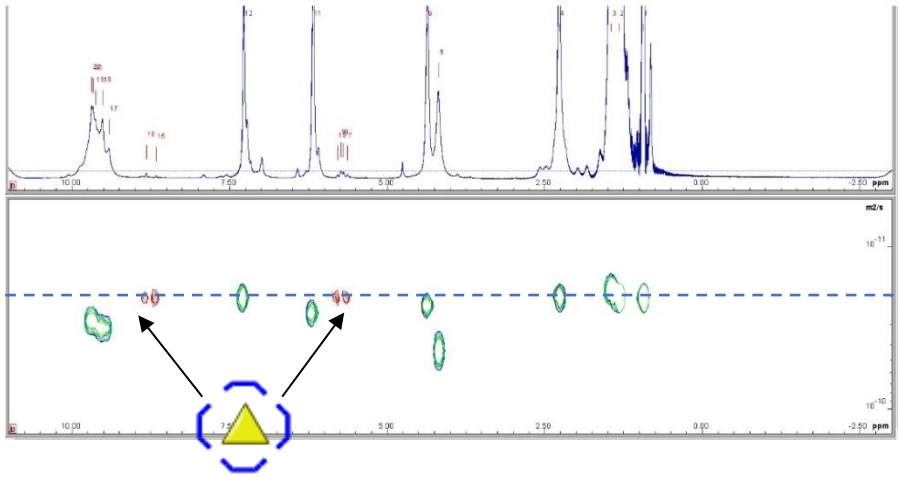

Figure S34. DOSY NMR (600 MHz, $CDCl_3$, 298 K) of the mixture 1:1 of benzaldehyde **74a** and capsule **CR$_6$** (42.3 mM). The signals pattern associated to **74a** inside the capsule **CR$_6$** are aligned with the capsule diffusion coefficient.

Encapsulation of p-CF_3benzaldehyde 74b

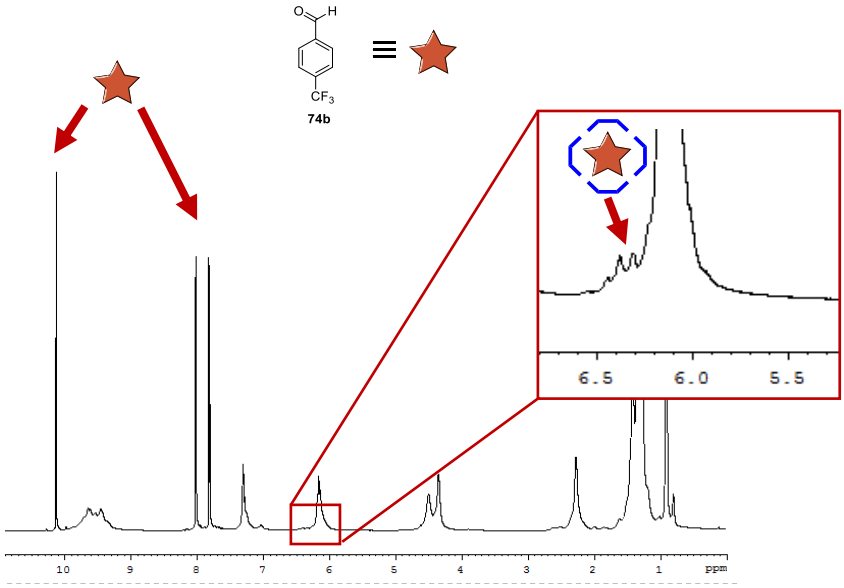

Figure S35. ^{1}H NMR spectrum (400 MHz, $CDCl_3$, 298 K) of the mixture of **74b** (0.846 mmol) and **CR_6** (0.0423 mmol).

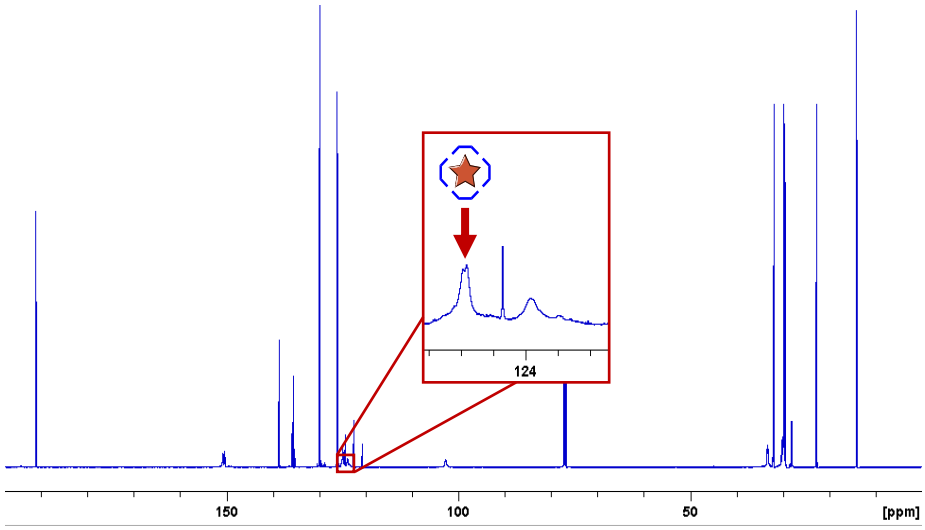

Figure S36. ^{13}C NMR spectrum (100 MHz, $CDCl_3$, 298 K) of the mixture of **74b** (0.846 mmol) and **CR_6** (0.0423mmol).

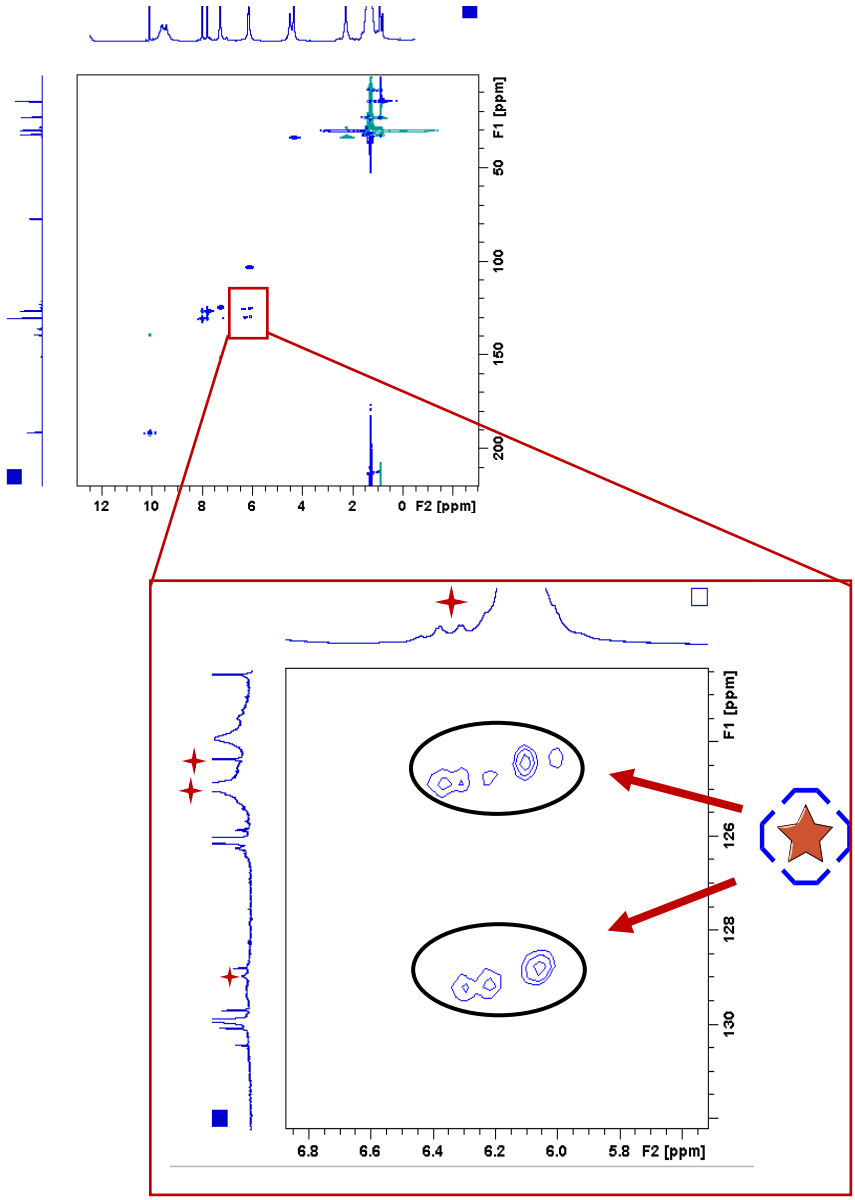

Figure S37. HSQC NMR spectrum (400 MHz, $CDCl_3$, 298 K) of the mixture **74b** (0.846 mmol) and **CR_6** (0.042 mmol). ^1J correlations attributable to the aromatic protons of **74b** inside the nanocontainer **CR_6** are marked.

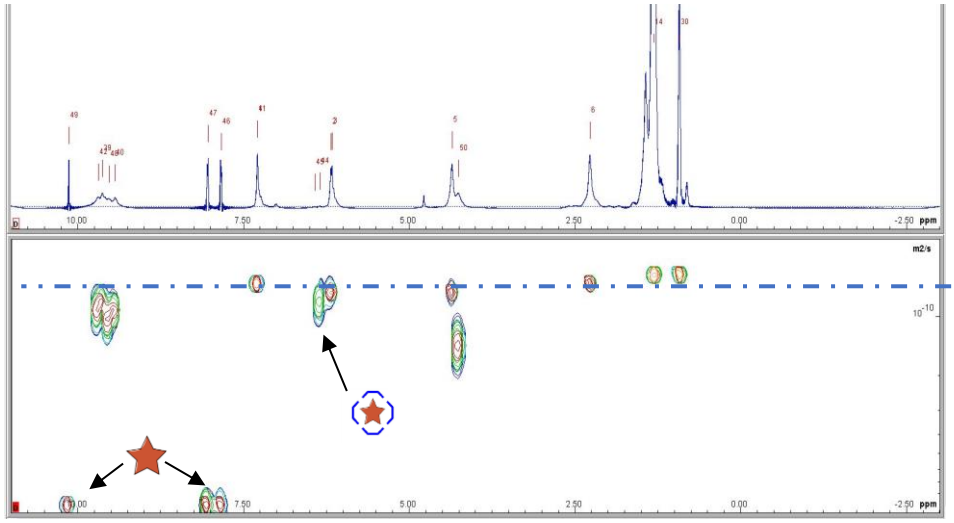

Figure S38. DOSY NMR (600 MHz, $CDCl_3$, 298 K) of the mixture of **74b** (0.846 mmol) and capsule **CR_6** (0.042 mmol).

As indicated in Figure S38, the signals pattern associated to **74b** inside the capsule **CR_6** are aligned with the capsule diffusion coefficient.

Encapsulation of p-chloroaniline A

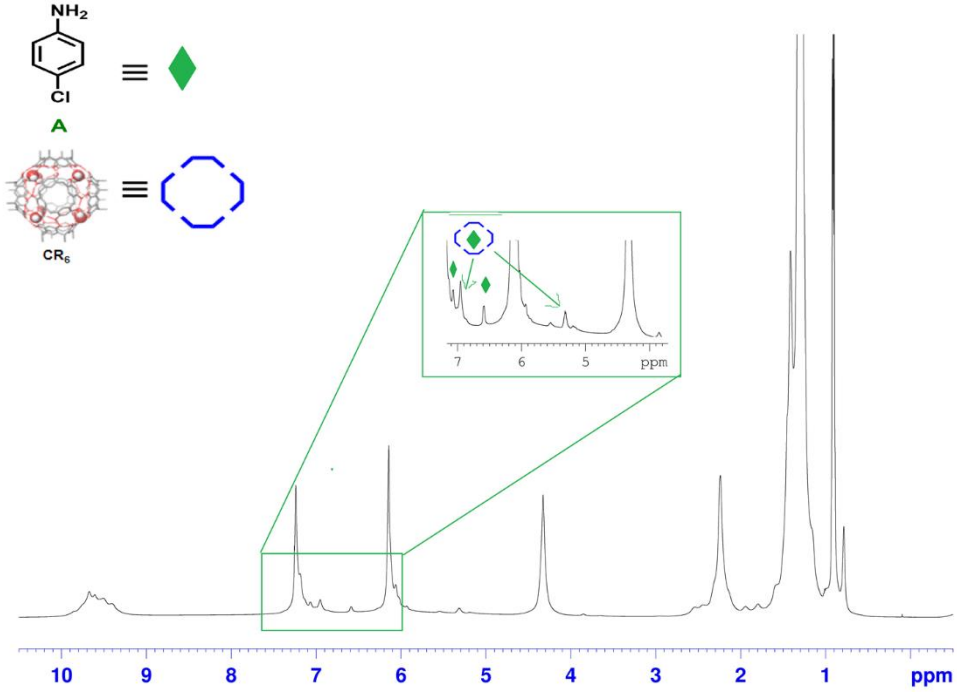

Figure S39. ^{1}H NMR spectrum (600 MHz, $CDCl_3$, 298 K) of the mixture of **A** (42.3 mM) and **CR$_6$** (42.3 mM)

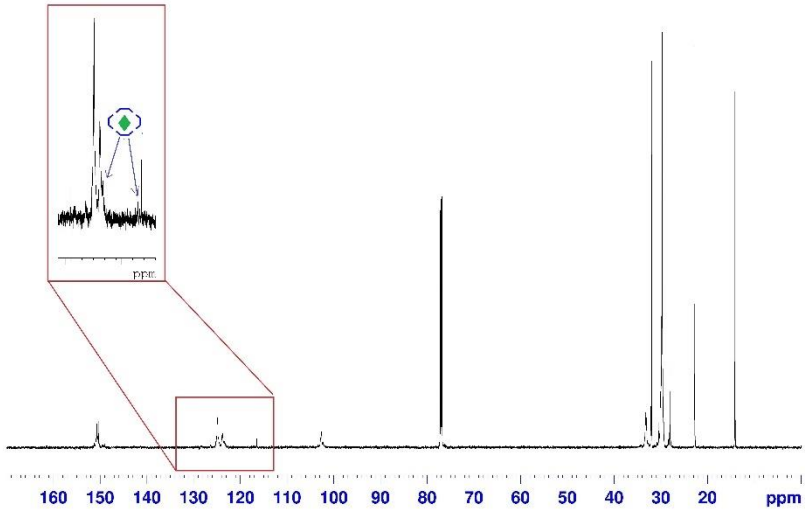

Figure S40. ^{13}C NMR spectrum (150 MHz, $CDCl_3$, 298 K) of the mixture of *p*-chloroanililne **A** and **CR$_6$**, 42.3 mM each component.

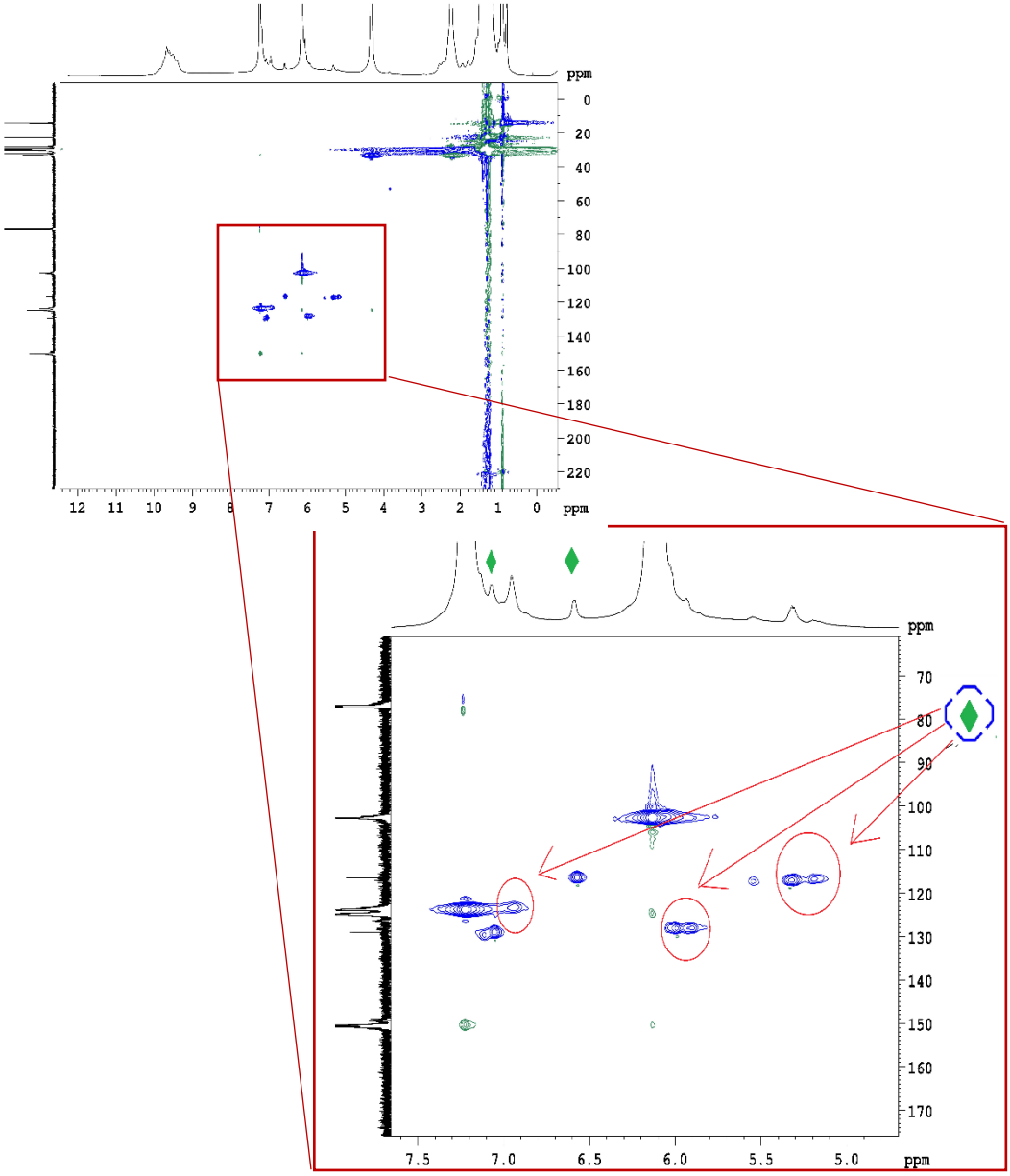

Figure S41. HSQC NMR spectrum (600 MHz, $CDCl_3$, 298 K) of the mixture **A** (42.3 mM) and **CR$_6$** (42.3mM).

7.3.11 Computational studies

The computational studies were performed by Dr. Paolo Della Sala from University of Salerno.

All calculations were performed using the ONIOM method implemented in the Gaussian16 package. M062X/dgdzvp level of theory was used for guests inside the capsule, OH groups of the resorcinarene units and for the 8 water molecules, while the semiempirical method PM6 was employed for all the other atoms.

The electronic zero-point corrected energies, enthalpies, and Gibbs free energies, expressed in Hartree, are reported in Tables S30 and S31. Enthalpy and Gibbs free energy in Table S30 are expressed in Kcal/mol.

Thermodynamic corrections were calculated at 298.15 K and 1 atm for all optimized geometries.

Table S30. Electronic zero-point corrected energies, enthalpies, and Gibbs free energies, expressed in Hartree

	E(0)	E	H	G	Oniom total energy Or EE
CR_6	-4273.909243	-4273.668128	-4273.667184	-4274.182345	-4277.467861
A74a	-1015.877148	-1015.865698	-1015.864754	-1015.916145	-1016.072092
A74b	-1352.884161	-1352.869104	-1352.868159	-1352.929597	-1353.084142
A74a⊂CR_6	-5289.822501	-5289.568164	-5289.567220	-5290.111374	-5293.578003
A74b⊂CR_6	-5626.775674	-5626.515751	-5626.514807	-5627.072559	-5630.534705

E(0)= EE + Zero–point Energy
E= EE + Thermal Energy Correction
H= EE + Thermal Enthalpy Correction
G= EE + Thermal Free Energy Correction
EE= Electronic energy

Table S31. Relative enthalpies (ΔH) and Gibbs free energies (ΔG) (in kcal mol^{-1}) for the encapsulation processes of imines **A74a** and **A74b** inside the capsule.

	ΔH_r	ΔG_r
A74a⊂CR$_6$	-22.14	-8.08
A74b⊂CR$_6$	12.87	24.71

Referred to those of the capsule **CR$_6$** and the corresponding non-encapsulated imines

7.4 General Procedures for the Diels-Alder reaction

7.4.1 General procedure in presence of CR_6 and Try-X

Resorcinarene **16** (281.6 mg, 254.7 µmol, 1.56 equiv.) was weighed in a 4 mL vial. Then, 1.1 mL of water-saturated chloroform was added, and the mixture was homogenized in an ultrasonic water bath at 40 °C for 10 min. To this clear yellow solution, trityl-X (0.1- 0.26 equiv) was added and after 5 min under stirring, the dienophiles (163 µmol, 1 equiv.) followed by the diene (1 - 3 equiv.) were added. The solution was kept stirring at the appropriate temperature and time. The reaction was monitored by ^{1}H NMR analysis taking aliquots of the reaction mixture (30 µL) at various time intervals and diluting with chloroform-d. The reaction was stopped by adding 40 µL of DMSO and the mixture was purified by flash chromatography on silica gel to afford the desired title compounds. *Endo/exo* ratios were determined by ^{1}H NMR analysis via integration of proton signals of the title compounds in comparison with literature data[135].

7.4.2 General procedure in presence of CR_6

Resorcinarene **16** (281.6 mg, 254.7 µmol, 1.56 equiv.) was weighed in a 4 mL vial. Then, 1.1 mL of water-saturated chloroform was added, and the mixture was homogenized in an ultrasonic water bath at 40 °C for 10 min. To this clear yellow solution dienophile (163 µmol, 1 equiv.) followed by the diene (1 – 3 equiv.) were added. The solution was kept stirring at the appropriate temperature and time. The reaction was monitored by ^{1}H NMR analysis taking aliquots of the reaction mixture (30 µL) at various time

[135] J. Bah, J. Franzn, *Chem. Eur. J.,* **2014**, 20, 1066.

intervals and diluting with chloroform-d. The reaction was stopped by adding 40 µL of DMSO and the mixture was purified by flash chromatography on silica gel to afford the desired title compounds.

7.4.3 Reaction in presence of competitive guest

To a resorcinarene **16** (281.6 mg, 254.7 µmol, 1.56 equiv.) solution in water saturated chloroform-d (1.1 mL), tetrabutylammonium tetrafluoroborate (763.8 µmol, 18 equiv. respect to CR_6) was added. Then, TryCl (42.3 µmol, 0.26 equiv.), dienophile (163 µmol, 1.0 equiv.) and the diene (489 µmol, 3 equiv.) were added to the solution in this order. The reaction system was kept under stirring (1400 rpm) at 50 °C for 16 h. No formation of product was observed.

7.4.4 Reaction in presence of DMSO

To a resorcinarene **16** (281.6 mg, 254.7 µmol, 1.56 equiv.) solution in water saturated chloroform-d (1.1 mL), 90 µl of DMSO (1.27 mmol) were added. TryCl (42.3 µmol, 0.26 equiv.), dienophile (163 µmol, 1.0 equiv.) and the diene (489 µmol, 3 equiv.) were added to the solution in this order. The reaction system was kept under stirring (1400 rpm) at 50 °C for 16 h. No formation of product was observed.

*7.4.5 General procedure in absence of **CR_6** in presence of Try-X*

To a solution of water saturated chloroform (1.1 mL) TryOH (42.3 µmol, 0.26 equiv.), dienophile (163 µmol, 1.0 equiv.) and the diene (489 µmol, 3 equiv.) were added in this order. The reaction mixture was vigorously stirred at 50°C for the appropriate time. The reaction was monitored by ^{1}H NMR analysis taking aliquots of the reaction mixture (30 µL) at various time

intervals and diluting with chloroform-d. The reaction was not concentrated under reduce pressure but directly purified by flash chromatography on silica gel to afford the desired title compounds.

*7.4.6 General procedure in absence of **CR$_6$** and Try-X*

To a solution of water saturated chloroform (1.1 mL) dienophile (163 µmol, 1.0 equiv.) and diene (489 µmol, 3 equiv.) were added in this order. The reaction mixture was vigorously stirred at 50°C for the appropriate time. The reaction was monitored by ^{1}H NMR analysis taking aliquots of the reaction mixture (30 µL) at various time intervals and diluting with chloroform-d. The reaction was not No formation of product was observed.

7.4.7 NMR experiments as evidence of encapsulation of tritylChloride

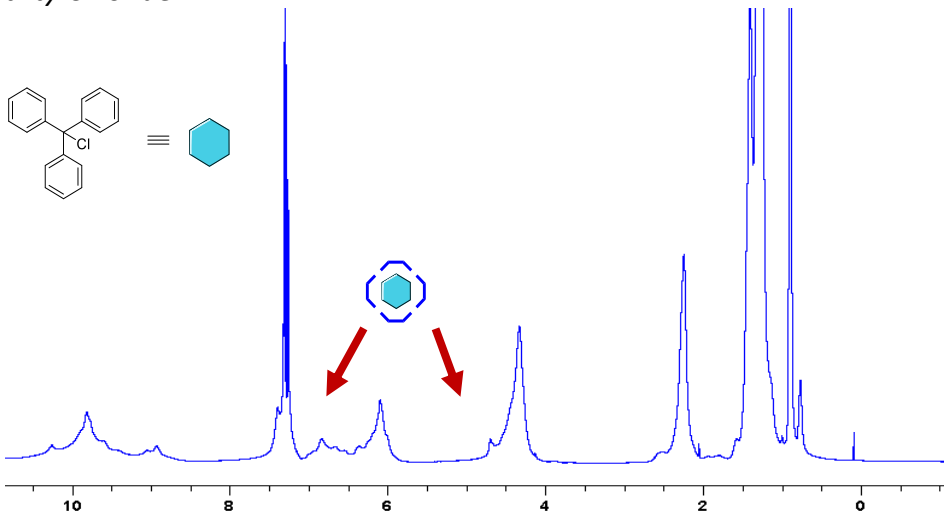

Figure S42. ^{1}H NMR spectrum (600 MHz, $CDCl_3$, 298 K) of the mixture **TryCl** (42.3 mM) and **CR$_6$** (21.2 mM).

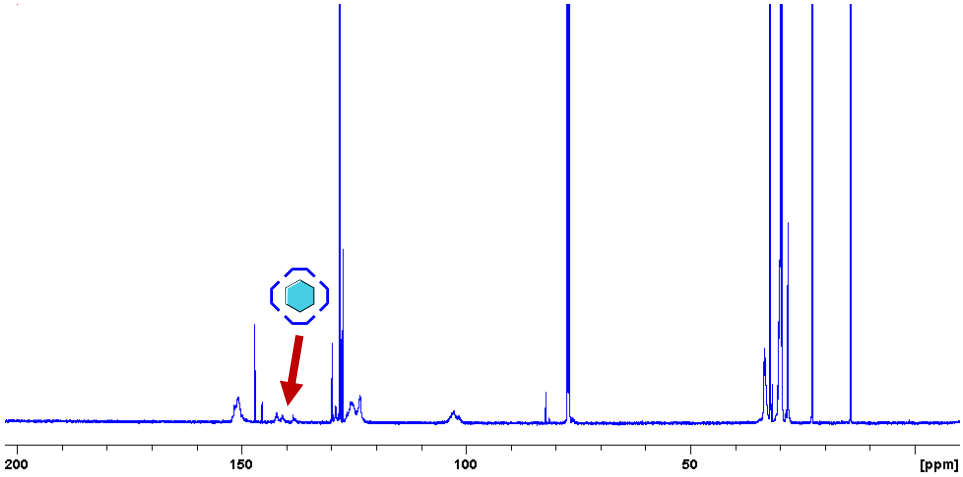

Figure S43. ^{13}C NMR spectrum (150 MHz, $CDCl_3$, 298 K) of the mixture **TryCl** (42.3 mM) and **CR_6** (21.2 mM).

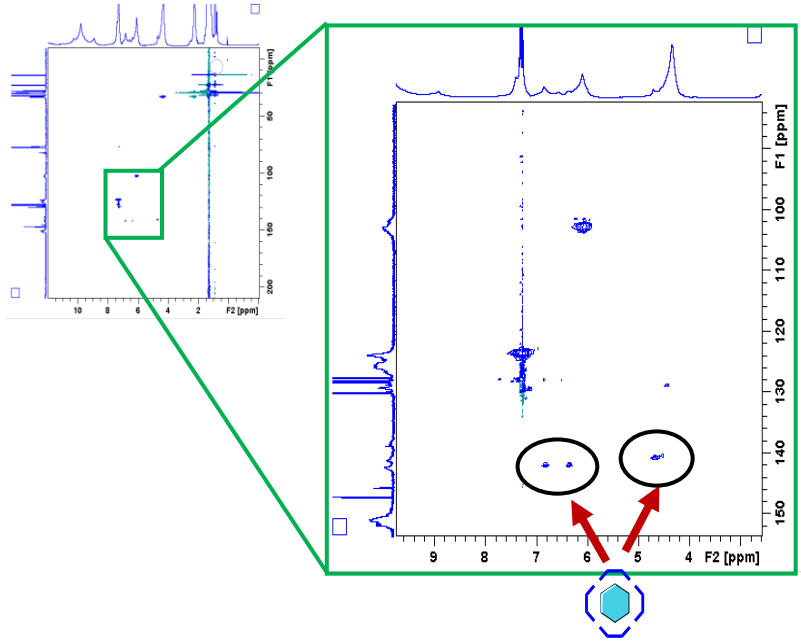

Figure S44 HSQC NMR spectrum (600 MHz, $CDCl_3$, 298 K) of the mixture **TryCl** (42.3 mM) and **CR_6** (21.2 mM). ^1J correlations attributable to the aromatic protons of **TryCl** inside the nanocontainer **CR_6** are marked.

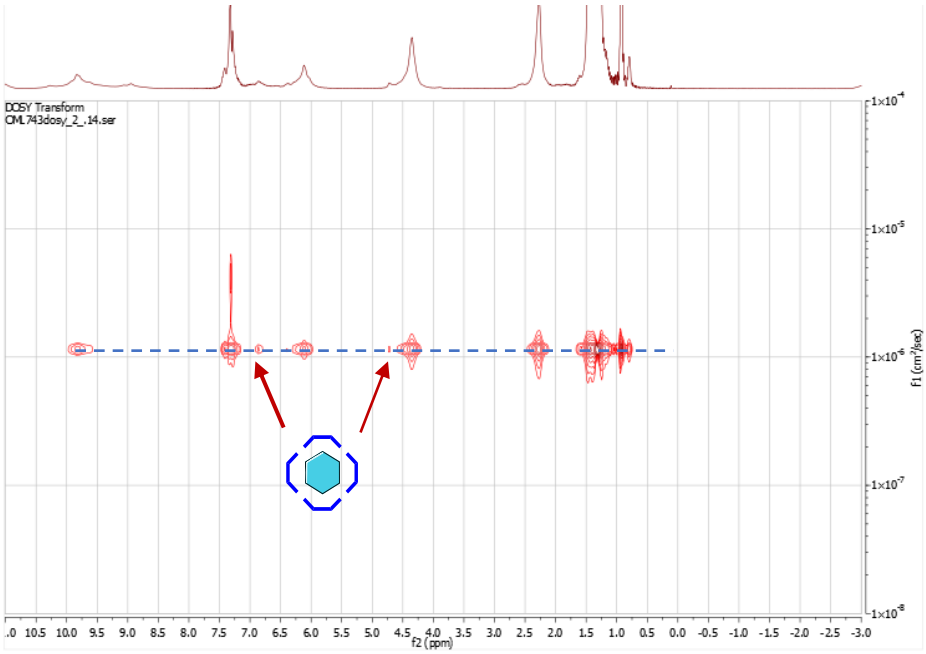

Figure S45. DOSY NMR (600 MHz, $CDCl_3$, 298 K) of the mixture of **TryCl** (42.3 mM) and **CR$_6$** (21.2 mM). The signals pattern associated to **TryCl** inside the capsule **CR$_6$** are aligned with the capsule diffusion coefficient.

7.4.8 Proof of the formation of trityl cation inside CR$_6$

UV-Vis experiments in presence of CR$_6$

Resorcinarene **16** (281.6 mg, 254.6 µmol, 1 equiv.) was weighed in a 4 mL vial. Then, 1 mL of water-saturated chloroform-d was added, and the mixture was homogenized in an ultrasonic water bath at 40 °C for 10 min. Initial concentration of **CR$_6$**: 42.3 Mm. To this clear yellow solution trityl-X was added (2 equiv vs CR_6, for an initial concentration of 84.6 mM). After 2

h under stirring, the solution was diluted to the final concentration and the UV-Vis spectra were recorded.

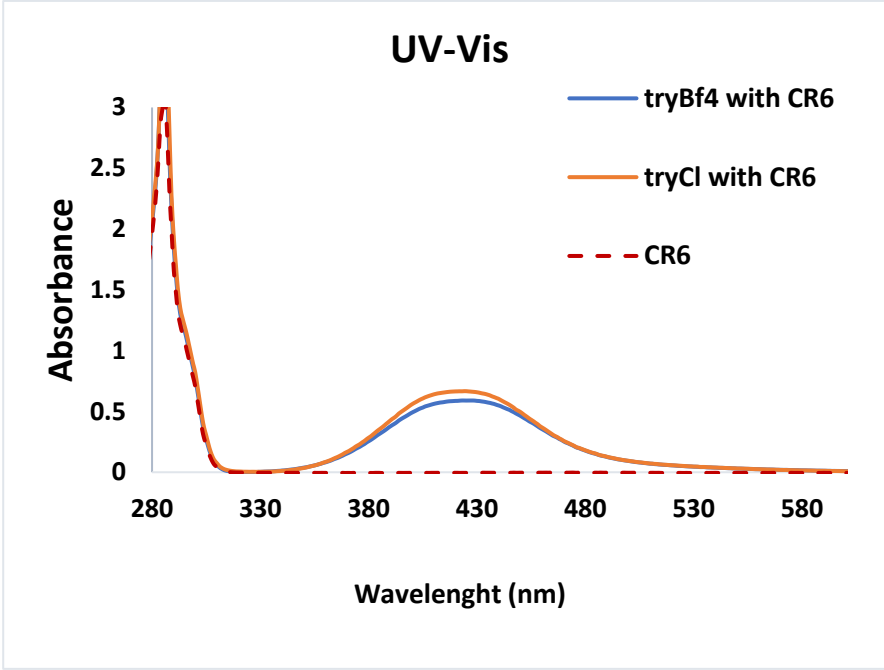

Figure S46. UV-Vis spectra of the mixture **TryBF$_4$/CR$_6$**, **TryCl/CR$_6$** (0.08mM/0.04 mM) and **CR$_6$** alone (0.04 mM) in water-saturated $CDCl_3$.

UV-Vis experiments in absence of CR$_6$

To a solution of 1 mL of water-saturated chloroform-d TryX was added for an initial concentration of 84.6 mM. After 2 h under stirring, the solution was diluted to the final concentration and the UV-Vis spectra were recorded.

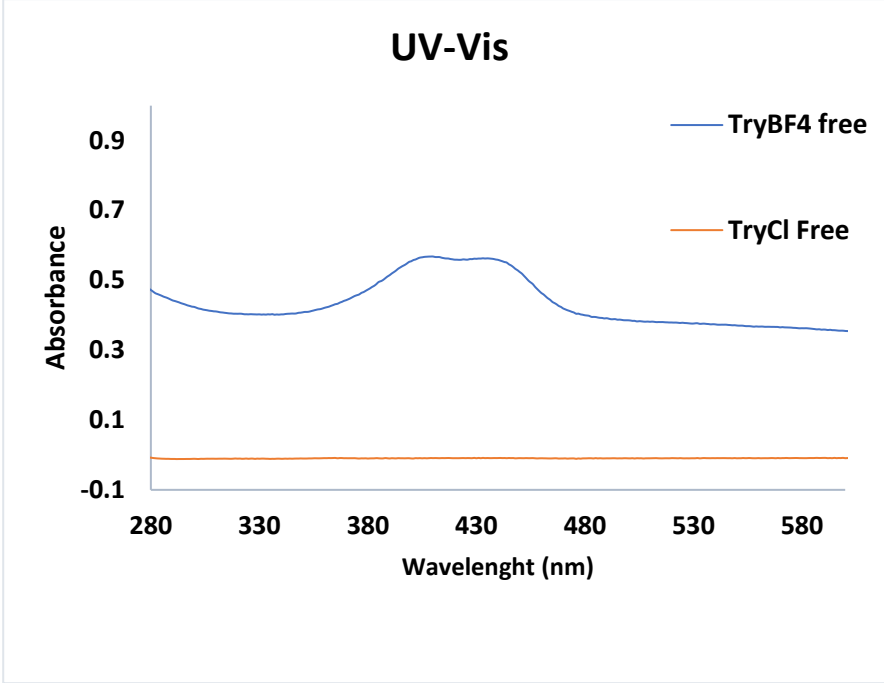

Figure S47. UV-Vis spectra of $TryBF_4$ and TryCl (0.08 mM) in water-saturated $CDCl_3$.

List of publications

S. Gambaro, M. De Rosa, A. Soriente, C. Talotta, G. Floresta, A. Rescifina, C. Gaeta, P. Neri, *A hexameric resorcinarene capsule as a hydrogen bonding catalyst in the conjugate addition of pyrroles and indoles to nitroalkenes, Org. Chem. Front.***, 2019**, *6*, 2339.

S. Gambaro, P. La Manna, M. De Rosa, A. Soriente, C. Talotta, C. Gaeta, P. Neri, *The Hexameric Resorcinarene Capsule as a Brønsted Acid Catalyst for the Synthesis of Bis(heteroaryl)methanes in a Nanoconfined Space, Front. Chem*., **2019**, 7, 687.

S. Gambaro, C. Talotta, P. Della Sala, A. Soriente, M. De Rosa, C. Gaeta, P. Neri, *Kinetic and Thermodynamic Modulation of Dynamic Imine Libraries Driven by the Hexameric Resorcinarene Capsule*, *J. Am. Chem. Soc.,* **2020**, *142*, 35, 14914.

Appendix: Template Synthesis of a bis-calix[4]pyrrole macrocycle

The following work has been performed at the Institut Català d'Investigació Química (ICIQ) in Tarragona under the supervision of Prof. Pablo Ballester.

A1. Introduction: Calix[4]pyrroles as receptors

Calix[4]pyrroles are macrocyclic compounds formed by four pyrrole units held together by four sp^3 hybridized carbon atoms (*meso*-carbons) [1]. Calix[4]pyrroles are conformationally flexible, and can adopt multiple conformations in solution, characterized by the relative orientation of the pyrrole units in the macrocycle: *cone, partial cone*, *1,3-alternate* and *1,2-alternate* conformation, fig. A1. In non-polar solvents, such as dichloromethane and chloroform, the most favored conformation is the *1,3-alternate* conformation, while in more polar solvents, such as acetone, acetonitrile and methanol, the population of alternative conformations increases[2].

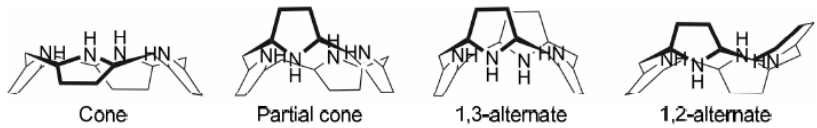

Figure A1. Representation of four possible conformations adopted by calix[4]pyrrole

[1]a) P. A. Gale, J. L. Sessler, V. Kral, V. Lynch, *J. Am. Chem. Soc.*, **1996**, *118*, 5140; b) P. A. Gale, J. L. Sessler, V. Kral, Chem. Commun., **1998**, *1*-8; c) P. A. Gale, P. Anzenbacher, J. L. Sessler, Coord. Chem. Rev., **2001**, *222*, 57.

[2] J. R. Blas, J. M. Lopez-Bes, M. Marquez, J. L. Sessler, F. J. Luque, M. Orozco, *Chem. Eur. J.*, **2007**, *13*, 1108.

Calix[4]pyrroles are effective receptors for anions[3] and ion-pairs[4], displaying a *host-separated* binding geometry in the latter case. As initially suggested by Sessler, the calix[4]pyrrole core can bind anions by establishing four hydrogen bond interactions with the four pyrrole NHs. This binding produces a conformational change of the calix[4]pyrrole to the *cone* conformation generating an electron-rich shallow cavity, opposed to the bound anion, that is able to bind cations which are complementary in size and shape.

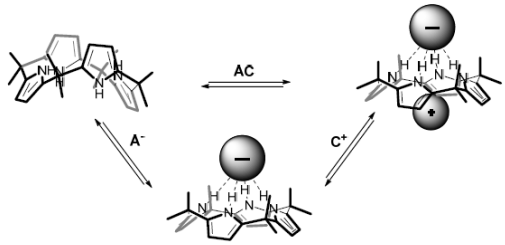

Figure A2. Binding sequence by a calix[4]pyrrole receptor proposed by Sessler.

In the last years, a wide number of calix[4]pyrrole derivatives with enhanced recognition properties have been described. For example, the elaboration of the meso carbon atoms with aryl groups affords the so called aryl-extended calix[4]pyrroles ("two walls" or "four walls" depending on the number of substituted meso carbon, fig. A3)[5]. For example, the α, α, α, α-isomer of aryl-extended calix[4]pyrrole in cone conformation presents a deep aromatic cavity ideal for the binding of anions and neutral polar

[3] L. Sessler, D. E. Gross, W. S. Cho, V. M. Lynch, F. P. Schmidtchen, G. W. Bates, M. E. Light, P. A. Gale, *J. Am. Chem. Soc.*, ***2006**, 128*, 122818.
[4] S. K. Kim, J. L. Sessler, *Acc. Chem. Res.*, **2014**, 47, 25256.
[5] P. Anzenbacher, K. Jursíková, V. M. Lynch, P. A. Gale, J. L. Sessler, *J. Am. Chem. Soc.,* **1999***, 121,* 11020; b) L. Bonomo, E. Solari, G. Toraman, R. Scopelliti, M. Latronico, C. Floriani, *Chem. Commun. (Cambridge, U. K.)*, **1999**, 2413.

guests[6]. The guest can establish H-bond interactions with the pyrrole NHs groups of the calix[4]pyrrole core and additional non-covalent interactions with the aromatic walls of the host. The introduction of ionizable groups, such as amines and carboxylic acids, can provide the calix[4]pyrrole scaffold with water-solubility and allows binding studies in the water[7].

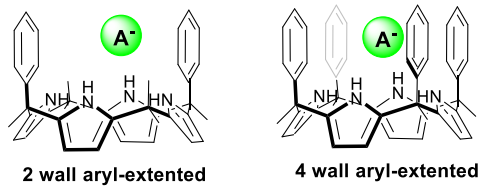

Figure A3. Examples of aryl-extented calix[4]pyrrole derivatives.

Other notable examples are the so-called strapped-calix[4]pyrrole[8]. Such systems present one or more bridging ''*straps*'' that spread from the calix[4]pyrrole core, creating cyclic (or polycyclic) systems, fig. A4. They often present enhanced affinities and greater selectivity toward the guests, compared to the non-strapped analogous and these properties can be attributed to a synergic interplay between the presence of a deeper cavity and additional binding/recognition sites on the *strap*. A special class of *strapped* calix[4]pyrrole is represented by the calix[4]pyrrole *strapped* by another calix[4]pyrrole, also called bis-calix[4]pyrroles, in which two aryl-extended calix[4]pyrroles are covalently connected by two bridging units, fig. A4.

---

[6] a) G. Gil-Ramírez, E. C. Escudero-Adán, J. Benet-Buchholz, P. Ballester, *Angew. Chem., Int. Ed.*, **2008**, *47*, 4114.
[7] B. Verdejo, G. Gil-Ramírez, P. Ballester, *J. Am. Chem. Soc.*, **2009**, *131*, 31789.
[8] C. H. Lee, H. Miyaji, D. W. Yoon, J. L. Sessler, *Chem. Commun.*, **2008**, 244.

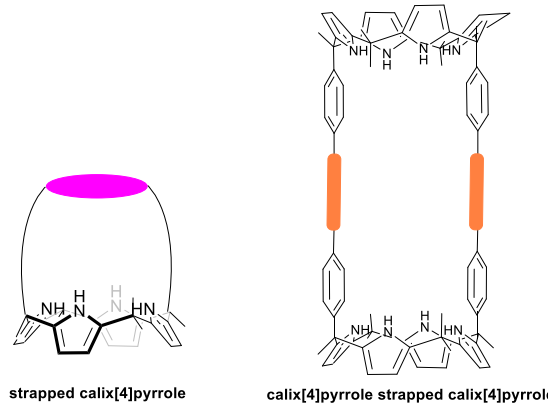

Figure A4. Representation of a strapped calix[4]pyrrole (left) and calix[4]pyrrole-strapped calix[4]pyrrole (right).

In 2012, Ballester's group reported the first example of a bis-calix[4]pyrrole macrocycle **2**. Macrocycle **2** was obtained by a Hay-coupling reaction of calix[4]pyrrole **1** templated by 1 equiv. of 4,4'-bipyridine bis-*N*,*N*'-oxide**.** Macrocycle **2** can bind ditopic linear bis-amidepyridyl-*N*-oxides in a 1:1 molar ratio. Addition of 1 equiv. of a tetrabutylammonium salt (e.g. Cl-, OCN-), produced the formation of four particles aggregates with pseudorotaxane topology[9].

[9] V. Valderrey, E. C. Escudero-Adan, P. Ballester, *J. Am. Chem. Soc.*, **2012**, *134*, 10733.

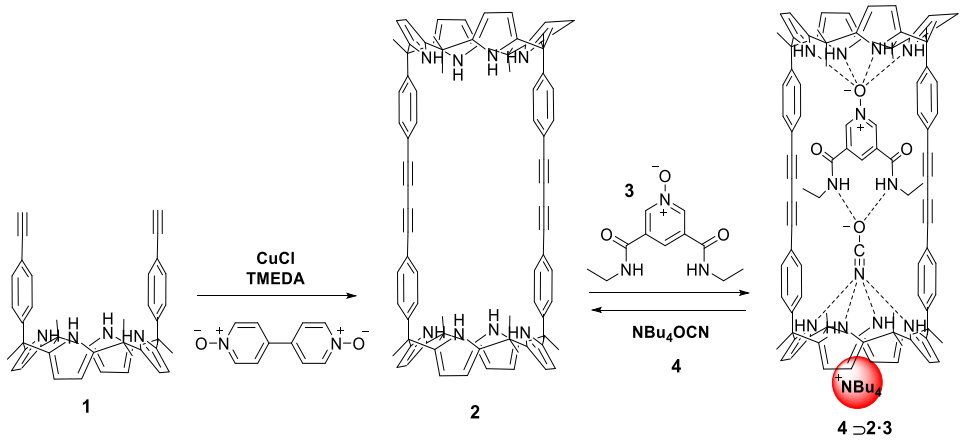

Figure A5. Synthesis of **2** and formation of pseudo rotaxane **4** ⊃**2·3.**

On the basis of this consideration and with the aim to extend the study on bis-calix[4]pyrroles, a new macrocycle **6** was designed, fig. A6. We envisioned the formation of the same type of architecture observed for **2**, but with higher selectivity towards monoatomic anions, such as chloride or bromide, over polyatomic anions owing the better fit with the new cavity.

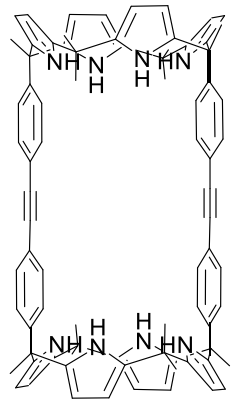

Figure A6. Structure of the bis-calix[4]pyrrole macrocycle **6.**

A2. Results and discussion

According to our retrosynthetic approach, consisting in a template Sonogashira reaction, we proposed two synthetic routes: **A**, starting from an asymmetric iodo-alkynil-calix[4]pyrrole **7** and **B**, starting from the diiodocalix[4]pyrrole **8** and dialkynilcalix[4]pyrrole **9**, depicted in fig. A7.

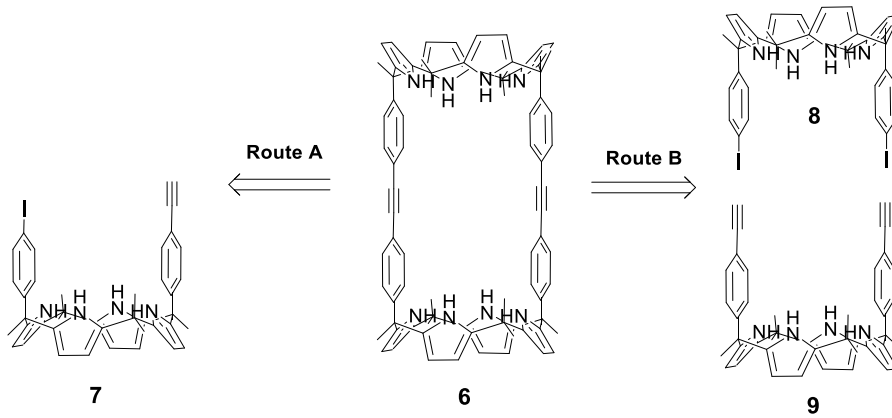

Figure A7. Representation of the two possible routes for the synthesis of macrocycle **6.**

For route A, precursor **7** was synthetized following the synthetic strategy depicted in fig. A8. Briefly, the acid catalysed condensation of the commercially available 4-iodo acetophenone **10** with an excess of freshly distilled pyrrole afforded the dipyrromethane **11** in 60% yield. Next, **11** was reacted in acetone in the presence of boron trifluoride ethyl ether, in highly dilution conditions, affording two calix[4]pyrrole stereoisomers α,β-**8** (not synthetic useful) and α,α-**8,** depending on the relative orientation of the 1,3-*meso* phenyl substituents, in 9% and 10% yield.

The mono-Sonogashira cross-coupling reaction of α,α-**8** with the propargylic alcohol produced **12** in a 45% yield. Finally, the basic treatment of **12** afforded **7** in 60% yield.

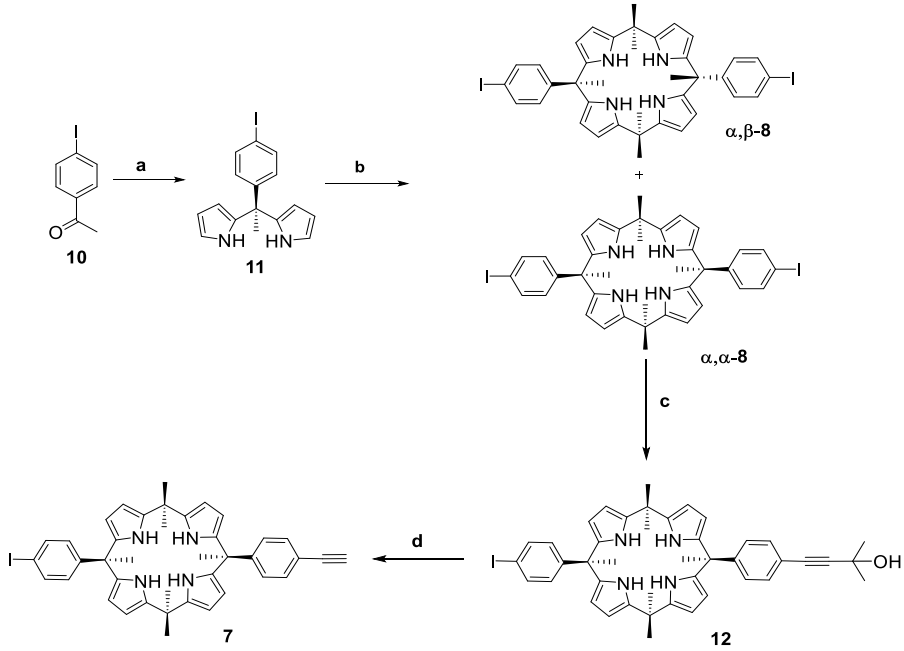

Figure A8. Synthesis of precursor **7**. Reagents and conditions: a) pyrrole, CF_3COOH, (60%) b) acetone $BF_3(OEt)_2$, (10%); c) propargylic alcohol, $PdCl_2(PPh_3)_2$, CuI, Et_3N, toluene (45%); d) KOH, toluene, (60%).

We choose as potential templates, the electron-rich ditopic guests terephthalate and isophtalate salts, **13**•TBA_2 and **14**•TBA_2 respectively. NMR titration experiments in acetonitrile-d_3 suggested the addition of 0.5 equiv. of template guest to a millimolar solution of **7** produces the formation of 2:1 complexes. The guests interact with NHs groups of two units of **7** simultaneously, by establishing multiple H-bond interactions.

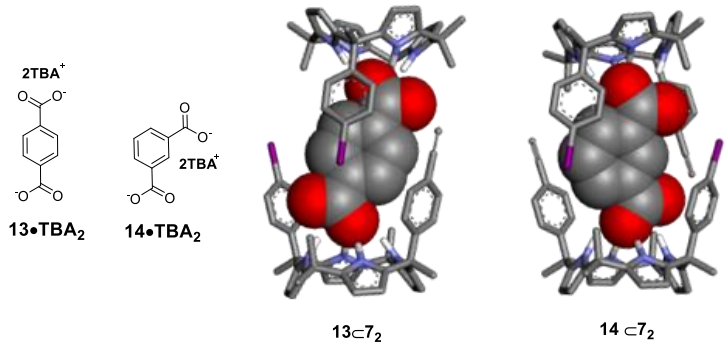

Figure A9 Structure of **13**•TBA_2 and **14**• TBA_2 (left) and Energy-minimized (MM3) structures of **13** ⊂ **7_2** and **14** ⊂ **7_2** (right). Host represented as stick and ball model and guest as CPK model.

In detail, the addition of 0.5 equiv. of 13•TBA_2 to a 2 mM acetonitrile-d_3 solution of **2** produced the downfield shift of the proton signals corresponding to the pyrrolic NHs. These changes pointed out to H-bond interactions between the pyrrole NHs and the oxygen atoms of the carboxylate moiety of the guest. Moreover, the proton of the encapsulated guest appeared as a single broad peak upfield shifted compared to the free counterpart. This result also confirmed the encapsulation of the guest inside the cavity and, the formation of the symmetric homodimeric complex **13⊃7_2**. Addition of incremental amounts of the guest (1 equiv.) provoked the splitting of the signal of the guest inside into two broad peaks. This result suggested the dissociation of the **13⊂7_2** complex and the formation of non-symmetric complex **13⊂7**. Titration experiments with isophtalate (SA1), produced similar results.

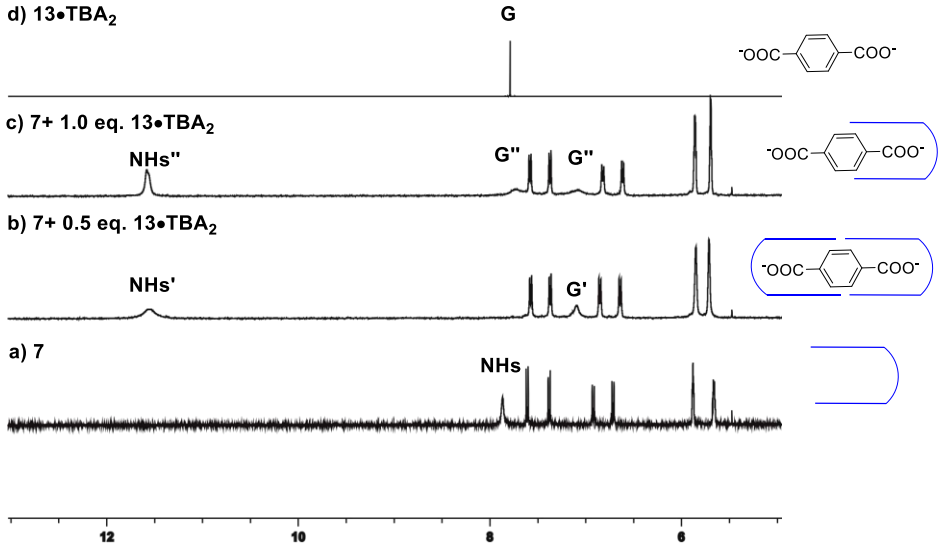

Figure A10 Selected region of the ^{1}H NMR spectra (400 MHz, CD_3CN, 298 K) of free receptor **7** (2 mM) (a) and incremental additions of 13•TBA_2: 0.5 equiv (b) and 1.0 equiv (c); 13•TBA_2 free (d). Primed letters correspond to **13⊃7$_2$**, double primed letters correspond to **13⊃7**.

Based on these preliminary results, we started to investigate the potential of synthetic Route A, scheme A1. The reactions were monitored by HPLC and ^{1}H NMR spectroscopy. We tested several reaction conditions (Table 1).

Initially, attempts in the synthesis of macrocycle **6** were carried out with $Pd(PPh_3)_2Cl_2$/CuI, a common combination of catalyst and co-catalyst for the Sonogashira reaction, in presence and in absence of the guests (entry 1, Table 1). Unfortunately, no trace of macrocycle **6** was detected. Alternatively, the reaction produced mainly insoluble polymeric products and traces of molecule **15**, derived from the Hay coupling between two molecules of **7**. The Hay coupling is a classical side reaction of the

Sonogashira reaction in the presence of copper salts, which, in presence of oxygen, promotes the alkyne-alkyne coupling[10]. Considering this, we carried out reactions replacing CuI co-catalyst by $AuClPPh_3$[11] and also without any co-catalyst[12] (entries 2-3, Table 2). In any case we could detect macrocycle **6**. Alternatively, we obtained Hay-coupling product **15** and insoluble polymers. Then we decided to replace the catalyst[13] $Pd(PPh_3)_2Cl_2$ by $Pd(OAc)_2$. We did not detect the macrocycle as a reaction product (entry 4, Table 4). Interestingly, carrying out the reaction using $Pd_2(dba)_3$ and Et_4NOAc as base, and without any templating guest, traces of **6** and the product of the mono cross-coupling reaction **16** were observed (Entry 5, Table 1). When the reactions were carried out in presence of **13** or **14**, an increase of the amount of macrocycle was detected. In detail, in presence of **13** the ratio macrocycle **6**/opened form **16** was 8/2, while with **14** was 6/4 ratio, thus indicating that the terephthalate **13** is a better template in driving the Sonogashira reaction towards **6**.

[10] P. Siemsen, R. C. Livingston, F. Diederich, *Angew. Chem. Int. Ed.*, **2000**, *39*, 2632.
[11] B. Panda, T. K. Sarkar, *Synthesis*, **2013**, *45*, 817.
[12] N. Leadbeater, B. J. Tominack, *Tetr. Lett.*, **2003**, *48*, 8653.
[13] S. Urgaonkar, J. G. Verkade, *J. Org. Chem.*, **2004**, *69*, 5752.

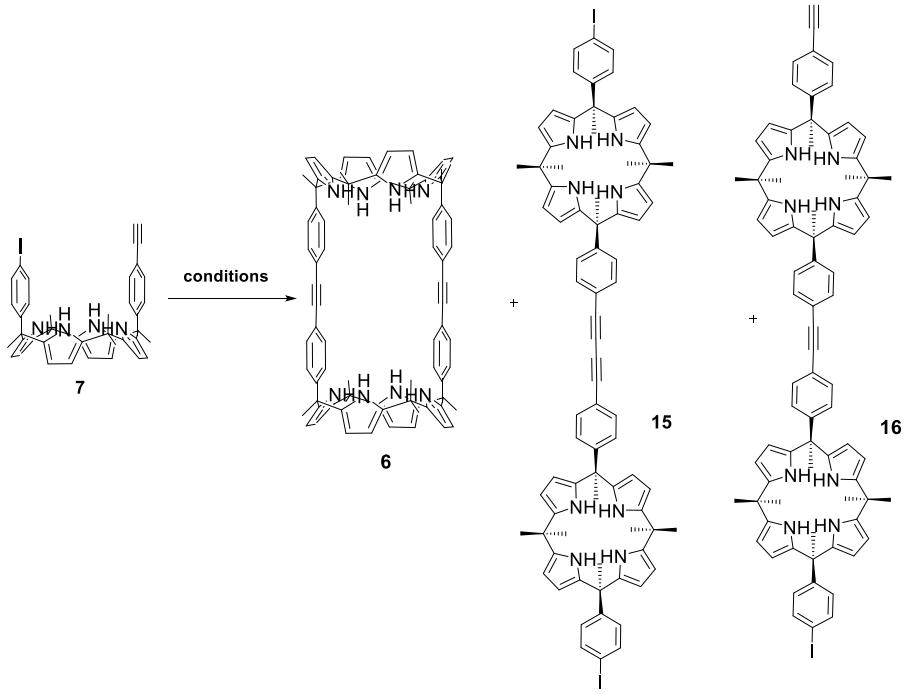

Scheme A1. Synthesis of **6** starting from **7.**

Table A1: Optimization reaction conditions for the synthesis of **6.**

Entry[a]	Catalyst	Co-catalyst	Base	Template	Products[b]
1	$Pd(PPh_3)_2Cl_2$	CuI	DIPEA	No **13** **14**	Polymers+**15**
2	$Pd(PPh_3)_2Cl_2$	$AuClPPh_3$	Et_3N	No **13** **14**	Polymers+**15**

3	$Pd(PPh_3)_2Cl_2$	--	Et_3N	No **13** **14**	Polymers+**15**
4	$Pd(OAc)_2$	--	Et_4NOAc	No **13** **14**	Polymers+**15**
5	$Pd_2(dba)_3$	--	Et_4NOAc	No **13** **14**	**16** + traces of **6** **6**+**16** in 8/2 ratio[c] **6**+**16** in 6/4 ratio[c]

[a]Reaction conditions: **7** (7Mm), catalyst and cocatalyst (2.1 Mm), **13-14** (3.5 Mm) and base 70Mm) in acetonitrile (3 mL), [b]By comparison of rt and UV-Vis spectra. [d]Determined by integration of area in HPLC analysis.

These results suggested that the first Sonogashira cross coupling reaction does not depend on the presence of the template but mainly on the reaction conditions. Template **13** is essential to favour the second intramolecular reaction to yield macrocycle **6** over the intermolecular one that would yield oligo and polymeric products. Terephthalate **13** binds the two calix[4]pyrrole units of dimer **15** and orients the two reacting groups in close proximity to facilitate the intramolecular reaction, fig. A11.

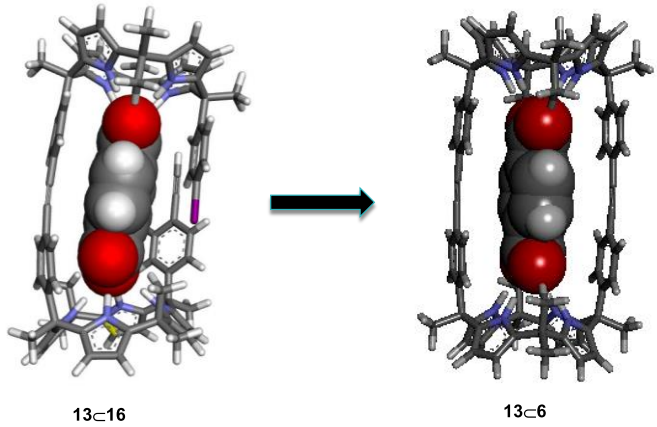

Figure A11 Scheme of the intramolecular reaction to form macrocycle **6.** Energy-minimized (MM3) structures of complexes **13⊂16** and **13⊂6**.

After having optimized the reaction conditions, we scale-up the reaction (50 mg of **6**). We obtained the pure macrocycle **6** in 5% yield after several purification steps (see experimental section for details). The ^{1}H NMR spectrum of the yellow solid in $CDCl_3$ solution displayed sharp signals corresponding to the protons of the macrocycle. β-pyrrole protons (H_5 and H_4) appeared as two signals resonating at 5.98 and 6.05 ppm while the pyrrole NHs appeared as a broad peak at 6.91 ppm. The doublets attributed to the aromatic protons of the macrocycle walls (H_1 and H_2) resonates at 6.92 and 7.51 ppm.

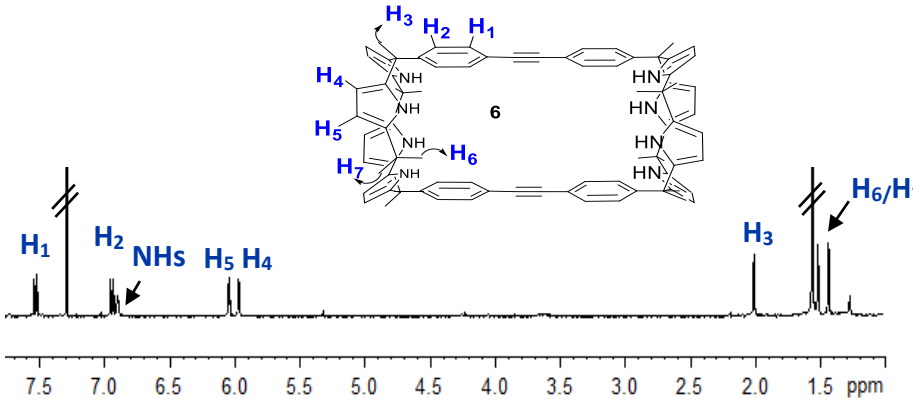

Figure A12 ^{1}H NMR (400 MHz, $CDCl_3$, 298 K) of the bis-calix[4]pyrrole macrocycle **6.**

Additionally, the same conditions were used also for synthetic route **B** and the macrocycle was detected in the crude. Unfortunately, in this case we were not able to isolate the pure compound because of the residual di-iodocalix[4]pyrrole **8**, that presented a very close R_f to the desired target.

Due to the covid-19 pandemic I did not have time to test the binding properties of this new bis-calix[4]pyrrole macrocycle.

A3. Conclusions

We have evaluated different reaction conditions for the synthesis of the new bis calix[4]pyrrole macrocycle **6**. We demonstrated that the Sonogashira reaction catalysed by $Pd_2(dba)_3$ in combination with the inorganic base Et_4NOAc in presence of terephthalate **13** as template were the best conditions found so far to obtain macrocycle **6**. However, purification steps need to be improved. The results suggested that the

template plays a crucial role to favour the second intramolecular reaction by arranging the two reactive ends of the opened dymer **16** in close proximity to afford macrocycle **6**.

A4. Experimental Section

A4.1 General remarks

All reagents were obtained from commercial suppliers and used without further purification. Anhydrous solvents were obtained from a solvent purification system SPS-400-6 from Innovative Technologies, Inc. All solvents were of HPLC grade quality, commercially obtained and used without further purification. Routine ^{1}H NMR spectra were recorded on a Bruker Avance II 400 Ultrashield NMR spectrometer. Chemical shifts are given in ppm, relative to TMS. Analytical HPLC experiments were performed using a HPLC1100 Agilent instrument.

A4.2 Synthetic procedures

The precursors α,α–**8**, **9** and the guests **13•TBA$_2$** and **14•TBA$_2$** were synthesized according to reported procedures[9].

*A4.2.1 Procedure for the synthesis of **12***

In a 25 mL schlenk flask 100 mg of α,α–**8** (0.1 g, 0.12 mmol, 1 equiv), CuI (1.18 mg, 0.006 mmol, 0.05 eq) and the $Pd(PPh_3)_2Cl_2$ (4.36 mg, 0.006 mmol, 0.05eq) are dissolved in 10 mL of toluene under inert conditions. Afterwards, triethylamine (1.64 mL, 0.62 mmol, 5 eq) and 2-methyl-3-butyn-2-ol (0.06 mL, 0.62 mmol, 5 eq) are added in one portion. The

reaction is stirred for 1 h at room temperature and 10 mL of DCM are added to the mixture. Then, the organic phase is washed with 20 mL of HCl 0.5 M and 20 mL of water. The organic phase is collected, dried with sodium sulfate and filtered. The solvent was removed under reduced pressure. The product **12** was purified through column chromatography using a 9:1 DCM:Hexane obtained as a brown-dark orange solid (yield = 45 %).

^{1}H NMR (500 MHz, $CDCl_3$, 298 K) δ 7.54 (d, J= 8.79 Hz, 2H,), 7.28 (d, J= 8.45 Hz, 2H), 7.20 (br, 4H, NHs), 6.90 (d, J= 8.45 Hz, 2H), 6.72 (d, J= 8.79 Hz, 2H), 5.92 (m, 4H), 5.61 (m, 4H), 1.87 (s, 3H,), 1.85 (s, 3H,), 1.61 (s, 6H), 1.59 (s, 6H), 1.52 (s, 6H). ^{13}C NMR (125 MHz, $CDCl_3$, 298 K) δ 148.6, 148.2, 139.0, 138.9, 137.1 136.5, 136.3, 131.3, 129.3, 127.7, 121.1, 106.4, 106.3, 103.7, 103.6, 93.9, 92.3, 82.4, 66.0, 45.0, 44.9, 35.5, 31.9, 30.4, 28.2, 28.0, 27.9. M.p. = 170 ºC. ESI- m/z calcd for $C_{43}H_{44}IN_4O$ $(M-H)^-$ 759.2654, found 759.2565.

*A4.2.2 Procedure for the deprotection of **12***

In a round bottom flask of 100 mL 300 mg of 12 are dissolved (0.3g, 0.207 mmol, 1eq) in 40 mL of dry toluene. Powdered sodium hydroxide (0.336 g, 7.12 mmol, 20 eq) is added to the solution. The orange mixture is stirred at 90°C for 12 h under Ar atmosphere. The reaction mixture is washed with

30mL of HCl 0.5M and the organic the aq. phase extracted 3 times with 30 mL DCM. The combined organic phases are washed then with water 2 x 60 mL, filtered and concentrated under reduced pressure to give **7** as brown solid (60%) ^{1}H NMR (500 MHz, CD_2Cl_2, 298 K) δ 7.55 (d, J= 8.48 Hz, 2H,), 7.35 (d, J= 8.44 Hz, 2H,), 7.27 (br, 4H,), 6.92 (d, J= 8.44, 2H), 6.71 (d, J= 8.47, 2H), 5.92 (m, 4H), 5.62 (m, 4H), 3.08 (s, 1H), 1.86 (s, 3H), 1.85 (s, 3H), 1.62 (s, 6H), 1.51 (s, 6H). ^{13}C NMR (125 MHz, CD_2Cl_2, 298 K) δ 149.4, 148.4, 139.1, 139.0, 137.0, 136.3, 136.2, 131.7, 129.9, 127.8, 120.4, 106.4, 193.5, 92.0, 83.7, 77.1, 45.0, 44.8, 35.3, 30.3, 27.5, 27.4, 27.1. M.p. =273.3 ºC. ESI- m/z calcd for $C_{40}H_{38}IN_4$ $(M-H)^-$ 701.2153, found 701.2147.

A4.2.3 General procedure for the optimization reaction conditions

In a 10mL schlenk flask 15 mg of **7** (0.015 g, 21 µmol, 1 eq) are dissolved together with, catalyst/co-catalyst (6.3 µmol, 0.3 eq), guest (10,5 µmol, 0.5eq), base (210µmol, 10 eq) in 3 mL of ACN under inert conditions. The reaction was monitored by HPLC normal phase (Waters corporation) using a 40/60 Hexane:DCM mixture as the eluent, until the total consumption of **7.** Afterwards, 5 mL of DCM are added to the mixture. The organic phase is washed with 50 mL of HCl 0.5 M and 5 mL of water. Then, the organic phases are collected, dried with sodium sulfate, filtered and concentrated under

reduced pressure. The crude was analyzed by ^{1}H NMR in order to confirm the presence or not of the target compound.

*A4.3.1 Synthesis of **6**: Route A*

In a 25mL schlenk flask **7** (0.051 g, 71 µmol, 1 eq), $Pd_2(dba)_3$ (0.019g, 21.3 µmol, 0.3 eq), 13·TBA_2 (10,5 µmol, 0.5eq), Et_4NOAc (0.21 710µmol, 10 eq) are dissolved in 10 mL of ACN under inert conditions. After 3h, in the mixture was added 15 mL of DCM. The organic phase was washed with 15 mL of HCl 0.5 M and 15 mL of water. The organic phases are collected, dried with sodium sulfate and concentrated under reduced pressure. At this point, several attempts were done in order to isolate **6** pure: precipitation or crystallization in ACN are not useful purification method whereas the combination of a first filtration on a path of silica to remove the catalyst using DCM as solvent and then a TLC semipreparative with Hexane/DCM 40/60 as eluent is found the best protocol to get **6** pure as yellow powder in 5% yield (2 mg).

^{1}H NMR (400 MHz, $CDCl_3$, 298 K) δ 7.52 (d, J= 8.7 Hz, 2H,), 6.93 (d, J= 8.7 Hz, 2H,), 6.04 (t, J= 3.2, 2H), 5.97 (t, J= 3.16, 2H,), 2.01 (s, 3H), 1.52 (s, 3H), 1.44 (s, 3H). ^{13}C NMR (125 MHz, $CDCl_3$, 298 K) δ 147.2, 137.0, 136.0, 131.7, 127.3,

121.6, 105.6, 105.1, 89.7, 44.9, 35.7, 30.5, 30.1, 29.0. MALDI+ m/z calculated for $C_{80}H_{76}N_8$ [M+] 1448.6187, found 1448.6158.

*A4.3.1 Synthesis of **6**: route B*

In a 10 mL Schlenk flask α,α-**8** (0.015 g, 19 µmol, 1 eq), **9** (0.012 g, 19 µmol, 1 eq), $Pd_2(dba)_3$ (0.019g, 5.7 µmol, 0.3 eq), **13**·TBA (19 µmol, 0.5eq), and Et_4NOAc (0.06g, 190µmol, 10 eq) are dissolved in 3 mL of ACN under inert conditions. After 3h, in the mixture was added 5 mL of DCM. The organic phase was washed with 5 mL of HCl 0.5 M and 5 mL of water. The organic phases are collected, dried with sodium sulfate and concentrated under reduced pressure. The crude was filtered on a path of silica using DCM as eluent to remove the catalyst. Several attempts to purify the crude were done but, it has not been possible to isolate the pure product **6** using these reaction conditions.

A4.3 Figures

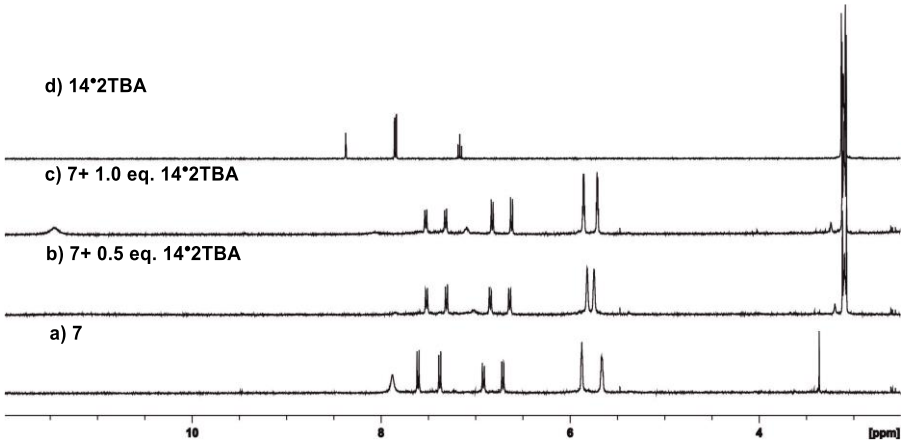

Figure SA1. Selected region of the ^{1}H NMR spectra (400 MHz, CD_3CN, 298 K) of free receptor **7** (2 mM) (a) and incremental additions of 14•TBA_2: 0.5 equiv (b) and 1.0 equiv (c); 14•2TBA free.

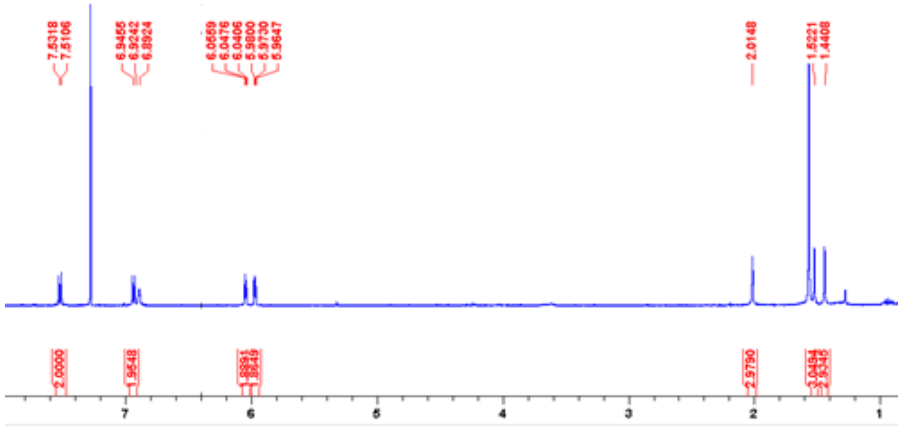

Figure SA2. ^{1}H NMR spectrum (400 MHz, $CDCl_3$, 298 K) of **6**

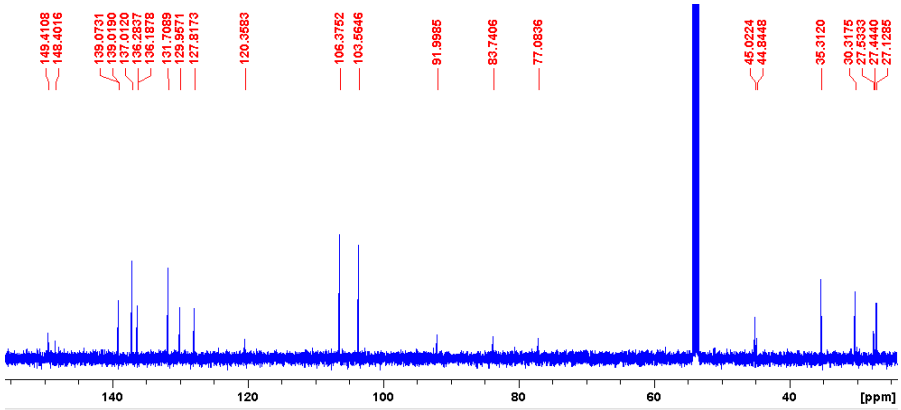

Figure SA3. ^{13}C NMR (125 MHz, $CDCl_3$, 298 K) of **6**

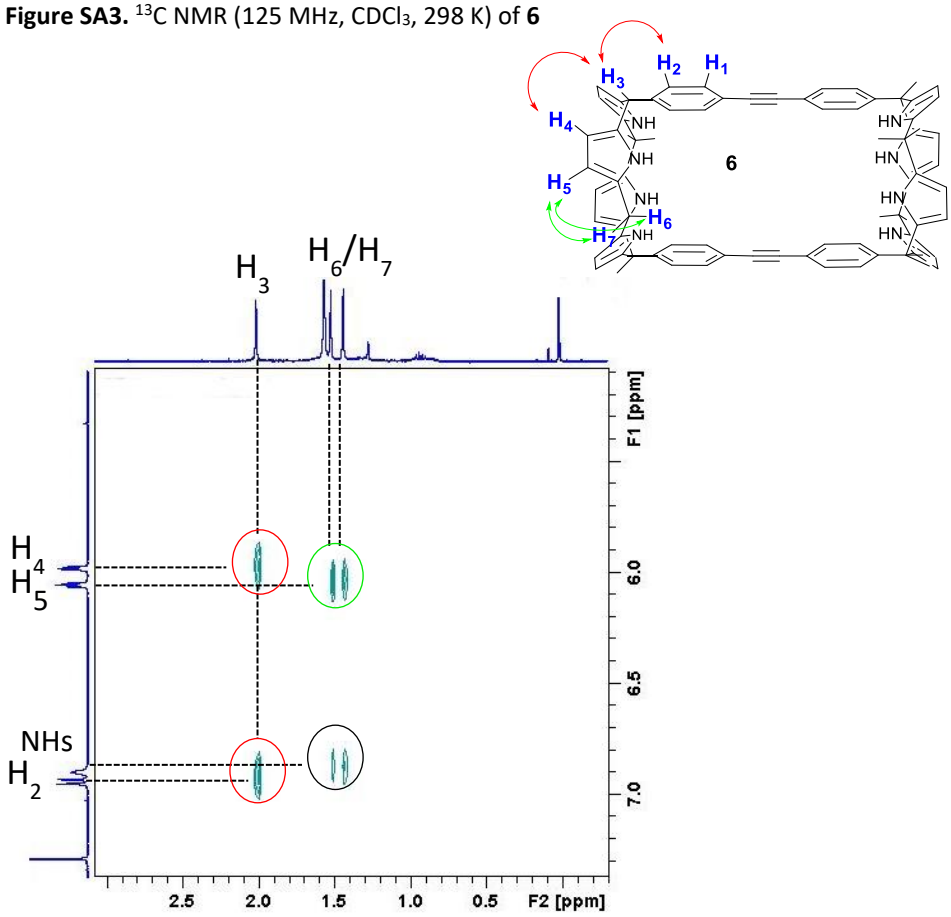

Figure SA4. Selected region of NOESY NMR spectrum (400 MHz, $CDCl_3$, 298 K) of **6.**